AD-A256 340

1. AGENCY USE ONLY (Leave blank)

2. REPORT DATE

3. REPORT TYPE AND DATES COVERED
FINAL 01 Feb 89 TO 31 Jan 92

4. TITLE AND SUBTITLE
BIOPHYSICAL AND BIOCHEMICAL MECHANISMS IN SYNAPTIC TRANSMITTER RELEASE

5. FUNDING NUMBERS
AFOSR-89-0270
61102F
2312
A2

6. AUTHOR(S)
DR RODOLFO R. LLINAS

7. PERFORMING ORGANIZATION NAME(S) AND ADDRESS(ES)
Dept of Psysiology and Biophysics
550 First Avenue
New York, NY 10016

8. PERFORMING ORGANIZATION REPORT NUMBER
AFOSR-TR- 92 0901

9. SPONSORING / MONITORING AGENCY NAME(S) AND ADDRESS(ES)
Dr Haddad
AFOSR/NL
Building 410
Bolling AFB DC 20332-6448

10. SPONSORING / MONITORING AGENCY REPORT NUMBER

11. SUPPLEMENTARY NOTES

12a. DISTRIBUTION / AVAILABILITY STATEMENT
Approved for public release,
distribution unlimited.

12b. DISTRIBUTION CODE

13. ABSTRACT (Maximum 200 words)

The initial question addressed in 1989 was that of synaptic vesicle movement as determined by direct microscopic visualization. This research demonstrated that vesicles were actually mobilized from the point of injection in the axon to the active zones, i.e. the place where synaptic transmitter is released. It was also found that a change in either oxygenation or the surface properties of vesicles can lead to no movement or, to change in movement direction. The second aspect of synapse work performed that year was a demonstration of the category of calcium channel that is responsible for transmitter release. The work in 1990 demonstrated that miniature potentials could be modulated in the squid synapse by injection of Synapsin I and of protein kinase II. In the third year of the grant, 1991, the first demonstration of calcium microdomains in synaptic transmission was performed.

14. SUBJECT TERMS

15. NUMBER OF PAGES

17. SECURITY CLASSIFICATION OF REPORT	18. SECURITY CLASSIFICATION OF THIS PAGE	19. SECURITY CLASSIFICATION OF ABSTRACT	20. LIMITATION OF ABSTRACT
(U)	(U)	(U)	(UL)

The research supported by the Air Force during the summers of 1989, 1990 and 1991 generated significant studies in four different aspects of synaptic transmission.

1. Characterization and isolation of voltage-dependent calcium channels responsible for transmitter release in the squid giant synapse as well as in the neuromuscular junction in mammals.

2. The dynamics, directionality and specificity of synaptic vesicle migration in relation to transmitter release.

3. The effect of Synapsin I, an intracellular chemical modulator of synaptic vesicular mobility, and its effect in the regulation of the vesicular release and synaptic facilitation in tonic synapses.

4. Finally, the presence of well-specified calcium concentration microdomains in relation to transmitter release, was demonstrated for the first time in 1991, using aequorin.

The initial question addressed in 1989 was that of synaptic vesicle movement as determined by direct microscopic visualization. This study marked the first time in which isolated mammalian vesicles were injected into a working synapse. This research demonstrated that vesicles (made fluorescent by Texas Red) were actually mobilized from the point of injection in the axon to the active zones, i.e. the place where synaptic transmitter is released. It was also found that a change in either oxygenation or the surface properties of vesicles can lead to no movement or, to change in movement direction. These results were published in 1989 in

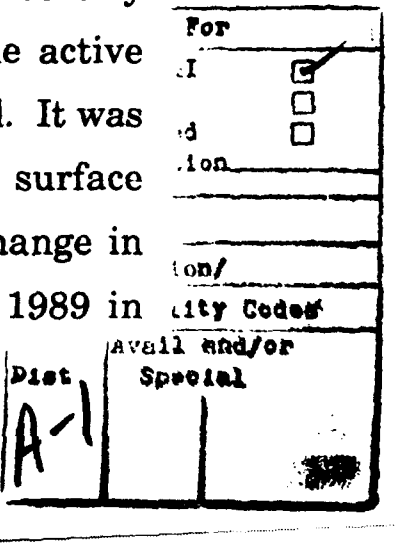

PNAS. A second aspect of vesicular mobility relating to the paper mentioned above was published in the *Journal of Neuroscience* in 1989, showing that Synapsin I modulates vesicular flow in the squid axoplasm.

The second aspect of synapse work performed that year was a demonstration of the category of calcium channel that is responsible for transmitter release. In fact the channel now known as a P-channel was isolated in the squid, as well as in mammalian cerebellum. These results were first published in 1989 in the *Biophysical Journal*, Volume 55, page 438a, and in PNAS, Volume 86, pages 1689–1693.

The work in 1990 related mostly to the study of Synapsin I in transmitter release. The studies demonstrated that miniature potentials could be modulated in the squid synapse by injection of Synapsin I and of protein kinase II and was published in *PNAS*, Volume 87, page 8257–8261. Another aspect of synaptic research investigated during the same summer related to the effect of Synapsin I on the neuromuscular junction in crayfish. This research was published in the *Biological Bulletin*, Volume 179, page 229.

In the third year of the grant, 1991, the first demonstration of calcium microdomains in synaptic transmission was performed. The study was done using a new type of aequorin that allowed direct visualization of calcium concentration sites at the presynaptic terminal. A paper was published in *Science* in 1992,

in Volume 256, page 677. Another study published in *PNAS* the same year, Volume 89, page 330, reported the fact that the P-type channels present in the squid are responsible for neuromuscular transmission in mammals.

The Journal of Physiology

Volume 412
1989

The molluscan neuropeptide FLRFamide potentiates transmission at the isolated squid giant synapse

BY G. A. COTTRELL*, J. W. LIN†, R. LLINÁS† and M. SUGIMORI†. **Department of Biology and Preclinical Medicine, University of St Andrews, KY16 9TS. †Department of Physiology and Biophysics, New York University Medical Center, N.Y. 10016, and Marine Biological Laboratory, Woods Hole, MA 02543, USA*

Peptides of the Phe-Met-Arg-Phe-NH_2-(FMRFamide-) series have many actions on neurone perikarya (Cottrell & Davies, 1987). The action of one such peptide in synaptic transmission at the giant synapse of the squid (*Loligo pealei*) was determined using Phe-Leu-Arg-Phe-NH_2 (FLRFamide), which occurs in cephalopods (Martin & Voigt, 1987). Pre- and postsynaptic recordings were made (see Llinás *et al.* 1981) and peptide solutions microinjected close to the synaptic junction.

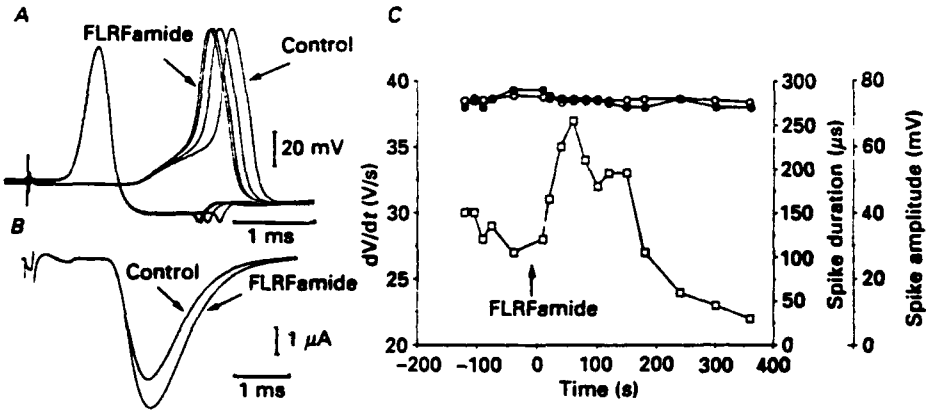

Fig. 1. (*A*) Pre- and postsynaptic recordings showing increase in postsynaptic response in the absence of presynaptic effect after injecting FLRFamide from a micropipette containing 1 mM FLRFamide in ASW (4 mM Ca). (*B*) EPSCs before and 75 s after injection. The response recovered after 6 min. (*C*) FLRFamide increased the rate of rise of the EPSP (□) without changing pre-spike width (●) or amplitude (○).

FLRFamide ($n = 9$) potentiated transmission, whereas control injections were without effect ($n = 3$). Potentiation was detected as an increase in size of the EPSC (Fig. 1*B*) and also as an increase in rate of rise (Fig. 1*A*, *C*) and amplitude of EPSP. No change in presynaptic membrane potential, spike amplitude or duration (Fig. 1*A*. *C*) was detected. FMRFamide injected into the blood supply to the ganglion has also been observed to potentiate transmission (S. Hess, personal communication).

G.A.C. thanks the William Ramsay Henderson Trust for financial support. Supported by AFOSR850368.

REFERENCES

COTTRELL, G. A. & DAVIES, N. W. (1987). *J. Physiol.* **382**, 51–68.
LLINÁS, R., STEINBERG, I. Z. & WALTON, K. (1981). *Biophys. J.* **33**, 323–352.
MARTIN, R. & VOIGT, K. H. (1987). *Experientia* **43**, 537–543.

Reprinted from THE BIOLOGICAL BULLETIN, Vol. 177, No. 2, October 1989
Printed in U.S.A.

Preliminary molecular structure of FTX and synthesis of analogs that block I_{Ca} in the squid giant synapse.

B. CHERKSEY, R. LLINAS, M. SUGIMORI, AND J.-W. LIN (Dept. Physiology and Biophysics, NYU Medical Center, New York, NY 10016).

FTX, a specific P channel blocker, is one of many channel blocking factors contained in the venom of the American funnel web spider. We have previously reported (Cherksey *et al.* 1988, *Biol. Bull.* **175**: 304; Llinas *et al.* 1989, *PNAS* **86**: 1686) on the use of FTX to construct an affinity gel for the isolation and characterization of P-type Ca^{++} channels from squid optic lobe and mammalian CNS.

Purification and structural analysis of FTX have been performed. FTX could not be adequately purified by reverse phase HPLC using acetonitrile:water gradients. FPLC on Superose indicated that FTX was of low molecular weight (200–400 Da), but did not effect an adequate purification. Anion exchange methods were ineffective. However, cation exchange on Mono S permitted a high level of purification of FTX, with elution of the active factor at approximately 0.8 *M* NaCl. Purified FTX exhibited a sharp UV absorption at 220 nm. No ring (aromatic) structure was detected. The absorption at 220 nm showed a pronounced shift with acidification suggesting that FTX possesses a titratable amine group. FT-IR (Fourier transform infrared spectroscopy) indicated the presence of C-C, C-N, N-H, C-H, and the absence of C=O, absorptions. These results ruled out the possibility that FTX is a small peptide and suggest that it is a polyamine. The known polyamine glutamate channel blockers (which contain ring structures) are ineffective as presynaptic blockers.

On the basis of these results, model compounds were constructed with the general structure of arginine-polyamine:

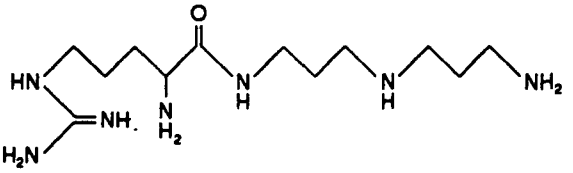

These compounds exhibited the selectivity of FTX, but not its potency. Compounds of the structure arginine-polyamine-arginine were ineffective as blockers. Thus, the free terminal amine is critical for efficacy, perhaps being the moiety that actually enters the pore of the channel. The arginyl group, perhaps via its strong charge, may act to secure the toxin in the channel. Therefore, the difference in potency between FTX and the model compounds may be due to the negative charge on the carbonyl of the latter, which, on the basis of FT-IR spectra, is absent from FTX.

Reprinted from THE BIOLOGICAL BULLETIN, Vol. 177, No. 2, October 1989
Printed in U.S.A.

Dose-response for FTX blockade of presynaptic $I_{(Ca)}$ in the squid giant synapse. R. LLINAS, M. SUGIMORI, J-W. LIN, AND B. CHERKSEY (Dept. Physiology and Biophysics, NYU Medical Center, New York, NY 10016).

The dose-response relationship for the blocking action of FTX (a toxin fraction from *Agalenopsis aperta* venom, Sugimori *et al.* 1988 *Biol. Bull.* **175**: 308; Cherksey *et al.* 1988, *Biol. Bull.* **175**: 304, Llinas *et al.* 1989, *PNAS*, **86**: 1689) on the voltage-dependent presynaptic calcium current (I_{Ca}) in the squid stellate ganglion, was determined from voltage clamp measurements. In addition to the purified toxin, we tested the raw venom, and a synthetic poly-amine with an arginine at one end, constructed on the basis of chemical analysis of the FTX fraction (Cherksey *et al.* 1989, these Abstracts). These substances were added to the bathing solution in concentrations ranging from 0.2 to 190 nl/ml (volume of venom or liquid synthetic toxin in nl/ml seawater). Each of the three fractions had an ED_{50} of 5 nl/ml and produced a total blockade at 80–100 nl/ml. The block caused by 100 nl/ml had a time course of about 20 min and was very slowly reversible. Comparing the degree of calcium current block with the reduction of the post-synaptic potential, we concluded that the effect of the toxin on synaptic release is totally ascribable to its calcium blocking effect. We reached a similar conclusion about the synthetic polyamine. But because the same volume of raw venom and the synthetic polyamine produced about the same degree of block, we conclude that the active toxin may be more potent, and that the structure of the naturally occurring polyamine is therefore probably a variant of the synthetic product. Finally, we tested some polyamines with an arginine at each terminal of the chain, but I_{Ca} was not blocked. Thus, the polyamine may require the terminal amine to penetrate the channel and produce the block; the arginine group may hold the molecule in place.

The Biological Bulletin Vol. 179, #229, 1991

Effects of synapsin I on synaptic facilitation at crayfish neuromuscular junction.

K. R. DELANEY, Y. YAMAGATA, D. W. TANK, P. GREENGARD, AND R. LLINAS (Marine Biological Laboratory, Woods Hole, MA 02543).

The effects of presynaptically injected phospho- and dephospho-synapsin I on transmitter release were studied in excitatory claw opener junctions in crayfish. We examined release evoked by presynaptic action potentials delivered at 0.5 Hz, which does not produce facilitation, and at higher frequencies (5–50 Hz) where facilitation is prominent. Consistent with previous work on squid giant synapse (Llinas *et al.*, 1985, *PNAS* **82**: 3035) and Mauthner cell synapses (Hacket *et al.*, 1990, *J. Neurophysiol.* **63**: 701), reduction of excitatory junction potentials (EJPs) obtained with 0.5 Hz stimulation was seen 5–30 min after injection. This reduction was coincident with the appearance of Texas red labeled synapsin I in the preterminals contacting the postsynaptic muscle fiber (8 of 9 expts.). The EJP amplitude continued to decline linearly over the course of 60–120 min to near zero. In addition, the rate of facilitation of the EJP during short stimulus trains at 5, 20, and 50 Hz was reduced following this injection. Moreover, high rates of release, which are normally produced and maintained during several minutes of stimulation at frequencies around 30 Hz, were not maintained following dephosphosynapsin I injection. These effects were not seen following the injection of phosphorylated synapsin I ($n = 1$). We conclude that synapsin I can modulate facilitated and unfacilitated transmitter release at this tonic junction.

Reprint Series
1 May 1992, Volume 256, pp. 677–679

SCIENCE

Microdomains of High Calcium Concentration in a Presynaptic Terminal

R. Llinás,* M. Sugimori, and R. B. Silver

Microdomains of High Calcium Concentration in a Presynaptic Terminal

R. Llinás,* M. Sugimori, R. B. Silver

Increases in intracellular calcium concentration are required for the release of neurotransmitter from presynaptic terminals in all neurons. However, the mechanism by which calcium exerts its effect is not known. A low-sensitivity calcium-dependent photoprotein (*n*-aequorin-J) was injected into the presynaptic terminal of the giant squid synapse to selectively detect high calcium concentration microdomains. During transmitter release, light emission occurred at specific points or quantum emission domains that remained in the same place during protracted stimulation. Intracellular calcium concentration microdomains on the order of 200 to 300 micromolar occur against the cytoplasmic surface of the plasmalemma during transmitter secretion, supporting the view that the synaptic vesicular fusion responsible for transmitter release is triggered by the activation of a low-affinity calcium-binding site at the active zone.

The role of intracellular free calcium as a trigger for initiating presynaptic transmitter release in chemical synapses was proposed as the "calcium hypothesis" several decades ago (*1*). The mechanism for this Ca^{2+}-dependent transmitter release remains unresolved, partly because the concentration of Ca^{2+} and the distribution of Ca^{2+} concentration within presynaptic terminals during transmission are unknown.

Presynaptic voltage-clamp studies in the giant squid synapse demonstrated a very short (200 μs) latency between Ca^{2+} entry and postsynaptic response, suggesting that Ca^{2+} channels are located at the site of vesicle accumulation and neurotransmitter release (*2*). Moreover, direct measurement of presynaptic Ca^{2+} currents suggested that intracellular free Ca^{2+} concentrations ($[Ca^{2+}]_i$) near the Ca^{2+} channels could be on the order of several hundred micromolar (*3*). Computer models based on these data suggested that the $[Ca^{2+}]_i$ falls off steeply away from the cytoplasmic mouth of the Ca^{2+} channels (*4–7*). These small domes of increased $[Ca^{2+}]_i$ are called microdomains. Each Ca^{2+} channel opening is thought to produce a rapid (microseconds) increase in $[Ca^{2+}]_i$, which rapidly returns to its pre-opening value when the channel closes (*6*). Neurotransmitter release would thus be triggered by a large transient increase in $[Ca^{2+}]_i$ adjacent to the synaptic vesicles.

We have now tested directly the existence of such $[Ca^{2+}]_i$ microdomains by using aequorin (a protein that emits light in the presence of free Ca^{2+}) (*8, 9*) injected in the presynaptic terminal of the giant squid synapse (*10*). In the presence of aequorin, transient increases in $[Ca^{2+}]_i$ appear as flashes of light localized in time and space.

We designed special methodology to identify, image, and characterize these flashes of light. Fluorescent *n*-aequorin-J (minimum Ca^{2+} sensitivity of 10^{-4} M) was injected into the presynaptic terminal (Fig. 1A) (*11*), and its distribution in the terminal was continually monitored by epifluorescence microscopy (*12*). Once the terminal was fully loaded with *n*-aequorin-J (Fig. 1B), the presynaptic fiber was continuously stimulated at 10 Hz (*13*), and a well-defined, stable set of quantum emission domains (QEDs) appeared as white spots (Fig. 1C) (*14*). The superposition of the fluorescent images of the terminal digit (Fig. 1B) and the QEDs (Fig. 1C) revealed that the distribution of QEDs coincided with the presynaptic terminal (Fig. 1D). QEDs were particularly evident at the center of the digit, where most synaptic contacts occur.

We also determined the distribution and number of QEDs in an unstimulated presynaptic terminal at high magnification (Fig. 1F). When QEDs were integrated for 30 s during tetanic stimulation (Fig. 1G), they were found to be organized in regions resembling semicircles or line segments and were approximately equally spaced over the presynaptic digit (Fig. 1, C and G).

Each QED fell within a contiguous rectilinear juxtaposition of approximately 16 pixels (0.25 μm by 0.25 μm per pixel). The size distribution of the QEDs was determined after measuring more than 15,000 such events for both long-term image integrations (1,500 to 5,000 video frames); serially repeated shorter integrations [600 to 1,200 national television standard code (NTSC) video frames]; and sets of single video frames. QEDs fluctuated in size from 0.25 to 0.6 μm^2 (Fig. 2), with a mean of 0.313 μm^2 (range, ~0.25 μm^2 to ~0.375 μm^2). QED patterns such as those shown in Figs. 1 and 2 (areas 0.375 to 0.625 μm^2) represent individual QEDs occurring at nearly identical frame locations, with a small overlap. On average, these sites occupied 8.4% of the presynaptic-postsynaptic membrane contact area, which is close to the 5 to 10% determined by ultrastructural studies (*15*). The number of QEDs in a 70 μm by 40 μm contact area (*15*) was about 4500 (based on actual counting of QEDs in the contact area), quite close to the 4400 calculated for the number of active zones (range 3580 to 5400) from measurements and analysis of transmission electron micrographs (*16*).

The $[Ca^{2+}]_i$ reached during presynaptic activation (200 to 300 μM) was determined by sampling the number of QEDs over consecutive 10-, 15-, or 30-s periods. Many loci repeated periods of photon emission within consecutive sampling periods, as

R. Llinás and M. Sugimori, Department of Physiology and Biophysics, New York University Medical Center, 550 First Avenue, New York, NY 10016, and the Marine Biological Laboratory, Woods Hole, MA 02543. R. B. Silver, Section and Department of Physiology, Cornell University, Ithaca, NY 14853–6401, and the Marine Biological Laboratory, Woods Hole, MA 02543.

*To whom correspondence should be addressed, at the Department of Physiology and Biophysics.

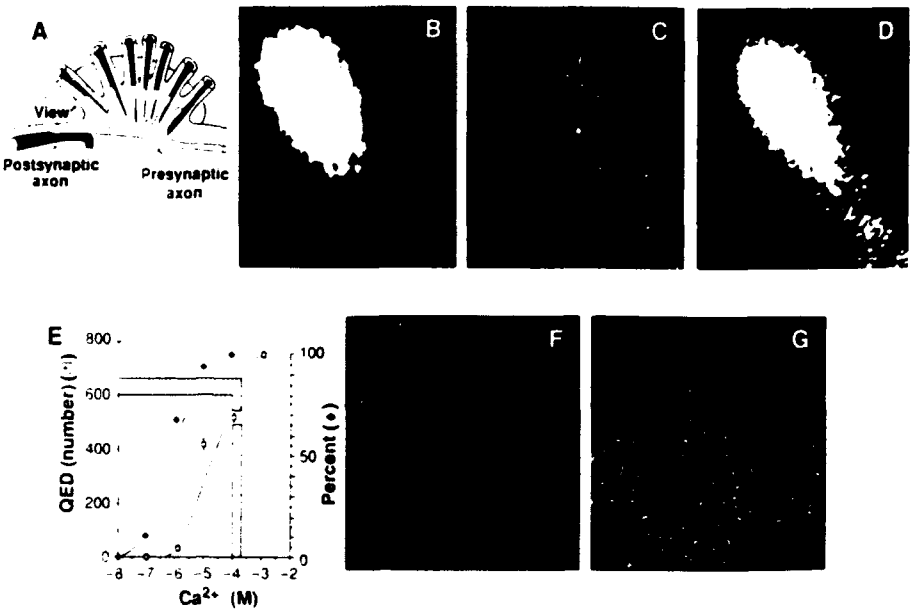

Fig. 1. (**A**) Diagram of the giant squid synapse showing the spatial organization of the presynaptic and the postsynaptic elements. The square (arrow) denotes the location of the synaptic junction shown in (B). (**B**) Fluorescence image of a presynaptic digit injected with a fluorescent preparation of *n*-aequorin-J. (**C**) Video image of photons emitted from QEDs. Image represents the accumulated light emission from *n*-aequorin-J elicited by Ca^{2+} entry during tetanic stimulation (10 s, 10 Hz). (**D**) Superposition of the images in (B) and (C). (**E**) The number of light emissions generated by *e*-aequorin (◆) and *n*-aequorin-J (□) (600 to 650 over a period of 3 s) corresponds to a $[Ca^{2+}]_i$ near 10^{-4} M, about two orders of magnitude less sensitive than the *e*-aequorin response (stippled bar) (*8*, *9*). (**F**) QEDs in an unstimulated terminal (30 s, 10 mM extracellular Ca^{2+}). (**G**) QEDs in the same terminal as in (F) during tetanic stimulation (10 s, 10 Hz).

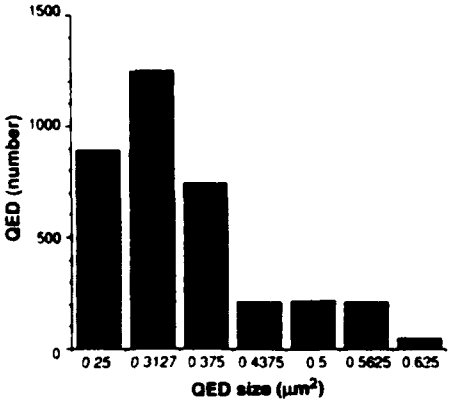

Fig. 2. Distribution of QED size (n = 2500).

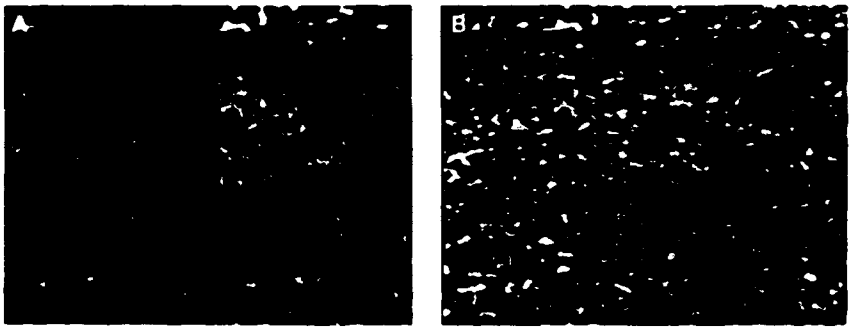

Fig. 3. (**A**) The center portion of two QED images obtained during consecutive 15-s recording intervals from the same area of terminal; the left panel (red) shows the first interval after stimulation; the right panel (blue) shows the subsequent 15-s period (blue). (**B**) The superposition (>93%) of the QEDs from consecutive 15-s recording intervals in (A) (red and blue) appears yellow.

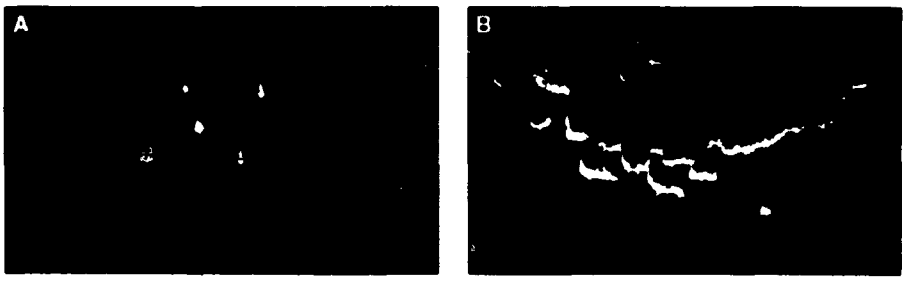

Fig. 4. Three-dimensional projection after image integration (4800 frames, 30-Hz sampling rate) of the QED image in a terminal bulb of a presynaptic fiber (**A**) before stimulation and (**B**) during stimulation, illustrating the steepness of the Ca^{2+} microdomain profiles. Image intensities were segmented into an 8-bit range, with the maximum intensity corresponding to the video intensity level of 255 (white) and the lowest to a level of 0 (black), with intermediate levels ranging from high (red) through intermediate (yellow and green) to low (blue) probabilities that a particular microdomain would be active.

shown in Fig. 3, A and B, for two consecutive 15-s periods, indicating that Ca^{2+} entry tended to be organized temporally and spatially. QEDs detected during the first 15-s period (Fig. 3A, red) and those detected during the second 15-s period (Fig. 3A, blue) are shown as yellow spots in Fig. 3B. When the second period is compared to the first period, there is an area correspondence of ~95%; when the order for comparison was reversed, the correspondence was 87%. Subsequent sequential 15-s periods, having correspondences between 93 and 98.81%, indicate that within such time most of the sites of Ca^{2+} entry to the terminal are activated.

Prolonged integrations (1200 to 5000 video frames) were performed during stimulation to determine the percentage of the total presynaptic terminal area containing QEDs. Figure 4 corresponds to the terminal bulb of a presynaptic fiber before (Fig. 4A) and during (Fig. 4B) stimulation (as in Fig. 1A). The average clearly describes areas of high probability of light emission and the pronounced differences between the prestimulation and stimulatory conditions. Because of the long integration times used, fused rather than discrete QEDs were observed in both cases. The distribution of $[Ca^{2+}]_i$ was not random and often formed ringlike structures, lines, or combinations of these. These patterns probably correspond to the "fingerprints" of clawlike postsynaptic dendrites that contact the presynaptic digit in the active zone (*17*).

Detailed analysis of the temporal and spatial distribution of QEDs suggests that once a microdomain is activated, the tem-

poral repeat frequencies at which a particular microdomain is activated differ from those of the same microdomain before stimulation. Upon activation, three classes of temporal repeat frequencies, not seen under prestimulation conditions, appeared, the primary temporal class having a mean delay period between the initial activation and subsequent activation of 1.37 s, which may indicate temporal requirements or constraints upon reestablishing microdomain activation. Under stimulation, the lifetime of a QED averaged 200 ms, clearly a high value that is likely attributable to the photon efficiency and lag characteristics of the camera and light-intensity losses through the optical system. Under most conditions, QEDs that occurred as singlets or doublets did not occur at high frequency at any particular microdomain. Analysis of the activation dynamics of individual microdomains suggested a quasi-sequential activation, that is, a low probability of immediate reactivation. One possible mechanism for this refractory period may be related to the high $[Ca^{2+}]_i$ at the active zone or to the low number of readily releasible vesicles. In fact, high $[Ca^{2+}]_i$ depresses Ca^{2+} channel activity by blocking the channel and increasing its inactivation (*18*). Also, it is well documented that an average of one vesicle is normally released per active zone (*15*, *19*, *20*). In fact, in squid, the quantum content is 5000, close to the value of 4500 measured here; thus, there must be an average of one vesicle per active zone. The presence of such "lateral inhibition," by activation of a certain number of channels in an active zone patch (average measured area, 0.313 μm^2), would temporarily depress local channel activity. If this were so, a special kinetics would operate, in which the probability of release is related to the previous activity in any given active zone (*21*). This prospect adds an interesting new variable to incorporate into models of transmitter release.

The distribution of Ca^{2+} microdomains suggests that these sites are active zones where increased $[Ca^{2+}]_i$ triggers neurotransmitter release by binding to a low-affinity Ca^{2+}-binding site at the presynaptic vesicles and activating the release process. Such a mechanism would safeguard the synapse from large amounts of spontaneous transmitter release because probably more than one Ca^{2+} channel must be activated per active zone to trigger exocytosis (*6*). Also, there would be enough time to replace the expended vesicles (*6*). The short delay between Ca^{2+} entry and transmitter release suggests that only vesicles near the QEDs would be released by a given action potential (*2*). The fact that $[Ca^{2+}]_i$ attains such high concentrations at release sites must be taken into account in the study of the mechanisms of membrane fusion.

REFERENCES AND NOTES

1. B. Katz, *The Release of Neurotransmitter Substances. The Sherrington Lectures X* (Thomas, Springfield, IL, 1969).
2. R. Llinás, in *Approaches to the Cell Biology of Neurons*, W. M. Cowan and J. A. Ferenceili, Eds. (Society for Neuroscience, Bethesda, MD, 1977), vol. 2, pp. 139–160.
3. _____, I. Z. Steinberg, K. Walton, *Biophys. J.* **33**, 323 (1981).
4. J. E. Chad and R. Eckert, *ibid.* **45**, 993 (1984).
5. S. M. Simon, M. Sugimori, R. Llinás, *ibid.*, p. 264a.
6. S. M. Simon and R. Llinás, *ibid.* **48**, 485 (1985).
7. R. S. Zucker and A. L. Fogelson, *Proc. Natl. Acad. Sci. U.S.A.* **83**, 3032 (1986).
8. O. Shimomura, B. Musicki, Y. Kishi, *Biochem. J.* **261**, 313 (1989).
9. O. Shimomura, S. Inouye, B. Musicki, Y. Kishi, *ibid.* **270**, 309 (1990).
10. A preliminary note on these results has appeared [R. Llinás, M. Sugimori, R. B. Silver, *Biol. Bull.* **181**, 316 (1991)].
11. The compound *n*-aequorin-J, a chemically modified low-sensitivity form of a naturally occurring photoprotein (*8*), was pressure-injected (tip concentration 5%) [R. Llinás, J. R. Blinks, C. Nicholson, *Science* **176**, 1127 (1972)] into the presynaptic terminal. To aid in localization of aequorin within the preparation, 5% of the aequorin injected was also fluoresceinated.
12. Video images were obtained with the use of a direct optical extension onto a dual-microchannel plate-intensified Video-Intensified Microscopy (VIM) camera system (Hamamatsu Argus 100, Hamamatsu Photonics, Inc., Bridgewater, NJ), operated in photon-counting mode, or a Nikon Optiphot-pol microscope modified to simultaneously record multispectral luminescent specimens (R. B. Silver, unpublished data), that is, we obtained differential interference contrast (DIC) or fluorescence images (Dage/MTI Model 68 SIT camera) and single-photon aequorin images (Hamamatsu C2400-20 VIM camera, pedestal set to background-shot noise). Video systems were operated at an NTSC frame-sampling rate of 30 Hz. The background signal of the optical system was typically fewer than 60 events per minute (determined for 10^3 or 10^4 s over the entire field); signal-to-noise ratio was ~150:1.
13. Stellate ganglia from small *Loligo pealii* were dissected and synaptic transmission was monitored with standard methods [R. Llinás, I. Z. Steinberg, K. Walton, *Biophys. J.* **33**, 289 (1981)]. Results were obtained from 27 synapses bathed in artificial seawater (10 mM Ca^{2+}).
14. Video images were processed, filtered, and analyzed to assist in QED feature extraction and quantification with a Hamamatsu Argus 100 imaging system or an Imagel-AT (Universal Imaging Corp., West Chester, PA) running on a Dell 325 AT-bus computer. Aequorin luminescence images of QEDs, seen as discrete spots on an otherwise dark background, were analyzed as single-video frames, as integrations of multiple-video frames (range, 10 to 4800), or as digitized sequential frames. Calibration curves were constructed by measuring the number of Ca^{2+}-dependent light flashes (within 33-ms frame-integration periods), each resulting from a discrete interaction of Ca^{2+} with an aequorin molecule (*8*, *9*), that accumulated during the 3 s after 20 pl of aequorin was injected into 10^{-3} to 10^{-8} M Ca^{2+} [R. B. Silver, *Dev. Biol.* **131**, 11 (1989)]. Two procedures were followed for accumulating information: (i) light-emission points were accumulated during 3 s of stimulation, and the QED distribution was studied; (ii) two portions of the recording field were individually accumulated and compared.
15. D. W. Pumplin, T. S. Reese, R. Llinás, *Proc. Natl. Acad. Sci. U.S.A.* **78**, 7210 (1981).
16. D. W. Pumplin and T. S. Reese, *Neuroscience* **3**, 685 (1978).
17. J. Z. Young, *Brain Res.* **57**, 457 (1973).
18. G. P. H. Young *et al.*, *Proc. Natl. Acad. Sci. U.S.A.* **81**, 5155 (1984).
19. J. Korn, A. Mallet, A. Triller, D. S. Faber, *J. Neurophysiol.* **48**, 679 (1982).
20. A. Triller and H. Korn, *ibid.*, p. 708.
21. R. Llinás, T. L. McGuinness, C. S. Leonard, M. Sugimori, P. Greengard, *Proc. Natl. Acad. Sci. U.S.A.* **82**, 3035 (1985).

22. We thank O. Shimomura (Marine Biological Laboratory) for the custom aequorin preparations. Supported by the NIH (NS13742 to R.L.), the U.S. Air Force (AFOSR89-0270 to R.L.), the NSF (DGB-9005343 to R.B.S.), and the Cornell–U.S. Army Biotechnology Center of Excellence Program (24629-LS-UIR to R.B.S.).

8 December 1991; accepted 6 March 1992

Proc. Natl. Acad. Sci. USA
Vol. 89, pp. 3330–3333, April 1992
Neurobiology

P-type voltage-dependent calcium channel mediates presynaptic calcium influx and transmitter release in mammalian synapses

(funnel-web spider toxin/polyamines/neuromuscular junction/synaptosomes)

O. D. UCHITEL*†, D. A. PROTTI*, V. SANCHEZ*, B. D. CHERKSEY‡, M. SUGIMORI‡, AND R. LLINÁS‡

*Instituto de Biologia Celular Facultad de Medicina, Universidad de Buenos Aires, Paraguay 2155, Buenos Aires 1121, Argentina; and ‡Department of Physiology and Biophysics, New York University Medical Center, 550 First Avenue, New York, NY 10016

Contributed by R. Llinás, January 2, 1992

ABSTRACT **We have studied the effect of the purified toxin from the funnel-web spider venom (FTX) and its synthetic analog (sFTX) on transmitter release and presynaptic currents at the mouse neuromuscular junction. FTX specifically blocks the ω-conotoxin- and dihydropyridine-insensitive P-type voltage-dependent Ca^{2+} channel (VDCC) in cerebellar Purkinje cells. Mammalian neuromuscular transmission, which is insensitive to N- or L-type Ca^{2+} channel blockers, was effectively abolished by FTX and sFTX. These substances blocked the muscle contraction and the neurotransmitter release evoked by nerve stimulation. Moreover, presynaptic Ca^{2+} currents recorded extracellularly from the interior of the perineural sheaths of nerves innervating the mouse levator auris muscle were specifically blocked by both natural toxin and synthetic analogue. In a parallel set of experiments, K^+-induced Ca^{45} uptake by brain synaptosomes was also shown to be blocked or greatly diminished by FTX and sFTX. These results indicate that the predominant VDCC in the motor nerve terminals, and possibly in a significant percentage of brain synapses, is the P-type channel.**

Ca^{2+} influx through voltage-dependent Ca^{2+} channels (VDCCs) is the trigger for the release of neurotransmitters from the nerve terminals (1, 2). Three major types of VDCC named T, L, and N were described in neuronal cells (3). The high-threshold L and N VDCCs are sensitive to the blocking effect of ω-conotoxin (ω-CgTX), and only the L type is affected by Ca^{2+} channel antagonists of the 1,4-dihydropyridine (DHP) class. An intermediate-threshold VDCC channel called the P channel was identified in the Purkinje cells of mammalian cerebellum and found to be insensitive to DHP and ω-CgTX, but very sensitive to a low molecular weight fraction of the venom of the funnel-web spider *Agelenopsis aperta* (4). This funnel-web spider toxin (FTX) was also effective in blocking Ca^{2+} conductance and synaptic transmission at the squid giant synapse (4). Evoked release of neurotransmitter was shown to be dependent on Ca^{2+} influx through the N-type VDCC in sympathetic neurons by the inhibitory effect of ω-CgTX and the lack of effect of DHP (5). By contrast, substance P release from dorsal root ganglia neurons (6, 7) and catecholamine release from chromaffin cells (8) are strongly inhibited by DHP, consistent with a major participation of L-type channels. However, mammalian motor nerve terminals are normally insensitive to either ω-CgTX or DHP (9–11). Furthermore, in brain synaptosomes, K^+-evoked Ca^{2+} uptake and transmitter release are only partially sensitive to ω-CgTX and DHP (12, 13). Thus the identity of the VDCC involved in transmitter release in the majority of the synapses at the mammalian central and peripheral nervous system has not been defined. The experiments presented here were designed to study the effect of FTX on transmitter release and Ca^{2+} influx at the mammalian neuromuscular junction and on Ca^{2+} uptake by cerebral cortex synaptosomes in order to determine whether a particular type of VDCC is more commonly involved in mammalian synaptic transmission.

MATERIAL AND METHODS

Electrophysiological Techniques. Experiments were performed with the nerve–muscle preparation from male Swiss mice (25–30 g). Muscles were removed after cervical dislocation and pinned out in a Sylgard-coated chamber containing 1–2 ml of physiological solution (normal Ringer solution: 135 mM NaCl/5 mM KCl/2 mM $CaCl_2$/1 mM $MgSO_4$/12 mM $NaHCO_3$/1 mM NaH_2PO_4/11-mM D-glucose, pH 7.4) kept at room temperature. The solution was oxygenated by continuous bubbling with a mixture of 5% CO_2 and 95% O_2. Miniature endplate potentials and evoked endplate potentials were recorded intracellularly. Glass microelectrodes of 5–15 MΩ resistance filled with 2 M KCl were used. The electrodes were inserted into the muscle fibers near the endplate regions, which were located visually at the ends of intramuscular branches of the phrenic nerve (Fig. 1*A*). The mean quantal content (m) of transmitter release was measured in muscles incubated in low Ca^{2+} (1.2 mM)/high Mg^{2+} (6 mM) by use of the failure-method equation $m = \log e^{N/Nf}$, where N is the total number of nerve stimuli and Nf is the total number of endplate-potential failures (14). The phrenic nerve was stimulated at 0.5 Hz. Miniature endplate amplitudes were corrected assuming a −80 mV membrane potential and their frequency of appearance counted over 0.5–3 min. The levator auris muscle (15) was used to study the presynaptic motor nerve terminals currents. The presynaptic currents were recorded with glass microelectrodes of 5–15 MΩ resistance filled with 2 M NaCl and placed inside the perineural sheath of small nerve branches near the endplate areas (Fig. 1*A*) (16, 17). The nerves were stimulated by using suction electrodes coupled to a pulse generator with associated stimulus isolation unit (0.1 ms). The recording microelectrodes were connected to an Axoclamp 1A amplifier (Axon Instruments, Burlingame, CA). The signals were digitized (Scientific Solutions, Labmaster A/D converter), stored, and analyzed by a computer.

Preparation of Synaptosomes and Measurement of Ca^{2+} Uptake. Cerebral cortex from three rats was homogenized in 0.32 M sucrose with a manual Teflon/glass homogenizer. The homogenate was centrifuged at 3000 × g for 10 min at 4°C, and the supernatant was further centrifuged at 20,000 × g for 20 min. The pellet was resuspended in 0.32 M sucrose and seeded in a 0.8–1.4 M sucrose gradient. After 2 hr of

The publication costs of this article were defrayed in part by page charge payment. This article must therefore be hereby marked "*advertisement*" in accordance with 18 U.S.C. §1734 solely to indicate this fact.

Abbreviations: VDCC, voltage-dependent Ca^{2+} channel; FTX, funnel-web spider toxin; sFTX, synthetic FTX; DHP, 1,4-dihydropyridine; ω-CgTX, ω-conotoxin.

†To whom reprint requests should be addressed.

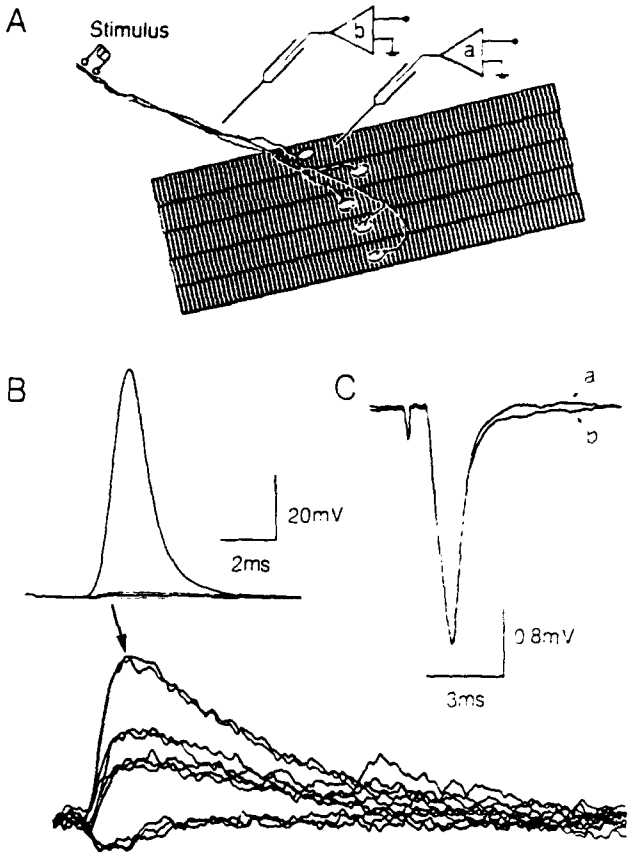

FIG. 1. (*A*) Schematic drawing of a nerve–muscle preparation indicating the position of the intracellular (a) and extracellular (b) recording microelectrodes. (*B*) Upper trace, intracellularly recorded muscle fiber action potential elicited by phrenic nerve stimulation; lower trace, a similar recording 10 min after the bath application of FTX (1 μl/ml) in normal Ringer solution. (*C*) Perineural recordings of presynaptic currents in a paralyzed muscle (normal solution plus 30 μM curare) before (trace a) and after (trace b) bath application of FTX (1 μl/ml).

centrifugation at 50,000 × *g*, the bands in 0.8–1, 1–1.2, and 1.2–1.4 M layers were pooled and slowly diluted 1:4 in Ca^{2+}-free 132 mM NaCl. After centrifugation at 35,000 × *g* for 15 min, the pellet was resuspended in solution A (132 mM choline chloride/1.2 mM $CaCl_2$) or solution B (65 mM choline chloride/1.2 mM $CaCl_2$). Samples from A and B suspension (500 μl, 500 μg of protein) were incubated for 10 min at 32°C with or without toxin. $^{45}Ca^{2+}$ uptake was started by the addition of $^{45}Ca^{2+}$ (0.3 μCi/μmol; 1 μCi = 37 kBq) in 200 μl of Na^+ Ringer solution, for basal uptake, or Na^+/K^+ Ringer solution for K^+-stimulated uptake (final K^+ concentration, 65 mM). Uptake was stopped after 15 or 30 s with the addition of 3 ml of 5 mM EGTA buffer solution. This suspension was rapidly filtered under vacuum through Whatmann GF/B filter paper and washed three times with 132 mM choline chloride/5 mM KCl, 1.2 mM $CaCl_2$/1.3 mM $MgCl_2$/10 mM glucose/5 mM Tris, pH 7.4. Filters were dried and immersed in scintillation fluid for measurement of radioactivity. FTX was purified chromatographically from the crude venom of American funnel-web spiders (Spider Pharm, Black Canyon, AZ). Synthetic FTX (sFTX) was prepared as described (18).

RESULTS

Hemidiaphragms incubated in normal Ringer solution were treated with FTX (1 μl/ml). After a few minutes, muscle contraction elicited by nerve stimulation was abolished. Intracellular recording showed that nerve stimulation failed to trigger transmitter release in a high percentage of trails. When transmitter release was evoked, small endplate potentials were recorded with fluctuating amplitude multiples of the miniature endplate potential amplitude (Fig. 1*B*). Neuromuscular transmission and contraction was restored a few minutes after the preparation was washed with normal solution.

The effect of FTX on the conducted nerve action potential was tested by studying the presynaptic currents recorded in the perineurum near the endplate areas in a curare-treated preparation. The negative signal recorded is associated with Na^+ currents in the final nodes of Ranvier and initial portions of the unmyelinated terminals and with the K^+ currents from the nerve endings (16). The lack of effect of FTX on these currents indicates that the toxin has no effect on the presynaptic action potential (Fig. 1*C*).

The inhibitory action of FTX on synaptic transmission was further characterized by studying the effect of various concentrations of FTX on quantal content of evoked transmitter release. The muscles were incubated in a low Ca^{2+}/high Mg^{2+} solution. The control values for mean quantal content of evoked release were between 1.1 and 2.8. A 50% inhibition of the quantal content of evoked release was obtained with a submicromolar concentration of FTX (Fig. 2). In contrast, evoked neuromuscular transmission was completely insensitive to 5 μM ω-CgTX tested under similar conditions (10).

FTX has been reported to be a low molecular weight, nonaromatic polyamine. Synthetic arginine-polyamine (spermidine) adducts were found to have FTX-like activity (sFTX) (18). Quantal content of transmitter release was inhibited in a dose-dependent manner with low millimolar concentrations of sFTX (Fig. 2). As a control the effect of spermidine was studied. At concentrations up to 3 mM, spermidine had no effect on neuromuscular transmission.

Spontaneous transmitter release was also affected by FTX and by sFTX. A 50–100% increase in miniature frequency was observed in muscles treated with 0.5 μl of purified toxin per ml or with 1 mM sFTX. The amplitude of the miniature endplate potentials was substantially reduced (over 40%) without major alterations in their time course.

To further investigate the inhibitory mechanism of FTX on synaptic transmission, the effect of the toxin on the presynaptic Ca^{2+} currents was studied. Presynaptic currents were

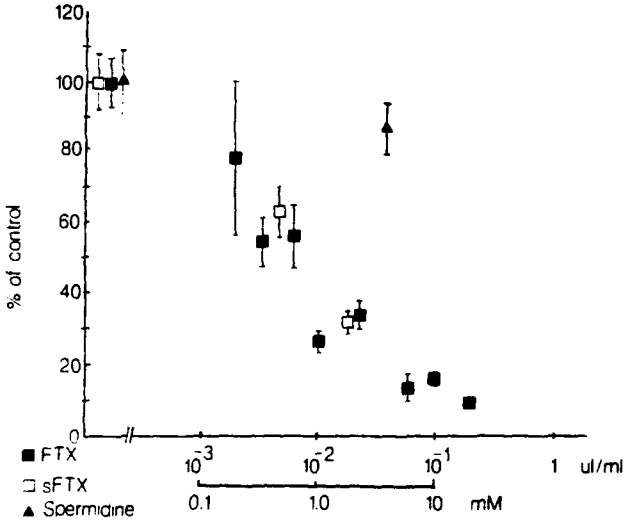

FIG. 2. Effect of FTX (■), sFTX (□) and spermidine (▲) on the quantal content of evoked release at the neuromuscular junction of the mouse diaphragm incubated with 1.2 mM Ca^{2+} and 6 mM Mg^{2+}. Each point is the mean ± SE of at least six muscle fibers. The μl/ml scale applies to FTX; the mM scale applies to sFTX and spermidine.

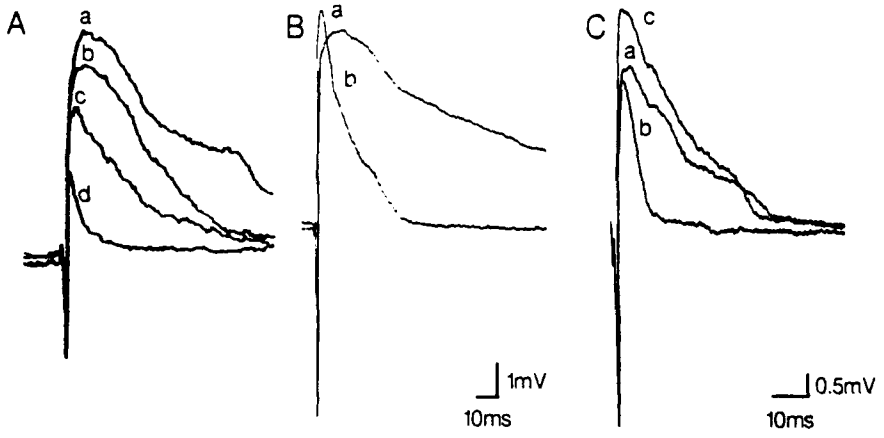

FIG. 3. Effect of Cd^{2+}, FTX, and sFTX on the presynaptic currents. Perineural recordings of presynaptic currents were obtained in levator auris muscle incubated in normal Ringer solution plus 30 μM curare, 10 mM tetraethylammonium, 250 μM 3,4-diaminopyridine, and 100 μM procaine. (*A*) Before (trace a) and 30, 60, and 90 s after (traces b–d) the addition of 500 μM Cd^{2+} to the bath solution. (*B*) Before (trace a) and after (trace b) the addition of FTX (0.5 μl/ml). (*C*) Before (trace a) and after (trace b) the addition of sFTX (300 μM). For trace c, the Ca^{2+} concentration was raised to 6 mM in the presence of sFTX.

recorded in curare-treated muscles incubated with K^+-channel blockers (tetraethylammonium, 10 mM; 3,4-diaminopyridine, 250 μM). The nerve was stimulated every 30 s and monitored continuously from the same site before and throughout the application of the toxin. Typical waveforms recorded from the perineural sheath have a large negative (downward) component and a long-lasting positive component. The latter has been shown to be Ca^{2+}-dependent (17) and sensitive to the inorganic Ca^{2+}-channel blocker Cd^{2+} (Fig. 3*A*) but insensitive to ω-CgTX (19).

The addition of FTX (0.5 μl/ml) to the bath rapidly diminished the Ca^{2+} wave (Fig. 3*B*). With a higher concentration of FTX (1 μl/ml), only a brief positive wave remained that was still present after the addition of 15 mM Cd^{2+}, suggesting that it is not a Ca^{2+} component. Submillimolar concentrations of sFTX were also effective in blocking the slow, long-lasting Ca^{2+} component of the presynaptic currents (Fig. 3*C*). The blocking effect of the toxin was overcome by increasing the Ca^{2+} concentration in the bath solution in a manner similar to that reported for other divalent cations (20).

K^+-Stimulated $^{45}Ca^{2+}$ Uptake by Synaptosomes. The experiments presented above and our previous findings on the blocking action of FTX on squid giant synaptic transmission (4) prompted us to evaluate the effect of the toxin on central nervous system synapses. Synaptosomes have been widely used for the study of VDCCs. In nerve terminals, Ca^{2+} influx into synapotosomes can be estimated by measuring the $^{45}Ca^{2+}$ uptake when synaptosomes are depolarized by K^+.

FTX and sFTX were effective inhibitors of the K^+-induced $^{45}Ca^{2+}$ uptake in cerebral cortex synaptosomes (Fig. 4). FTX (0.7 μl/ml) reduced $^{45}Ca^{2+}$ uptake to the same level as that in the nondepolarized synaptosomes. However, 100 μM Cd^{2+} was more effective: it also blocked part of the non-K^+-dependent uptake. Submillimolar concentrations of sFTX were able to block the Ca^{2+} uptake in a dose-dependent manner. In contrast, spermidine or arginine alone or combined showed no significant blocking effect.

DISCUSSION

Electrophysiological studies have shown that VDCCs are heterogeneous (21). In peripheral neurons, the T-, L-, and N-type channels can be distinguished by their sensitivities to organic Ca^{2+}-channel antagonists and to ω-CgTX. The L-type is sensitive to modulation by DHPs, whereas N- and T-types are not sensitive. ω-CgTX blocks N- and L-channels, but not T-type channels in chicken sensory neurons and rat sympathetic neurons (3–5). In cerebellar Purkinje cells, the P-type VDCC was characterized by its lack of sensitivity to ω-CgTX and to DHP, and by its high sensitivity to FTX (4).

The nature of the VDCC subtype directly involved in transmitter release in mammalian central and peripheral nervous system is not well defined. Evoked release of transmitter by nerve stimulation at the mammalian neuromuscular junction is not affected by DHP antagonists unless Ca^{2+} channels have been previously activated by a DHP agonist (11). ω-CgTX is also ineffective against the nerve-

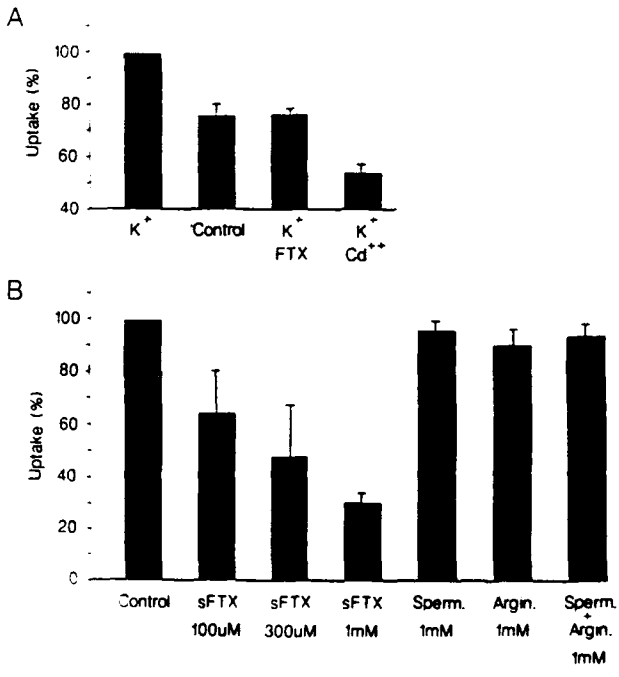

FIG. 4. Effect of FTX and sFTX on K^+-evoked $^{45}Ca^{2+}$ uptake in rat cerebral cortex synaptosomes. (*A*) Uptake of $^{45}Ca^{2+}$ in synaptosomes incubated in high K^+ (65 mM) in the absence or presence of FTX (1 μl/ml) or Cd^{2+} (100 μM). Control is the uptake in normal K^+ (5 mM). (*B*) Uptake of K^+ stimulated $^{45}Ca^{2+}$ in the presence of various concentrations of sFTx or 1mM spermidine (Sperm.), arginine (Argin.), or spermidine and arginine. For each experiment the control value (100%) was obtained by subtracting the uptake in normal K^+ to the uptake in high K^+. Each bar represents the mean ± SE.

stimulated evoked release; however, it is capable of reducing the frequency of spontaneous release of transmitter (10). Motor nerve terminal presynaptic Ca^{2+} currents measured with the intraperineural technique were found to be insensitive to DHP agonist (17) and also to ω-CgtTX (19). In contrast, the experiments presented in this paper showed the high potency of FTX in blocking synaptic transmission and presynaptic Ca^{2+} currents at the mouse neuromuscular junction. Therefore, from a pharmacological point of view the VDCCs involved in nerve-evoked transmitter release at the mammalian nerve terminals resemble the P-type channels described in Purkinje cells. Unfortunately, neither the electrophysiological characteristics of the motor nerve terminal channels at the single-channel level nor the macroscopic voltage-clamped currents are known. Therefore, it is not possible to compare their electrophysiological properties with the Ca^{2+} currents obtained from Purkinje cells.

In mammalian synaptosomes Ca^{2+} influx and depolarization-induced increases in intracellular Ca^{2+} have been found insensitive to DHP Ca^{2+}-channel antagonists, suggesting that L-type channels are not involved in transmitter release. ω-CgTX is a potent inhibitor of Ca^{2+} influx in avian and reptilian synaptosomes but is only partially effective on mammalian preparations, indicating that other types of VDCC must be involved in neurotransmitter release in the mammalian brain. The P-type channels seem to be widely distributed in the central nervous system, since they have been immunohistologically localized in numerous regions of mammalian brain (22). FTX-sensitive VDCCs were originally found in Purkinje cells, and a recent report (23) indicates that FTX-sensitive Ca^{2+} channels are also present in rat neurohypophysial nerve terminals.

Our findings, although preliminary, show that cerebral cortex synaptosomal Ca^{2+} influx is sensitive to FTX, suggesting that P-type channels may also be involved in transmitter release in central nervous system synapses. The potent effect of FTX in inhibiting Ca^{2+} uptake suggests that the population of synaptosomes sensitive to ω-CgTX may also be sensitive to FTX. Therefore, it might be possible that there are other types of VDCC with combined pharmacological properties. sFTX was as effective in blocking neuromuscular transmission as it was in blocking synaptosomal Ca^{2+} uptake, although the blocking concentration range was 3 orders of magnitude above that of the natural FTX. It has been suggested on the basis of organic structural studies including mass spectrometry, NMR, Fourier-transform infrared spectroscopy, and elemental analysis that naturally occurring FTX is a nonaromatic, decarboxylated polyamine (18). The difference in potency between FTX and the synthetic analog sFTX may be due to the presence of the carbonyl oxygen on sFTX. The biological specificities of both natural FTX and sFTX are identical in these studies, suggesting a remarkable similarity between the two. Our findings reaffirm the idea that polyamines, particularly amino acid-polyamine adducts, may play an important role in neuronal channel pharmacology. Thus, it is important to consider the possibility that nonaromatic polyamines resembling sFTX may normally be synthesized in the body and may exert a modulatory action on VDCCs and, hence, on transmitter release.

This work was supported by funding from Consejo Nacional de Investigaciones Cientificas y Tecnicas of Argentina, a grant from the Muscular Dystrophy Association of America, Fundacion Antorchas, U.S. Public Health Service grants (NS13742 and AG09480), and a grant from the Armed Forces Office of Scientific Research (AFOSR-89-0270).

1. Katz, B. (1969) *The Release of Neurotransmitter Substances* (Liverpool Univ. Press, Liverpool, U.K.).
2. Llinás, R. R. (1991) *Ann. N.Y. Acad. Sci.* **635**, 3–17.
3. Tsien, R. W., Lipscombe, D., Madison, D. V., Bley, K. R. & Fox, P. (1988) *Trends Neurosci.* **11**, 431–438.
4. Llinás, R., Sugimori, M., Lin, J. W. & Cherksey, B. (1989) *Proc. Natl. Acad. Sci. USA* **86**, 1689–1693.
5. Hirning, L. D., Fox, A. P., McCleskey, E. W., Olivera, B. M., Thayer, S. A., Miller, R. J. & Tsien, R. W. (1988) *Science* **239**, 57–61.
6. Perney, T. M., Hirning, L. D., Leeman, S. E. & Miller, R. J. (1986) *Proc. Natl. Acad. Sci. USA* **83**, 6656–6659.
7. Cazalis, M., Dayanithi, G. & Nordmann, J. J. (1987) *J. Physiol. (London)* **390**, 55–70.
8. Cena, V., Nicolas, G. P., Sanchez Garcia, P., Kirpekar, S. M. & Garcia, A. G. (1983) *Neuroscience* **10**, 1455–1462.
9. Olivera, B. M., Gray, W. R., Zeikus, R., Michael McIntosh, J., Vargas, J., Victoria de Santos, J. R. & Cruz, L. J. (1985) *Science* **230**, 1338–1343.
10. Protti, D. A., Szczupak, L., Scornick, F. S. & Uchitel, O. D. (1991) *Brain Res.* **557**, 336–339.
11. Atchison, W. D. (1989) *J. Pharmacol. Exp. Ther.* **251**, 672–678.
12. Reynolds, I. J., Wagner, J. A., Snyder, S. H., Thayer, S. A., Olivera, B. M. & Miller, R. J. (1986) *Proc. Natl. Acad. Sci. USA* **83**, 8804–8807.
13. Turner, T. J. & Goldin, S. M. (1985) *J. Neurosci.* **5**, 841–849.
14. Martin, A. R. (1966) *Physiol. Rev.* **46**, 51–66.
15. Angaut-Petit, D., Molgo, J., Connnold, A. L. & Faille, L. (1987) *Neurosci. Lett.* **82**, 83–88.
16. Mallart, A. (1985) *J. Physiol. (London)* **368**, 565–575.
17. Penner, R. & Dreyer, F. (1986) *Pflügers Arch.* **406**, 190–197.
18. Cherksey, B. D., Sugimori, M. & Llinas, R. R. (1991) *Ann. N.Y. Acad. Sci.* **635**, 80–89.
19. Anderson, A. J. & Harvey, A. L. (1987) *Neurosci. Lett.* **82**, 177–180.
20. Lin, J. W., Rudy, B. & Llinás, R. (1990) *Proc. Natl. Acad. Sci. USA* **87**, 4538–4542.
21. Miller, J. (1987) *Science* **235**, 46–52.
22. Hillman, D., Chen, S., Aung, T. T., Cherksey, B., Sugimori, M. & Llinás, R. R. (1991) *Proc. Natl. Acad. Sci. USA* **88**, 7076–7080.
23. Lemos, J. R. & Wang, G. (1991) *Soc. Neurosci. Abstr.* **17**, 342.

Reference: *Biol. Bull.* **181**: 315–361. (October, 1991)

Reports of Papers Presented at the General Scientific Meetings of the Marine Biological Laboratory

August 12–14, 1991

Short Reports are arranged (after the first featured article by Llinas et al.*) alphabetically by first author within the following categories: Neurobiology and Biophysics (pp. 316–333); Cell and Molecular Biology (pp. 333–342); Fertilization and Development (pp. 342–350); Physiology (pp. 350–356); and Systems and Ecology (pp. 357–361).*

All Short Reports were reviewed by members of our Special Editorial Board. Board members include: George Augustine (University of Southern California); David Epel (Hopkins Marine Station); Judith Grassle (MBL); Ehud Kaplan (Rockefeller University); George Langford (University of North Carolina); Jack Levin (VA Medical Center, San Francisco); James Olds (NIH); Robert Palazzo (MBL); Darrell Stokes (Emory University); Ivan Valiela (Boston University Marine Program); and Steven Zottoli (Williams College).

In addition to the reports contained in this issue, the following papers were also presented, by title, at the meetings. The abstracts of these papers are available from the MBL Archives.

Du, Jun, and Raquel Sussman. "mRNA analysis of a DNA-damage-inducible operon involved in mutagenesis of *E. coli*."

van Egeraat, Jan M., Richard N. Friedman, and John P. Wikswo. "Magnetic measurement of the spatial distribution of action currents in injured squid giant axons and squid giant synapses."

Fox, S. H., A. B. DuBois, and C. S. Ogilvy. "The effect of carbon dioxide on blood pressure, heart rate, intracranial pressure, and the Cushing response in bluefish (*Pomatomus saltatrix*)."

Kaplan, Ilene M., Barbara C. Boyer, and Lesley Carmichael. "The impact of socio-economic trends in the New England Conch (*Busy Con*) fishery on environmental changes and seafood inspection."

Nelson, Leonard, and Lucio Cariello. "Enzymatic correlates of *Arbacia punctulata* gametes exposed to pesticides."

Reynolds, G. T., and D. A. Hajduk. "Luminescence from polymerization of acrylamide."

Sheetz, Michael P. "Expansion and linearization of nuclear material visualized by video microscopy."

Silver, R. B. "Temperature induced spawning in *Echinarachnius parma* experiments? Knot when they're hot."

Sweet, Hyla C., and Barbara C. Boyer. "Multiple first quartet micromere deletions in eight-cell stage embryos of *Ilyanassa obsoleta*."

Zhong, Nan, and Robert M. Gould. "Partial cDNA sequence of phosphatidylinositol-specific phospholipase C (PI-PLC) from squid and dogfish nervous tissues by RNA-PCR."

Zhou, Zhimin, Gordon L. Fain, and John E. Dowling. "Amino acid receptors in isolated horizontal cells from the white perch retina."

Imaging Preterminal Calcium Concentration Microdomains in the Squid Giant Synapse

R. Llinás[1], M. Sugimori[1] and R. B. Silver[2] ([1]Department of Physiology and Biophysics, New York University Medical Center, New York, New York; and [2]Section and Department of Physiology, Cornell University, Ithaca, New York 14853-6401)

Intracellular calcium is the main trigger for transmitter release at most chemical synapses (1). The mechanisms by which calcium activates such release is presently unknown. The initial working hypothesis about the relationship between intracellular calcium concentration ($[Ca^{2+}]_i$) and transmitter release was based on results from the neuromuscular junction (2), and was proposed as a single-compartment release model. According to this model, vesicles are exocytosed following a fourth-order relation with respect to $[Ca^{2+}]_i$. This model, while useful, and clearly the best that could be made at the time, did not consider the many variables that regulate such parameters as $[Ca^{2+}]_i$ or vesicular availability. Moreover, calcium was thought to flow uniformly across the preterminal membrane, and the model of transmitter released did not adequately consider the ultrastructure of the presynaptic terminal. Present information regarding such parameters demand a more complete multi-compartment model.

Indeed, the possibility that calcium channels are localized at a discrete site in the preterminal was suggested in the late-70's (3). The suggestion came as a result of voltage-clamp experiments, which revealed the latency between the tail current calcium entry and transmitter release to be as short as 200 ms (3, 4). This morphological prerequisite of synaptic vesicles being directly apposed to the calcium channels was recently confirmed histologically (5). From voltage clamp data, the maximum $[Ca^{2+}]_i$ against the membrane was calculated to be about $10^{-4}M$ (4). These results shifted the focus from cytosolic residual calcium to the problem of what is now known as calcium microdomains (6–9). The term "calcium microdomains" refers to a very precise distribution of sites for $[Ca^{2+}]_i$ change. These microdomains were expected to occur against the inside of the presynaptic terminal at the active zone. In fact, each active calcium channel is thought to produce a rapid (*i.e.*, a few Ms) increase in $[Ca^{2+}]_i$, lasting for the duration of the average open time of the channel (8). This influx is thought to generate a $[Ca^{2+}]_i$ profile as high as 200–300 Mmoles in the proximity of the calcium channels. This being the case, transmitter release would be triggered by extraordinarily high transient calcium-concentration change in the immediate vicinity of the presynaptic release site where the vesicles are lodged (4, 8).

To test this hypothesis, a special type of signalling methodology was introduced. A hybrid synthetic n-aequorin/J (10), having a sensitivity to $[Ca^{2+}]_i$ in the order of 10^{-4}, was developed for this purpose by Dr. Shimomura. This aequorin was injected presynaptically at a concentration of 5%, in conjunction with "discharged" normal sensitivity aequorin made fluorescent to permit its intracellular localization. The distribution of the injected protein following impalement of the presynaptic terminal of the giant synapse of the squid *Loligo pealii* was visualized with a fluorescence microscope using a 40× water-immersion lens. Aequorin luminescence was then detected with a VIM camera operated in the photon counting mode; the images stored on videotape and characterized by digital image processing and analysis methods.

Results were obtained from eight different synapses bathed in artificial seawater (10 mM Ca^{2+}); one synapse was injected with normal aequorin, and the other seven injected with the n-aequorin/J. Upon tetanic stimulation, small points of light were detected over the preterminal region in the area of the "active zone" (Fig. 1).

These points had an average diameter of approximately 0.5 μm and were distributed over roughly 5–10% of the total area of the presynaptic membrane (with an average of 8.39 μ^2 per 100 μ^2) (Fig. 1). Results from all synapses were quite similar. They show that the portion of the presynaptic terminal forming the active zone emits light during presynaptic activation, indicating that the calcium concentration is elevated in the range of 10^{-4} M during this active period.

The location of these small light sources was determined by two methodologies. First, light-emission points were accumulated during several seconds of stimulation, and the spatial and temporal distribution of the blips was then studied. Second, to ensure that the location of the patches of blips were similar within repeating stimuli, sets of successive temporal image integrations of the recording were compared.

Both methods illustrated a similar distribution of microdomains and roughly the same size and intensity of light points. The results suggest that microdomains may belong to one of two varieties: (1) those frequently activated, and (2) those that, while repeating, activate less often. Finally, analysis of digitized sub-regions of the image field showed that the temporal and spatial distribution of microdomain action through time reflects the temporal cycling of active sites from one point of membrane to the next, during stimulation. This finding suggests that an even more complex modulation of activity may be present in these terminals. Indeed, in addition to calcium microdomains, compartmentalization of other parameters such as the degree of phosphorylation of synapsin I (11) may also show dynamic interaction, which would ensure a fine control of transmitter release from one impulse to the next. Of interest here is the possibility that a certain number of calcium channels may have to be active simultaneously in order to activate the aequorin signals observed here. In that case, the high level of $[Ca^{2+}]_i$ obtained at the microdomain may itself reduce, by a "lateral inhibition" type effect, the probability of further calcium channel activation in a given active site.

We extend our deep gratitude to Dr. Osamu Shimomura for his generous gifts of the custom aequorin preparations used in this study. The authors gratefully acknowledge research grant support from the NIH (NS 14014 to RL), the U. S. Air Force (OSRG85-0368 to RL), the NSF (DCB-9005343 to RBS) and the Cornell—U. S. Army Biotechnology Center of Excellence Program (24629-LS-UIR to RBS).

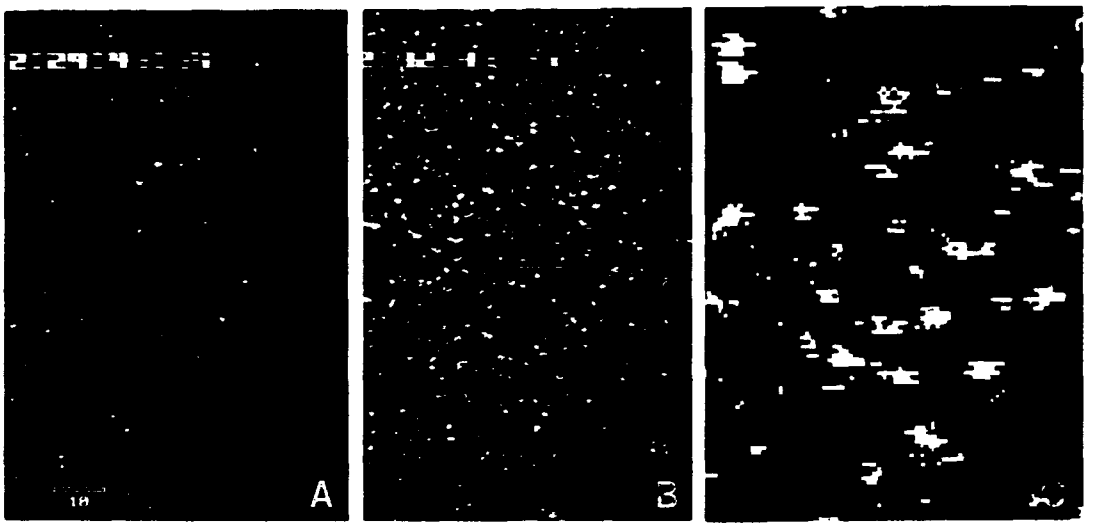

Figure 1. *Imagery of Ca^{2+}-dependent aequorin luminescence from pre-terminal of the squid giant synapse. Note the discrete sizes of individual blips. Pseudo-coloring is used to indicate brightness of each blip: white and red are the brightest blips, blue and violet blips are the least intense. Panel A: A 10-s integration of the pre-terminal 30 s prior to stimulation. Panel B: A 10-s integration of the same region of the pre-terminal shown in Panel A 60 s following the onset of tetanic stimulation. Note the increase in the number of blips compared to Panel A. Panel C: An enlarged image of calcium microdomains in the region indicated within the inset borders of Panel B. Bar = 10 μm.*

Literature Cited

1. **Katz, B. 1969.** *The Release of Neurotransmitter Substances.* The Sherrington Lectures X. Charles C. Thomas, Springfield, IL.
2. **Dodge, F. A., and R. Rachamimoff. 1967.** *J. Physiol. Lond.* **193:** 419–432.
3. **Llinás, R. 197?.** Pp. 139–160 in *Approaches to the Cell Biology of Neurons.* Soc. for Neurosciences, Bethesda, MD.
4. **Llinás, R., *et al.* 1981.** *Biophys. J.* **33:** 289–321.
5. **Robitaille, R., *et al.* 1990.** *Neuron* **5:** 773–779.
6. **Chad, J. E., and R. Ekert. 1984.** *Biophys. J.* **45:** 993–999.
7. **Simon, S. M., *et al.* 1984.** *Biophys. J.* **45:** 264a.
8. **Simon, S. M., and R. Llinás. 1985.** *Biophys. J.* **48:** 485–498.
9. **Fogelson, A. L., and R. S. Zucker. 1985.** *Biophys. J.* **48:** 1003–1007.
10. **Shimomura, O., *et al.* 1989.** *Biochem. J.* **261:** 913–920.
11. **Llinás, R., *et al.* 1985.** *Proc. Natl. Acad. Sci. U.S.A.* **82:** 3035–3039.

Synaptic Background Activity Influences Spatiotemporal Integration in Single Pyramidal Cells

Öjvind Bernander and Christof Koch (California Institute of Technology, 216-76, Pasadena, CA 91125)

Standard 1-D cable theory models the voltage behavior of spatially extended cable structures in response to synaptic inputs. These models usually assume R_m of 5–20,000 Ωcm^2 and a small number of activated synapses. Each synaptic input induces a transient increase in the membrane conductance, which is small relative to the total cell conductance. However, neurons do not exist in isolation, but are part of a heavily interconnected network of neurons that are spontaneously active: *e.g.*, in visual cortex at rates between 0.5–5 synaptic events per second [Hz] (1). Given that the average cortical pyramidal cell receives input from 10–20,000 synapses, this background activity can cause an added membrane conductance comparable to $G_m = 1/R_m$. In the light of recent evidence suggesting much higher values for R_m (2), this synaptic background activity may actually constitute the bulk of the effective membrane conductance. Here we study the overall effect of synaptic background activity on the spatial and temporal integrative properties of a single pyramidal cell.

A typical layer V pyramidal cell in the striate cortex was filled with HRP during *in vivo* experiments on anesthetized, adult cats: R_m = 21 MΩ and τ_m = 22 ms (3). Lengths and diameters of all 163 dendritic branches were measured, and the data was fed into a modified version of NEURON, a single cell simulator developed by M. Hines and J. Moore (4). Passive properties were set to: R_m = 100,000 Ωcm^2, C_m = 1 μm^{-2}, R_i = 200 Ωcm, and E_{rest} = −66 mV. Seven active Hodgkin-Huxley-like currents were located at the soma, including a calcium-dependent K current, giving such basic behavior as spike adaptation and primary slope of the curve relating injected current to the number of action potentials triggered. We modeled 4000 excitatory synapses using $g(t) = \text{const}\ te^{-t/t_{peak}}$ for the time-varying conductance in-

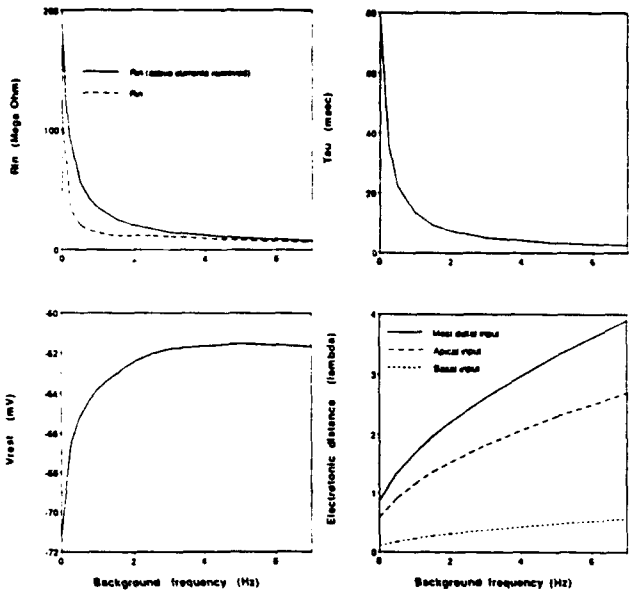

Figure 1. *Impact of synaptic background frequency (in synaptic events per second, Hz) on cellular parameters of the layer V cell described in the text. (a) Somatic input resistance, R_{in}, in the absence of any active currents (top curve: passive neuron) and in our standard model (bottom curve). Over this range, the somatic input conductance varies from 9.1 nS (at f = 0) to 151 nS (at f = 7 Hz). (b) Membrane time constant, τ_m measured at the cell body. (c) Somatic resting potential, V_{rest}. (d) Electrotonic distance, L, from the soma to three different locations (the distal end of a basal dendrite, a point halfway up the apical tree and the most distal point in layer I).*

crease (with g_{peak} = 0.5 nS and t_{peak} = 1.5 ms), 500 inhibitory synapses of the $GABA_A$ type (with g_{peak} = 1.0 nS and t_{peak} = 10 ms) and 500 of the $GABA_B$ type (with g_{peak} = 0.1 nS and t_{peak} = 40 ms). The density of inhibitory synapses was highest on, or close to, the soma, and vice versa for excitatory synapses.

Figure 1 illustrates what happens if the synaptic background activity, (f) is varied. In the absence of input (corresponding to slice conditions), R_m = 153 MΩ and τ_m = 80 ms, while V_{rest} is pulled between E_{leak} and E_K (−95 mV). At 1 Hz background activity, 5 synaptic events are impinging on the cell every ms, contributing a total of 24 nS to the somatic input conductance G_{in} (corresponding to 34%). Along with R_m, τ_m drops with increasing f. This drop is most dramatic between 0 and 2 Hz. Because of the reversal potential of the excitatory synapses (0 mV), the membrane potential throughout the cell is pulled towards more depolarizing potentials. That the spatial integrative properties vary with f is demonstrated in Figure 1d. The electronic distance of three locations are plotted *vs.* f. As we go from 0 to 2 Hz, the distance increases almost by a factor 3, making the cell much less compact, effectively isolating distal parts of the apical tree.

We showed that the synaptic background activity can modify the temporal integration behavior of the cell, by computing the minimal number of excitatory synapses necessary to generate at least one action potential. We compare the case in which all synapses are activated simultaneously with the case in which the inputs arrive asynchronously, smeared out over 25 ms. If f = 0, 115 synapses must fire simultaneously to generate a single action potential, while 145 are needed if the input is desynchronized. This small difference is due to the long integration period of the cell. If the background activity increases to f = 1 Hz, 113 synchronized synaptic inputs—spread out all over the cell—are sufficient to fire the cell. If, however, the synaptic input is spread out over 25 ms, 202 synapses are now needed to trigger a response from the cell. This is mainly due to the much smaller value of τ_m relative to the period over which the synaptic input is spread out. The difference between synchronized and unsynchronized synaptic input in evoking action potentials becomes much larger if periodic, repetitive synaptic input is considered.

The principal phenomenon reported here is the dramatic effect that network activity can have on the spatiotemporal integration behavior of single neurons. Our results show that the large values of R_m and τ_m reported by several groups for pyramidal cells (2, 5, 6) may simply reflect the lack of general synaptic background activity typically observed in slice preparations. This would also explain the lower values of V_{rest} seen in slices as compared to *in vivo* intracellular recordings. Thus, the overall activity of the network can alter the properties and the behavior of single neurons. Our prediction can be simply tested by recording from one cell and varying the overall network activity with the help of sensory afferents.

Literature Cited

1. **Leventhal, A. G., and H. V. B. Hirsch. 1978.** *J. Neurophysiol.* **41:** 948–962.
2. **Major, G., *et al.* 1990.** *J. Physiol.* **430:** 13P.
3. **Douglas, R. J., *et al.* 1991.** *J. Physiol.* In press.
4. **Hines, M. 1989.** *Int. J. Biomed. Comput.* **24:** 55–68.
5. **Anderson, P., *et al.* 1990.** *Symp. Quant. Biol.* **55:** 81–86.
6. **Spruston, N., and D. Johnston. 1991.** *J. Neurophysiol.* In press.

Journal of Physiology (1991), **436**, *pp.* 257–282
With 10 figures
Printed in Great Britain

REGULATION BY SYNAPSIN I AND Ca^{2+}–CALMODULIN-DEPENDENT PROTEIN KINASE II OF TRANSMITTER RELEASE IN SQUID GIANT SYNAPSE

BY R. LLINÁS*, J. A. GRUNER*†, M. SUGIMORI*, T. L. McGUINNESS‡, AND P. GREENGARD‡

*From the Marine Biological Laboratory, Woods Hole, MA, *Department of Physiology & Biophysics and †Department of Neurosurgery, New York University Medical Center, New York, NY and the ‡Laboratory of Molecular and Cellular Neuroscience, Rockefeller University, New York, NY, USA*

(*Received 3 August 1990*)

SUMMARY

1. Presynaptic or simultaneous pre- and postsynaptic voltage-clamp protocols were implemented in the squid giant synapse in order to determine the magnitude and time course of the presynaptic calcium current (I_{Ca}) and its relation to transmitter release before and after presynaptic injection of proteins. These included several forms of synapsin I, calcium–calmodulin-dependent protein kinase II (CaM kinase II) and avidin.

2. The quantities and location of these proteins were monitored by fluorescence video-enhanced microscopy during the electrophysiological measurements.

3. Presynaptic injection of dephosphorylated synapsin I inhibited synaptic transmission with a time course consistent with diffusion of the protein through the terminal and action at the active release zone. A mathematical model relating the diffusion of synapsin I into the terminal with transmitter release was developed to aid in the interpretation of these results.

4. Synapsin I inhibition of transmitter release was reversible.

5. The action of synapsin I was highly specific, as phosphorylation of the tail region only or head and tail regions prevented synapsin I from inhibiting release.

6. Injections of heat-treated synapsin I or of avidin, a protein with a size and isoelectric point similar to those of synapsin I, had no effect on transmitter release.

7. CaM kinase II injected presynaptically was found to facilitate transmitter release. This facilitation, which could be as large as 700% of the control response, was related to the level of penetration of the enzyme along the length of the preterminal. A mathematical model of this facilitation indicates a reasonable fit between the distribution of CaM kinase II within the terminal and the degree of facilitation.

8. The overall shape of the postsynaptic response was not modified by either synapsin I or CaM kinase II injection.

9. The data suggest that, in addition to releasing transmitter, calcium also penetrates the presynaptic cytosol and activates CaM kinase II. When activated, CaM kinase II phosphorylates synapsin I, which reduces its binding to vesicles

MS 8704

and/or cytoskeletal structures, enabling more vesicles to be released during a presynaptic depolarization. The amplitude of the postsynaptic response will then be both directly and indirectly regulated by depolarization-induced Ca^{2+} influx. This model provides a molecular mechanism for synaptic potentiation.

INTRODUCTION

Electrophysiological and morphological studies in the squid giant synapse preparation have yielded significant insights into the mechanisms of depolarization–release coupling in chemical transmission (Katz & Miledi, 1967; Llinás, Steinberg & Walton, 1981*a*, *b*; cf. Augustine, Charlton & Smith, 1987). Because both the pre- and postsynaptic terminals in this junction can be impaled directly (Bullock & Hagiwara, 1957; Hagiwara & Tasaki, 1958), the depolarization–release coupling process may be studied at its site of occurrence. We have recently examined some of the biochemical steps involved in the release process. Since the presynaptic terminal can generate action potentials (Miledi & Slater, 1966; Llinás, Sugimori & Simon, 1982), the effects of presynaptically injected proteins on depolarization–release coupling can be directly tested using spike activation. In addition, pre- and postsynaptic voltage clamping, combined with pharmacological blockade of Na^+ and K^+ conductances, allow precise measurement of the presynaptic Ca^{2+} current. Transmitter release can be inferred from the time course and amplitude of the postsynaptic potential (Llinás, Steinberg & Walton, 1976; Llinás *et al.* 1981*b*) or the postsynaptic current (Llinás & Sugimori, 1978; Augustine & Charlton, 1986), thereby allowing determination of the relationship between Ca^{2+} entry and transmitter release.

Several findings have suggested a prominent role for the protein synapsin I in synaptic transmission. For instance, synapsin I has been found to be nearly ubiquitous in presynaptic terminals, and to be closely associated with the cytoplasmic surface of small synaptic vesicles. It represents about 1% of the total neuronal protein in the mammalian brain (DeCamilli, Cameron & Greengard, 1983; Greengard, Browning, McGuinness & Llinás, 1987). Earlier experiments in the squid giant synapse have indeed shown that intracellular injection of synapsin I can block synaptic transmission, and that Ca^{2+}–calmodulin-dependent protein kinase II (CaM kinase II) has a facilitory effect (Llinás, McGuinness, Leonard, Sugimori & Greengard, 1985; Greengard *et al.* 1987).

Based on these and other findings, we hypothesized that synapsin I serves to immobilize synaptic vesicles by binding them to cytoskeletal elements, and that phosphorylation of synapsin I by CaM kinase II liberates vesicles from these attachments (Llinás *et al.* 1985; DeCamilli & Greengard, 1986; Greengard *et al.* 1987; McGuinness, Brady, Gruner, Sugimori, Llinás & Greengard, 1989; DeCamilli, Benfenati, Valtorta & Greengard, 1990).

The regulation of synapsin I phosphorylation is of central importance to this hypothesis. Synapsin I can be phosphorylated at three sites: site 1 is located in the globular head region of the molecule, while sites 2 and 3 are located in the elongated tail region. Previous studies have indicated that CaM kinase II is capable of phosphorylating synapsin I on its tail sites, while the head site can be phosphorylated either by cyclic AMP-dependent protein kinase or by Ca^{2+}–calmodulin-dependent

protein kinase I (Huttner & Greengard, 1979; Sieghart, Forn & Greengard, 1979; Huttner, DeGennaro & Greengard, 1981; Kennedy & Greengard, 1981; Czernick, Pang & Greengard, 1987; Nairn & Greengard, 1987). Phosphorylation of the tail region by CaM kinase II reduces the binding of synapsin I to synaptic vesicles (Huttner, Scheibler, Greengard & DeCamilli, 1983; Schiebler, Jahn, Doucet, Rothlein & Greengard, 1986; Benfenati, Bahler, Jahn & Greengard, 1989) as well as to actin (Bahler & Greengard, 1987; Petrucci & Morrow, 1987). It has been hypothesized that synapsin I cross-links synaptic vesicles to actin, and that upon phosphorylation of synapsin I by CaM kinase II, the vesicles are free to move from a 'reserve' pool to a 'releasable' pool (Llinás *et al.* 1985; Bahler & Greengard, 1987; Benfenati *et al.* 1989; DeCamilli *et al.* 1990). The size of the postsynaptic response would then depend on both the size of the inward calcium current and the number of vesicles available for release. Here we present results obtained following the injection of synapsin I and CaM kinase II which are consistent with this hypothesis. Some of the results have been reported in preliminary form (Llinás *et al.* 1985).

METHODS

Stellate ganglion preparation

Experiments were performed in the giant synapse of the squid *Loligo pealii* at the Marine Biological Laboratory, Woods Hole, MA, USA. After decapitation of the squid, the stellate ganglion was isolated from the mantle under running sea water and placed in the recording chamber. The connective tissue over its surface was removed while the ganglion was continuously superfused with artificial sea water for the duration of the experiment (Llinás *et al.* 1981*a*). The presynaptic terminal was impaled with two microelectrodes: one to inject current and the different proteins, and one to measure voltage, which provided the feedback signal for the voltage-clamp amplifier. Chemicals (TEA) and proteins (phosphorylated and dephosphorylated synapsin I, mock phosphorylated synapsin I, avidin and CaM kinase II) were injected into the presynaptic terminal, using pressure pulses 50–100 ms in duration, regulated to 10^5 N/m^2. The postsynaptic fibre was impaled with two electrodes, one for voltage recording, the other for current injection. A brief electrical stimulus to the presynaptic bundle via a bipolar electrode located proximal to the stellate ganglion was used to confirm the viability of the preparation prior to the initiation of each experiment. Following demonstration of synaptic transmission, the sodium and potassium conductances (g_K, g_{Na}) were blocked by bath application of tetrodotoxin (TTX: 5×10^{-6} M) and 4-aminopyridine (4-AP) (final concentration 1 mM). In addition, TEA was also injected presynaptically in some experiments (see Figs 6*A*, 9 and 10). Careful monitoring revealed that during this procedure the potential at the recording electrode depolarized transiently by 2–5 mV in successful injections. Only in those experiments where the membrane potential stabilized within 5 mV of the pre-injection membrane potential level was the experiment continued. In our initial experiments, dephosphorylated synapsin I was injected prior to any pharmacological intervention to investigate the action of synapsin I in the absence of the ionic channel blocker. The presynaptic as well as the simultaneous presynaptic and postsynaptic voltage-clamp and calcium current measurement techniques have been previously described (Llinás & Sugimori, 1978; Llinás *et al.* 1981*a*; cf. Augustine *et al.* 1987).

Visualization of intracellularly injected proteins

To visualize the proteins used in the presynaptic injections, the various forms of synapsin I and avidin were made fluorescent by conjugation to the dye Texas Red (see below). Binding of the dye to synapsin I did not alter its ability to: (a) be phosphorylated by CaM kinase II as assessed using the procedure of McGuinness, Lai & Greengard (1985); (b) bind to purified synaptic vesicles using the procedure of Schiebler *et al.* (1986); or (c) inhibit neurotransmitter release (present report). A high-gain fluorescence imaging system consisting of a Videcon camera attached to a microchannel plate-image intensifier (maximum light magnification, 10^6) allowed us to localize the protein in the

preterminal. The image was then analysed on a Hamamatsu C 1966 VIM image analysis system which gave a well-defined fluorescence profile. The movement of the labelled protein was measured at different times after the injection and its movement along the terminal was determined by entering the enhanced image into a computer for graphic analysis. The rate of protein movement was determined by measuring the advance of the wavefronts as the terminal filled, and then calculating the percentage area of the terminal which remained unfilled at each time point. As discussed below, after the protein had diffused several hundred micrometres and its concentration had declined, the wavefront became less well defined and thus its position gave an underestimate of the extent of protein movement into the terminal. The diffusion velocity of synapsin I and avidin measured in this way was typically 25–55 $\mu m\ min^{-1}$ (cf. Fig. 3C).

The location of CaM kinase II was indirectly determined by adding Texas Red-labelled bovine serum albumin (BSA) to the injection solution since the binding of dyes interfered with its solubility and/or its ability to phosphorylate synapsin I. Addition of labelled BSA to the CaM kinase II solution had no detectable effect on the ability of the enzyme to phosphorylate synapsin I *in vitro* or on its ability to enhance neurotransmitter release from the giant synapse.

In early experiments the volume of synapsin I injected into the presynaptic terminal was determined using ^{125}I-labelled synapsin I which was measured directly, using a gamma counter. In five trials, the volume injected was 0·05–1 pl, i.e. $\leqslant 10\%$ of the total volume of the terminal digit, corresponding to a maximal intracellular synapsin I concentration of 1·35 μM. Synapsin I, avidin and BSA had similar mobilities in the terminal.

Preparations of proteins

Dephosphorylated synapsin I was purified from bovine brain by modification (Bahler & Greengard, 1987) of the procedure of Schiebler *et al.* (1986). CaM kinase II was purified from rat forebrain as previously described (McGuinness *et al.* 1985), with the addition of hydroxylapatite chromatography inserted between the DEAE-cellulose chromatography and ammonium sulphate precipitation steps. The purified CaM kinase II (0·5 mg ml^{-1}) was dialysed extensively against 0·5 M-potassium acetate/10 mM-potassium phosphate, pH 7·4 (injection buffer) and stored at −70 °C until immediately before use. The catalytic subunit of cyclic AMP-dependent protein kinase, purified as described (Kaczmarek, Jennings, Strumwasser, Nairn, Walter, Wilson & Greengard, 1980), was a gift of Dr A. C. Nairn. Calmodulin was purified as described (Grand, Perry & Weeks, 1979). Avidin, a basic protein similar in size to synapsin I, was labelled with the fluorescent dye Texas Red. Texas Red-labelled avidin and Texas Red-labelled BSA were obtained from Molecular Probes (Eugene, OR, USA), dissolved in and dialysed extensively against the injection buffer, and stored in aliquots at −70 °C until immediately before use. Protein determinations were performed by the method of Peterson (1977) using BSA as the standard.

Synapsin I (0·35 mg ml^{-1}) was phosphorylated by incubation for 30 min at 30 °C in 50 mM-Tris-HCl, pH 7·5, 150 mM-NaCl, 0·4 mM-EGTA, 1 mM-dithioerythritol, 10 mM-$MgCl_2$, 100 μM-ATP with trace amounts of [γ-^{32}P]ATP, with either CaM kinase II (3·4 $\mu g\ ml^{-1}$), 0·7 mM-$CaCl_2$, 30 $\mu g\ ml^{-1}$ calmodulin and/or the catalytic subunit of cyclic AMP-dependent protein kinase (60 nM/0·1% Nonidet-P40). Mock phospho-synapsin I was prepared as above except that both kinases, $CaCl_2$, calmodulin and Nonidet-P40 were added while ATP was omitted from the reaction mixture. Synapsin I was phosphorylated to a stoichiometry of 2·0 mol mol^{-1} by CaM kinase II and 0·95 mol mol^{-1} by the catalytic subunit of cyclic AMP-dependent protein kinase, as confirmed by one- and two-dimensional peptide mapping of the phosphorylated synapsin I molecules (Huttner *et al.* 1981; Kennedy & Greengard, 1981; Kennedy, McGuinness & Greengard, 1983).

The synapsin I preparations to be fluorescently labelled were dialysed extensively against 0·1 M-Tris-HCl (pH 9·0), 50 mM-NaCl and then concentrated on an Amicon centricon 30 unit to a final protein concentration of 1 mg ml^{-1}. Conjugation to the fluorescent probe Texas Red (Molecular Probes, Eugene, OR, USA) was performed according to the method of Titus, Haugland, Sharrow & Segal, (1982). Briefly, 1 mg of Texas Red was dissolved in 250 μl of dimethylformamide and an aliquot was immediately added to the protein solution (0·5–1·0 ml) using a ratio of 0·04 mg Texas Red : 1 mg protein. Conjugation reactions were carried out for 1 h at 4 °C. Synapsin I, in both the labelled and unlabelled preparations, was purified away from kinases and/or unbound Texas Red by CM-cellulose chromatography at pH 8·0 (Ueda & Greengard, 1977). Synapsin I was eluted from the CM-cellulose column with injection buffer, concentrated as described above, dialysed overnight against the injection buffer, centrifuged at 450000 *g* for 15 min to remove large aggregates, and

either stored at 0 °C and used within 7 days of preparation or stored at −70 °C and thawed immediately before use. The absorbance ratio $A_{596\ 280}$ of the labelled synapsin I ranged from 0·7 to 1·3, giving an estimated molar dye:protein ratio of 5:1 to 12:1. One-dimensional SDS-gel electrophoresis confirmed that the fluorescence co-migrated with the synapsin I protein staining bands.

Data analysis

Electrophysiological responses were stored on a Nicolet 4094B digital oscilloscope and transferred to a Macintosh II computer for analysis. Peak amplitudes for the postsynaptic potentials (PSP) or currents (PSI) were determined using the average value of the pre-stimulus baseline as reference. In some experiments, the amplitude of the postsynaptic response was obtained by integrating the curves over the period required for the largest response to return to baseline. Indeed, in those cases where the shape of the response curve did not change as a function of stimulus amplitude, the integral of the response was proportional to the peak response amplitude at all stimulus levels. This was tested in three preparations in which integrals of postsynaptic currents or voltage responses were calculated and compared to peak-to-peak amplitudes. In each case, there was a high ($R^2 \sim 0{\cdot}95$) linear correlation between the peak amplitudes and the integrals of the responses when compared at various stimulus levels, and there was no apparent change in the shape of the responses. The maximum rate of rise of the response was determined by a computer algorithm which determined slopes for successive sets of five points 20 μs apart, beginning at the onset of the stimulus artifact to the time of the response peak. The maximum slope determined by the computer was overlaid on the raw waveform for visual verification. Statistical calculations (linear correlation coefficients, t tests) were performed using commercial statistics programs.

RESULTS

The database comprised fifty-two experiments involving injections of various dephosphorylated and phosphorylated forms of synapsin I, avidin and CaM kinase II. The results of these experiments are summarized in Table 1. More than 100 experiments, in which the preterminal had been injected with one of the above proteins, were excluded from this database for one of the following reasons: (a) failure to achieve normal pre- and postsynaptic resting membrane potential values after injection; (b) significant drop in membrane potential (more than 5 mV) or of input resistance and (c) leakage of dye into the extracellular compartment. Fine adjustments of the electrode positions were sometimes needed to maintain recording integrity. If a microelectrode came completely out of a terminal more than once, the data were discarded.

Synapsin I and transmitter release

Effect of dephosphorylated synapsin I on neurotransmitter release elicited by presynaptic action potentials

In twenty-one experiments, dephosphorylated synapsin I (synapsin I) was successfully injected into the final preterminal digit between 200 and 1100 μm from its distal end and allowed to diffuse throughout the remainder of the digit. In one experiment the postsynaptic potential elicited by presynaptic nerve stimulation was measured at regular intervals after injection of the protein. This allowed the release properties of the synapse to be determined in the absence of other pharmacological agents. As shown in Fig. 1, injection of synapsin I was accompanied by a reduction of transmitter release as measured by the decline in amplitude of the PSP. The postsynaptic response decreased in amplitude after this injection as the protein

diffused into the preterminal digit, without any change in the amplitude of the presynaptic action potential. This decrease in the postsynaptic response was almost complete 24 min after the injection.

These findings are in agreement with our initial observations that the injection of dephosphorylated synapsin I can block the release of transmitter induced by

TABLE 1. Summary of injection experiments

Injection	N	NC	I	F
CaM kinase II	9	0	1	8
Synapsin I	21	1	20	0
Mock phospho-synapsin I*	3	0	3	0
Heat-treated synapsin I	2	2	0	0
Head-tail-phosphorylated synapsin I	4	3	1	0
Head-phosphorylated synapsin I	7	1	6	0
Tail-phosphorylated synapsin I	2	2	0	0
Avidin	4	4	0	0
Total number	52	—	—	—

N, total number; NC, no change; I, inhibition of release; F, facilitation.
* Prepared as phospho-synapsin I except *not* phosphorylated.

presynaptic action potentials (Llinás *et al.* 1985) and with those recently published on Mauthner cell function in the vertebrate central nervous system (Hackett, Cochran, Greenfield, Brosius & Ueda, 1990).

Relation between dephosphorylated synapsin I diffusion into the terminal and neurotransmitter release evoked by presynaptic voltage steps

In order to establish the parameters that determine blockade of transmitter release by dephosphorylated synapsin I, calcium currents were measured before and at several intervals after injection of synapsin I. The presynaptic terminal was voltage clamped and transiently depolarized by rectangular voltage pulses of constant amplitude (40 mV) and duration (4·5 ms) from a holding potential of −65 mV. This allowed the time course and amplitude of the postsynaptic response to be determined as a function of the presynaptic I_{Ca} (Llinás *et al.* 1981*a*, *b*; Augustine, Charlton & Smith, 1985).

The decrease in postsynaptic response to constant amplitude voltage steps following synapsin I injection at the proximal end of the presynaptic digit is shown in Fig. 2. The presynaptic voltage step was repeated at the intervals indicated by the numbers to the left in the top panel of Fig. 2 which indicate time in minutes after injection. The results confirm our previous finding that synapsin I does not affect I_{Ca}, in contrast to its dramatic inhibition of the postsynaptic response (Llinás *et al.* 1985). Almost complete inhibition of the postsynaptic response occurred at about 25–30 min (see plot in Fig. 3*B*). In this experiment, g_K was not completely blocked, as TEA was not injected to avoid a possible interaction with the action of synapsin I. However, it can be seen that the initial rate and amplitude of I_{Ca} was unaffected by synapsin I. Furthermore, in subsequent experiments (see Fig. 6) it was observed that TEA, in amounts required to abolish the K^+ currents, did not interfere with the ability of synapsin I to block transmitter release.

In order to determine the mobility of synapsin I within the presynaptic cytosol, and to investigate the relationship between the location of synapsin I and transmitter release, a series of experiments were carried out in which synapsin I was injected at various locations along the preterminal. Synapsin I was labelled with the fluorescent

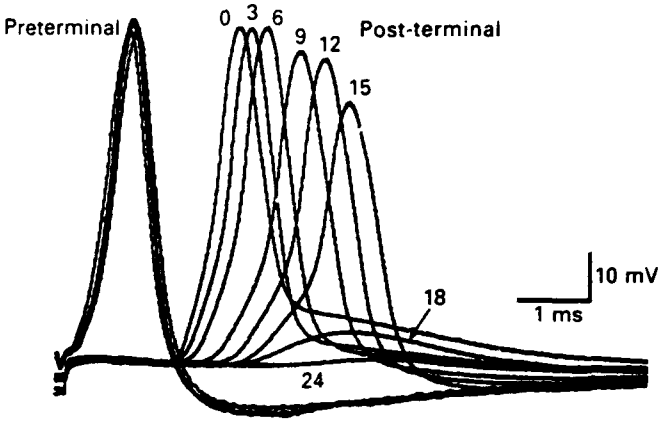

Fig. 1. Pre- and postsynaptic potentials from the squid giant synapse before and after presynaptic injection of synapsin I. Synaptic transmission was almost completely blocked 24 min after injection. No significant change in the presynaptic spike was observed. The decrement in postsynaptic spike amplitude was due to g_{Na} inactivation and g_K activation as the time required for the PSP to reach firing level was prolonged by the progressive block of synaptic transmission. The numbers give the time after synapsin I injection in minutes.

dye Texas Red and imaged using video-enhanced microscopy (see Methods) which allowed constant monitoring of the diffusion of the synapsin I–Texas Red conjugate. The results of two experiments are shown in Fig. 3. The initial diffusion rate of synapsin I into the presynaptic terminal, as determined by analysis of video-enhanced microscopic images of five individual injections, ranged between 23 and 108 μm min^{-1} (mean $\pm$ S.D. = 54 $\pm$ 33). This value is similar to that found for injection of similar proteins, such as avidin (see below). The amplitude of the postsynaptic response and the filling of the presynaptic terminal are plotted in Fig. 3*A* as a function of time for a synapse in which synapsin I was injected 300–400 μm proximal to the beginning of the synaptic zone region. Data for a synapse in which the injection was near the proximal edge of the active zone region are plotted in Fig. 3*B*. The maximal reduction in mean amplitude occurred after synapsin I had completely filled the presynaptic terminal (Fig. 3*B*).

The initial rate of filling of the presynaptic terminal was best fitted by a linear function. In cases where the injection was relatively small and/or more than several hundred micrometres from the end of the terminal, the fluorescence intensity became faint and the diffusion rate appeared to slow dramatically near the end of the terminal. In Fig. 3*B*, for example, the fluorescence was very low after the initial 5 min following injections. This did not occur for the injection shown in Fig. 3*A*, perhaps because of the relatively large size of the injection.

In contrast to the linear time course of filling of the terminal, the initial time course of postsynaptic inhibition was better fitted by an exponential curve. When the injection was further from the edge of the active zone, as in the experiment illustrated in Fig. 3A, the onset of inhibition was delayed for a period of time. In

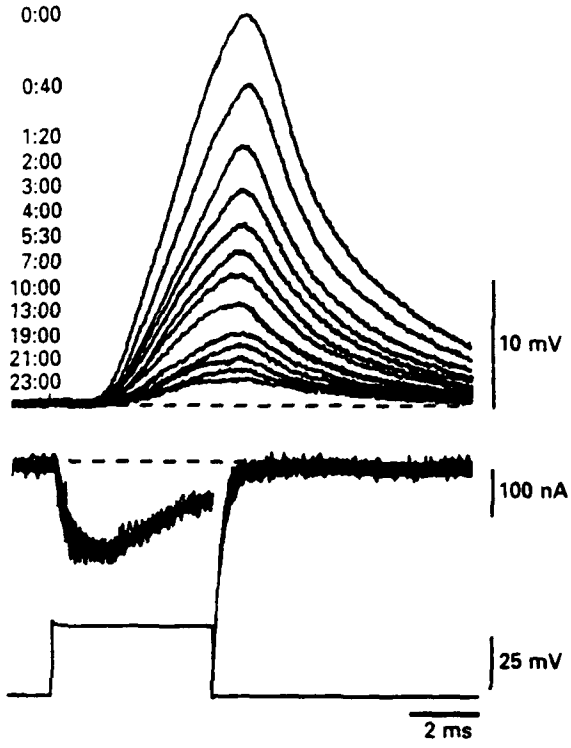

Fig. 2. Postsynaptic voltage (above) and presynaptic I_{Ca} (middle) following a presynaptic injection of synapsin I. A constant presynaptic voltage pulse was delivered at regular intervals before and after the injection (bottom). The postsynaptic responses illustrated were recorded at the intervals given by numbers to the left (in minutes).

some cases, the rate of reduction in PSP amplitude also appeared to decline as the wavefront approached the end of the terminal, suggesting that release from the most distal terminal region may not be as large as that from the rest of the preterminal.

Since the morphology of the preterminal varies quite markedly in length, position and diameter (Martin & Miledi, 1986), drawings were made of the terminals in all experiments in which dye-labelled proteins were injected. The amplitude of the postsynaptic potential is plotted as a function of time after synapsin I injection in Fig. 4 for five terminals (including those shown in Fig. 3) along with diagrams showing the movement of the dye through the terminal digit. The approximate position of the active synaptic release zone, as determined by microscopic observation, is indicated in Fig. 4*B*. Two injection sites were at the release zone; one was on the proximal edge, and two were several hundred micrometres distant from the proximal edge of the active zone. When synapsin I was injected at the *centre* of

the digit and the diffusion distance to the release sites was negligible, the blockade occurred almost immediately (up to 80% reduction within 1 min) in most cases. In such cases, presynaptic filling and complete blockade could occur in as little as 3–5 min, and the time to complete blockade was closely related to the time taken to

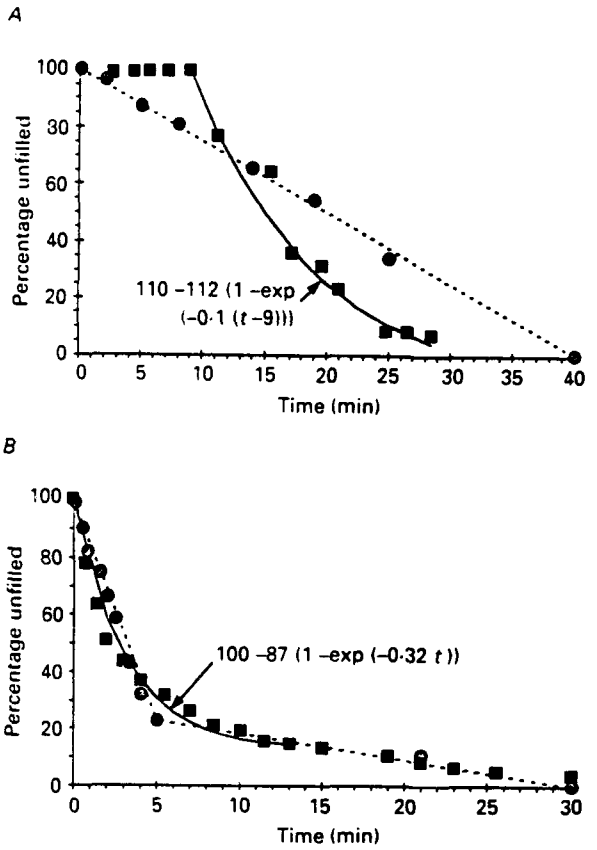

Fig. 3. Comparisons of the time course of PSP amplitude and terminal loading with Texas Red-labelled synapsin I, as determined by movement of the fluorescent wavefront. *A*, injection 300–400 μm from the proximal edge of the synaptic zone. Note linear filling of terminal by label (●). PSP amplitude began to decline exponentially about 10 min after synapsin I injection (■). *B*, injection near the proximal edge of the synaptic zone. Movement of label was initially linear, then slowed after 5 min while it diffused through the last third of the terminal (●). PSP amplitude began to decline immediately after injection, initially following an exponential time course, then becoming more linear after 10 to 15 min (■).

fill the entire terminal as determined by video analysis. In some cases the inhibition of transmitter release did not begin for up to 2 min after the injection, even in cases where synapsin I was deposited at the centre of the active zone region as, for example, injection no. 2 in Fig. 4. This small delay might be related to the size of the injections. Thus, in the case of injection no. 2, which was smaller than usual, diffusion to the release zone may have been prolonged.

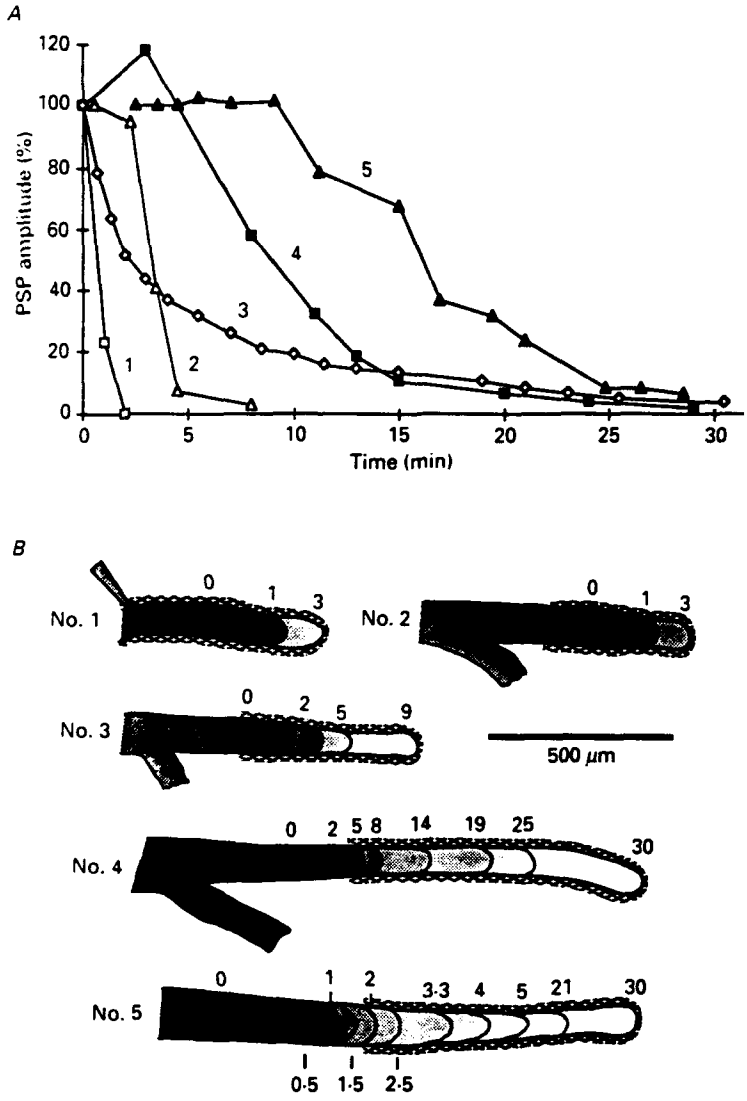

Fig. 4. Synapsin I loading and PSP amplitude. *A*, plot of PSP amplitude (as a percentage of pre-injection peak amplitude) as a function of time for five synapsin I injections at different points along the terminal finger as shown in *B*. Note progressively delayed onset and lower rate of inhibition when injection was farther from the end of the digit. *B*, reconstructions of terminals from video images showing the progression of the fluorescent wavefront at times (in minutes) indicated after injection. The electrode tip is indicated by black dot. Note that at $t = 0$, the volume of labelled synapsin I injected is indicated by the size of the region immediately surrounding the injection site. The location of the junction is indicated by the stippled pattern around the outside. The injection numbers (nos. 1–5) appear to the left of the reconstructions. Injections nos. 1 and 2 were within the active zone; no. 3 was near the proximal edge; and nos. 4 and 5 were approximately 200 and 400 μm proximal to the edge, respectively.

When synapsin I was injected close to the proximal border of the active zone area (injection no. 3), inhibition began within 1–2 min, but the time required for complete inhibition was longer, presumably because the protein had to travel farther to penetrate the entire terminal. As seen in Fig. 3*B*, and in Fig. 4 injection no. 3, 80% inhibition took 10 min to occur in this case. When synapsin I was injected several hundred micrometres from the terminal digit, a delay of 3–10 min was seen between injection and onset of blockade. In Fig. 4 injection no. 5 (300–400 μm from the active zone), synapsin I was not detected at the active zone until about 15 min after injection, while inhibition began at approximately 10 min. This temporal disparity may be accounted for by differences in threshold for visual detection *versus* synaptic inhibition, as discussed below.

Theoretical model for synapsin I action on synaptic transmission

In order to better understand the dynamics of terminal filling and PSP blockade, we developed a compartmental model for the diffusion of synapsin I into the presynaptic terminal in which n equal dimension compartments were placed end to end, and several compartments in the centre were filled with dye (or protein) at time 0 ($t = 0$). The fluorescent dye was then allowed to 'diffuse' through the compartments (Fig. 5). According to Fick's First Law of Diffusion

$$S_{ix} = -D_i \frac{\partial c_i}{\partial x},$$

where S = solute flow of the ith particle as a function of distance x, D = the diffusion coefficient, and c = concentration, the amount of dye diffusing between two compartments will depend on the difference in concentration between them. This is equivalent to assuming that at each time point, a fixed percentage ('D') of the dye in each compartment will move to either of the adjacent compartments. Here we have used a compartmental model, assuming for convenience that at each time point some percentage of the dye in each compartment, j, will move into each of the adjacent compartments, i.e.

$$c_{j,t} = (1-2D)\,c_{j,t-1} + D(c_{j-1,t-1} + c_{j+1,t-1}). \qquad (1)$$

where $c_{j,t}$ is the concentration of protein in compartment j at time t, and D is the 'diffusion coefficient' of the dye (here chosen to be 0·25).

The right-most compartment was closed to simulate the end of the terminal. To simulate the injection corresponding to the data shown in Fig. 3*A*, fourteen compartments 'distal' to the injection site at C_0 were used, with C_0 and the compartment on either side filled with 1000 units of dye at time 0.

Figure 5 shows the results of this simulation for the compartments C_n, where $n = -14$ to 14, from $t = 0$ to $t = 50$. As the dye moves through the terminal, the concentration in each compartment rises, but progressively more slowly with distance as the concentration gradient decreases along the terminal. Curve C_{13} is closer to C_{14} than to C_{12} because C_{14}, being the last compartment, only loses dye to C_{13}. The initial time of appearance of dye in each compartment is a linear function (indicated by the descending dashed line) since the diffusion rate at any point is

constant and independent of concentration. However, if there is a detection threshold for the fluorescence, say 1 unit (0·1% of the initial injection; horizontal dashed line), then beginning with compartment C_7, the diffusion rate of the dye will appear to slow significantly. Thus, between C_7 and C_{14}, the distances (times) between

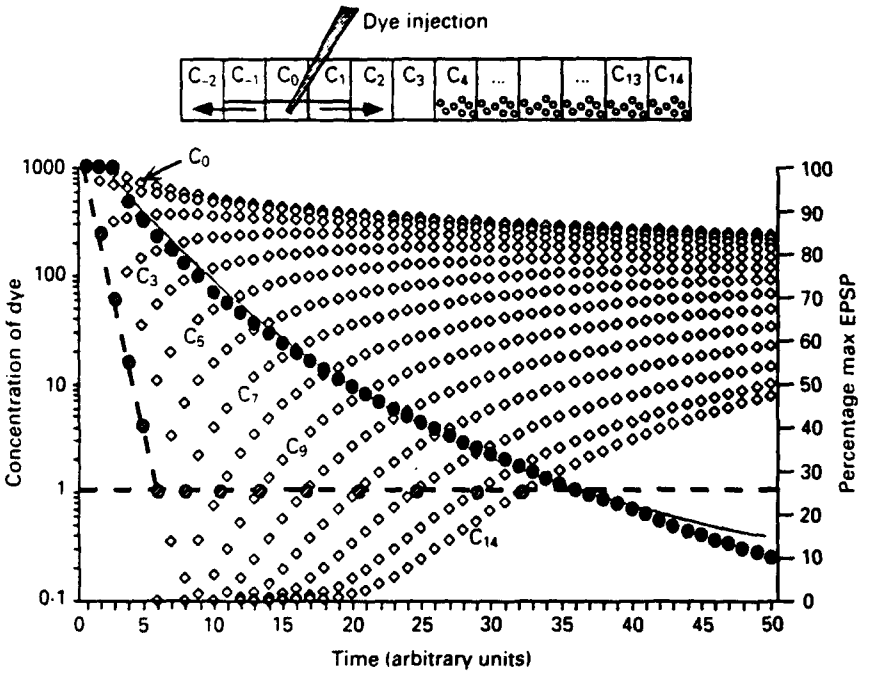

Fig. 5. Compartment model of diffusion of synapsin I along interior of the squid axon. The model consisted of twenty-nine compartments (C_{-14}–C_{14}; C_{-14}–C_{-3} not shown). The model illustrates the diffusion of synapsin I with respect to time in compartments C_0 (the centre of the 'injection') to C_{14} (the end of the terminal). The 'synaptic release zone' consisted of compartments C_4–C_{14}, each of which contained 1000 unbound 'vesicles.' A diffusion constant of 0·33 was assumed, with $k_3 = 300$. Curves marked with ◇ show the concentration of synapsin I (in arbitrary units) for compartments C_0 through C_{14} as a function of time after injection. Horizontal dashed line is hypothetical level for dye detection. The dye detection threshold generates a delay in visual detection of the dye in compartments C_7–C_{14} due to slow accumulation of dye (●). ● illustrate the theoretical decline of PSP amplitude in the presence of synapsin I.

the intersections of the horizontal threshold line and the concentration–time curves increase. These results are qualitatively consistent with the observed diffusion rate of labelled synapsin I, particularly the apparent slowing of the diffusion rate near the terminal end as in Fig. 3*B*.

Since the model for diffusion of synapsin I appeared to describe correctly the principal features of the dye movement, it was then expanded in an attempt to model the effects of synapsin I on transmission. This model, based on eqns (2) to (5) below, is based on the following assumptions. (a) The response amplitude (R) for a given stimulus is proportional to the sum of the vesicles released from all compartments

(eqn (2)). (b) The number of vesicles released from each compartment (N_{jR}) is proportional to the number of free vesicles in that compartment (N_{jF}) (eqn (3)). (c) The number of free vesicles in a given compartment equals the number in the starting pool at time 0 (V_0) less the number bound (N_{jB}) by synapsin I per compartment (eqn (4)). (d) The number of bound vesicles is proportional to the concentration of active (dephosphorylated, D) synapsin I (S_j^D) in a given compartment (j) (eqn (5)) (k_1, k_2 and k_3, are constants):

$$R = k_1 \sum_{j=-n}^{j} N_{jR}; \tag{2}$$

$$N_{jR} = k_2 N_{jF}; \tag{3}$$

$$N_{jF} = V_{0,j} - N_{jB}; N_{jF} \geq 0; \tag{4}$$

$$N_{jB} = k_3 [S_j^D]. \tag{5}$$

These equations reduce to eqn (6):

$$R = k_1 k_2 \sum_{j=-n}^{n} V_0 - (k_3 [S_j^D]) \tag{6}$$

The diffusion parameter D, the constant, k_3 (which presumably corresponds to the 'activity' of dephosphorylated synapsin I in terms of vesicle binding), the size and location of the injection (1000 units of synapsin I injected into each of compartments C_{-1}, C_0, and C_1), and the size of the active zone (compartments C_1 through C_{14}, each containing 1000 vesicles) were chosen to simulate the data of injection no. 4 (Fig. 4). For simplicity, we have assumed that the product of the constants $k_1 k_2 = 1$ in this simulation. The constant k_3 was then adjusted to produce approximately 90% inhibition at the final time point. The shape of this curve is neither linear nor exponential, as shown by superimposing an exponential curve whose parameters were adjusted to match the initial decline of the inhibition curve. In fact, as 'inhibition' proceeds, the curve becomes increasingly linear, precisely as seen with injections nos. 3, 4 and possibly 5. An important feature of the model which contributes to the changing rate of inhibition seen in this curve is the assumption that the number of free vesicles cannot be less than zero (eqn (4)). Thus when all vesicles in a compartment are bound, it cannot contribute further to inhibition.

Reversibility of synapsin I reduction of neurotransmitter release

In most experiments a rapid and profound block of synaptic transmission followed synapsin I injection, indicating that the release mechanism was totally overwhelmed. It was assumed that injection of a smaller amount of synapsin I might allow a recovery of synaptic transmission. This experiment would also serve as a test for any possible deleterious effects of the synapsin I injections on transmitter release *per se*.

As illustrated in Fig. 6, recovery of transmitter release was observed when a smaller amount of synapsin I was injected in a synapse which remained in excellent condition for 90 min after the injection. The pre-injection responses for a set of depolarization steps are shown in Fig. 6*A* and *B*. Similar sets of presynaptic pulses

were generated 12, 25 and 75 min later. In each case the corresponding presynaptic calcium currents (Fig. 6*A*) were comparable to the controls. The postsynaptic responses, which were markedly reduced at 12 and 25 min, recovered to nearly normal levels by 75 min. The plot of peak PSP amplitudes for each stimulus level as a function of time after injection (Fig. 6*B*) showed that recovery began between 12 and 25 min after the injections.

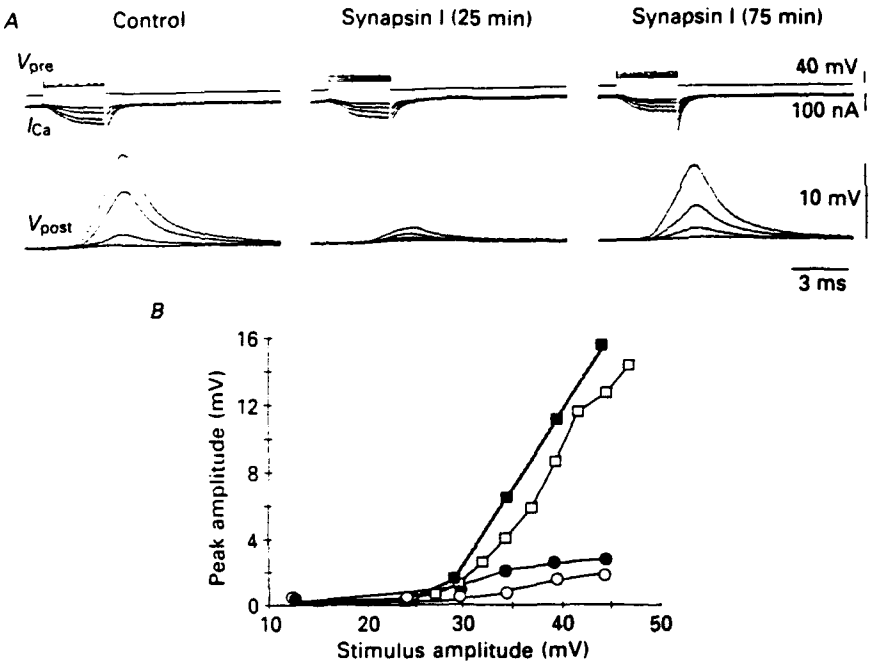

Fig. 6. Reversibility of synapsin I inhibition of neurotransmitter release. *A*, time course of recovery of transmission after synapsin I injection. Four presynaptic voltage-clamp steps (upper) were delivered at each time interval which resulted in a graded series of Ca^{2+} current (middle) and PSP (lower) responses. Postsynaptic responses were strongly depressed at 25 min compared to pre-injection responses, while presynaptic Ca^{2+} current was unaffected. PSP amplitudes recovered to near-normal levels by 75 min. *B*, plot of peak PSP values as a function of voltage-step amplitude showing maximum inhibition at about 12 min. ■, 0 min; ○, 12 min; ●, 25 min; □, 75 min.

Injection of phosphorylated synapsin I into the presynaptic terminal

Further experiments were designed to test the effect of phosphorylation of the various sites of synapsin I on its ability to affect transmission. Samples of phosphosynapsin I (in which only the head region or only the tail region, or both, were phosphorylated) were prepared and injected into a number of synapses (see Table 1).

Two examples of results from each type of injection are shown in Fig. 7. In the cases of synapsin I phosphorylated in the head and tail regions (head–tail-phosphorylated synapsin I; Fig. 7*A*), or synapsin I phosphorylated only in the tail region (tail-phosphorylated synapsin I; Fig. 7*B*), the injection had no effect on synaptic transmission. The slight increase after the injection and gradual reduction

of the synaptic response in the case of one tail-phosphorylated synapsin I injection (upper curve, Fig. 7*B*) was similar to responses seen in some control experiments where either avidin or heat-treated synapsin I was injected (see below). In contrast, transmission was inhibited by synapsin I phosphorylated only in the head region

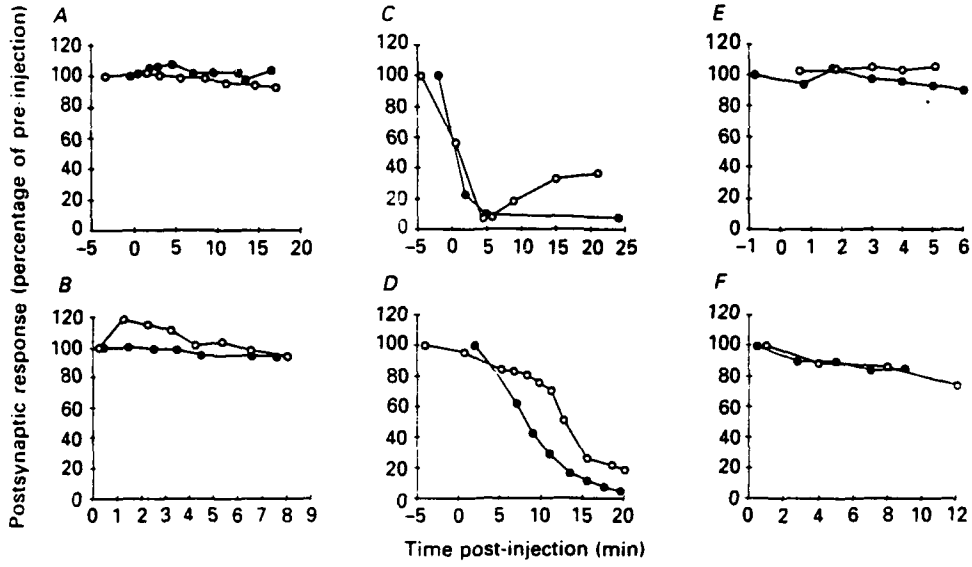

Fig. 7. Results of presynaptic injection of various phosphorylated forms of synapsin I. Two experiments are shown for each type of injection. Note that head and tail phosphorylation (*A*) or tail-only phosphorylation (*B*) of synapsin I prevented inhibition, while head phosphorylation (*C*) did not. *D*, injection of 'mock' phospho-synapsin I (prepared as head-tail-phosphorylated synapsin I except for the omission of ATP from the phosphorylation reaction) blocked transmission. Injections of heat-treated synapsin I (*E*) or avidin (*F*) did not affect transmitter release. Data are plotted as a percentage of pre-injection PSP amplitude.

(head-phosphorylated synapsin I; Fig. 7*C*). Note that there was some recovery from inhibition in the case of one of the head-phosphorylated synapsin I injections, indicating a reversible action as shown for dephosphorylated synapsin I in Fig. 6. In all of the cases illustrated in Fig. 7, the I_{Ca} was unchanged by the protein injection (not shown).

Since the ineffectiveness of some of the phosphorylated forms of synapsin I could have been due to inactivation of the protein during the phosphorylation reaction, it was felt that an additional control for the negative results with the phosphorylated forms of synapsin I was required. For this reason, 'mock' phospho-synapsin I was prepared (see Methods) in which both enzymes necessary for phosphorylating both the head and tail regions were present, but ATP was omitted to prevent actual phosphorylation. In this case, inhibition of transmission was observed exactly as seen with conventionally prepared synapsin I (Fig. 7*D*).

In summary, the results of injections of the phosphorylated forms of synapsin I confirmed our initial findings that phosphorylation of the tail region of synapsin I

abolishes its ability to block synaptic release (Llinás *et al.* 1985). Phosphorylation of the head region does not influence the inhibitory ability of synapsin I, nor does it reverse the effect of tail phosphorylation.

Injections of heat-treated synapsin I and of avidin

It was previously determined that heating the synapsin I molecule abolishes its ability to block synaptic transmission (Llinás *et al.* 1985). Examples of two such injections are shown in Fig. 7*E*. As an additional control for certain physical properties of synapsin I, Texas Red-labelled avidin was injected. Avidin is a protein which has a size ($M_r = 63000$) and pI (10·6) similar to those of synapsin I. These experiments were performed in a manner similar to those described for synapsin I. The postsynaptic response as a function of time after two avidin injection experiments is shown in Fig. 7*F*, which indicates little or no effect on transmission. The relationship between the postsynaptic response and the diffusion of avidin as reconstructed from video analysis for one of these injections is shown in Fig. 8. The diffusion rate was similar to that of synapsin I, ranging between 23 and 54 μm min^{-1} (mean $\pm$ S.D. $= 39 \pm 12$; $n = 4$). Avidin had no effect on transmitter release even when monitored up to 30 min after injection, at which time the fluorescence was relatively evenly distributed throughout the terminal. Note in the experiment illustrated in Fig. 8*C* that the diffusion rate for avidin is nearly constant along the entire length of the terminal.

CaM kinase II and transmitter release

Injection of CaM kinase II

The previous set of experiments indicated that synapsin I in its dephosphorylated form blocked synaptic transmission while tail-phosphorylated synapsin I had no effect. Further studies were designed to test the hypothesis that CaM kinase II acts to modulate the synapsin I-dependent binding of synaptic vesicles to the intracellular matrix. If the enzyme dissociates vesicles from their attachments by phosphorylating an endogenous synapsin I-like molecule, increasing the endogenous CaM kinase II normally present in the terminal should increase transmitter release. In our preliminary study in the squid synapse, the injection of CaM kinase II markedly facilitated transmitter release without significantly modulating the presynaptic Ca^{2+} current in each of three experiments (Llinás *et al.* 1985). The diffusion rate of CaM kinase II was not directly assessed because labelling with any of the usual dyes was found to interfere with its solubility and/or ability to phosphorylate synapsin I.

In the present study injection of of CaM kinase II was followed by facilitation of transmitter release in all but one experiment. In eight out of nine experiments, transmitter release was facilitated after the injection of CaM kinase II as shown for one synapse in Fig. 9. Blockage of transmission was seen in one experiment, although there was no obvious damage to the synapse. In five experiments which were analysed quantitatively, the mean per cent facilitation was 409 ± 157%. The maximal facilitation usually occurred between 10 and 20 min after injection. Presynaptic voltage steps of different amplitudes were applied to the presynaptic terminal while employing a double voltage clamp to determine I_{Ca} and postsynaptic

current (I_{post}). The double voltage clamp was preferable in order to prevent the postsynaptic potential from reaching the PSP reversal potential during facilitation by CaM kinase II, which would result in response saturation.

A double voltage-clamp experiment showing facilitation following CaM kinase II injection is illustrated in Fig. 9. The time course and amplitude of I_{post} (post-injection

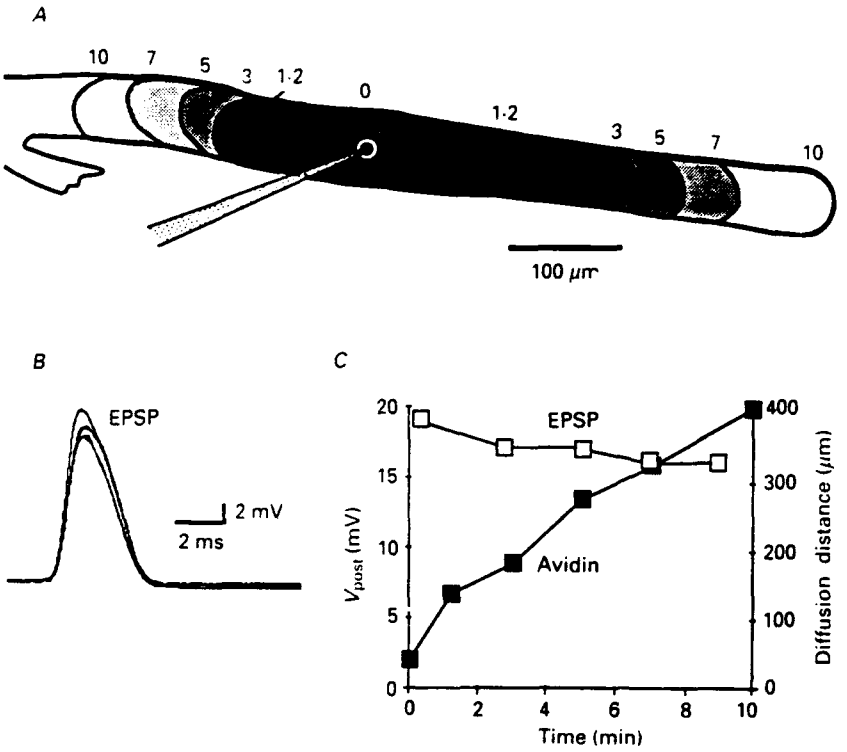

Fig. 8. Effect of injection of Texas Red-labelled avidin on synaptic transmission. *A*, diffusion of dye along synaptic digit as a function of time (numbers above drawing; in minutes), as determined by enhanced image from the video monitor. Black dot marks electrode tip; immediately surrounding stippled area is volume filled after initial injection. *B*, PSPs between 0 and 10 min following avidin injection showing this protein had a minimal effect on the PSP. *C*, plot of diffusion distance and PSP amplitude as a function of time showing linear avidin diffusion rate and minimal effect on transmission.

current) for three different times and levels of presynaptic depolarization are shown. Following CaM kinase II injection, the PSP was facilitated as early as 2 min post-injection, and increased in amplitude by over 600%. This facilitation was associated with a corresponding increase in the rate of rise in I_{post} for a given level of I_{Ca}. In Fig. 9*C*, the postsynaptic current increased to the point of saturation, as evidenced by the flattened top of the response. Note that, in this experiment, the amplitude onset kinetics (Llinás *et al.* 1981*a*, *b*) and the tail component of the macroscopic inward calcium current were not modified by CaM kinase II. Moreover, these currents were similar to those previously reported in the absence of CaM kinase II (Llinás *et al.* 1981*a*, 1982; Augustine *et al.* 1985). Figure 10 illustrates the relative enhancement

of the PSP and PSI following CaM kinase II injection for four experiments. The actual ranges of PSP and PSI amplitudes for each experiment are noted at the right. Data from three experiments overlap, while one synapse had a more delayed and slower rising facilitation. Exponential curves were then empirically fitted to this range of data (thin continuous lines).

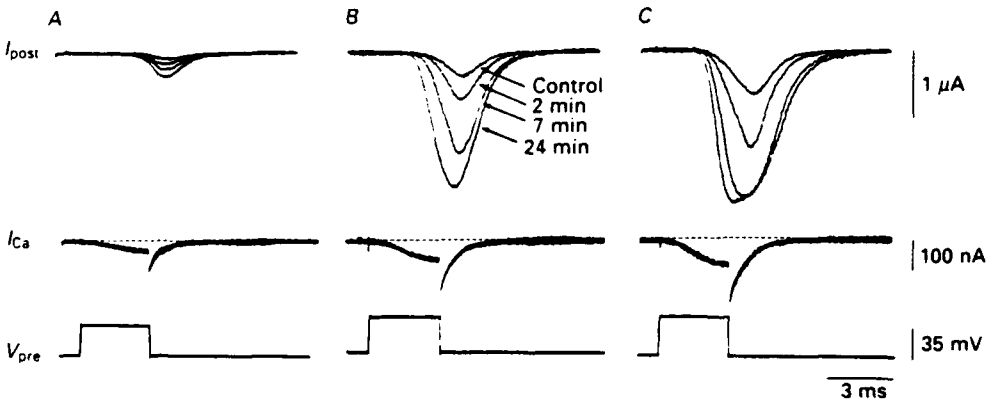

Fig. 9. Recordings showing time course of facilitation of synaptic transmission after CaM kinase II injection into the presynaptic digit. *A*, *B* and *C*: postsynaptic currents (upper traces) in response to 25, 30 and 35 mV presynaptic voltage-clamp steps (lower traces). Responses to each step were recorded before and at the three times after the injection noted in *B*. Note that I_{Ca} (middle traces) at each stimulus level was constant over time. At the highest stimulus level (*C*), postsynaptic response saturation occurred at 24 min.

Theoretical model for CaM kinase II action on synaptic transmission

If the hypothesis is correct that CaM kinase II acts on neurotransmitter release by regulating the phosphorylation state of synapsin I, then the model of vesicle release presented above should also apply to the facilitation produced by CaM kinase II. In particular, k_3 can be considered to be related to the degree of phosphorylation and inactivation of synapsin I by CaM kinase II. Starting with eqn (6) above, we may assume that the ratio of the concentrations of the phosphorylated to dephosphorylated synapsin I ($[S^P]/[S^D]$) is directly proportional to the concentration of CaM kinase II ([CK]), i.e.

$$\frac{[S^P]}{[S^D]} = k_4[CK], \tag{7}$$

where k_4 is a constant. Equation (6) can then be rewritten with respect to the individual compartments (j):

$$R = k_1 k_2 \sum_{j=-n}^{n} V_0 - \frac{k_3[S^T]_j}{1 + k_4[CK]_j}, \tag{8}$$

where $[S^T]_j$ is the total phosphorylated plus dephosphorylated synapsin I in each compartment.

To simulate an injection of CaM kinase II, eqn (1) was used to model diffusion of CaM kinase II through the terminal, with S^T set to a constant value in each

compartment. The parameters of the model (eqn (8)) were then adjusted to produce a curve which fell roughly in the centre of the range of experimental data. These values are shown as a thick line in Fig. 10. The specific parameter values were: $k_1 = k_2 = 1$. $S^T = 10000$. $k_3 = 1$. and $k_4 = 0{\cdot}0002$. The value of [CK] was set to

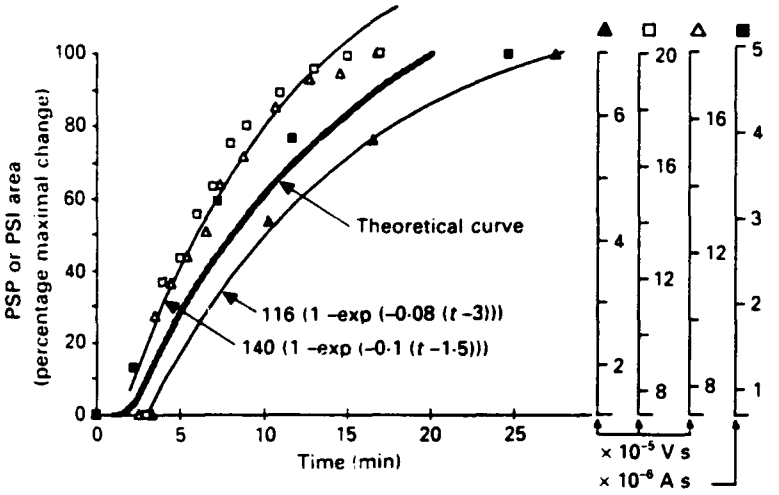

Fig. 10. The time course of synaptic facilitation by CaM kinase II in four experiments (absolute scales shown at right). Two empirically determined exponential curves (thin continuous lines) which enclose the entire data range were calculated. Parameters for the theoretical facilitation model were adjusted so the resulting inhibition curve would fall in the centre of the data range (thick stippled line).

5 units except for compartments C_{-2} through C_2 which were 'filled' with 1000 units. The active zone was modelled as extending from compartments C_3 through C_{14}; these compartments were each filled with 10^4 vesicles at time 0 ($V_0 = 10^4$). This model produced an exponential rate of facilitation very similar to that observed experimentally. As was the case with the synapsin I inhibition model, however, this curve was affected by the extent to which response facilitation was allowed. Thus it was assumed that a finite number of vesicles in the pre-terminal can be made available for release; i.e. the size of the 'releasable' pool is limited. (The same effect would be achieved if the rate of vesicle release during depolarization is limited.)

Analysis of maximum rate of rise of postsynaptic response

If synapsin I and CaM kinase II affect synaptic transmission by modulating the number of vesicles available for release–without modifying the dynamics of the release process *per se*, one would *not* expect the rate of vesicle release to change as a function of time. In fact, it would be expected that the effect of CaM kinase II on the probability of release (P) would be independent of time, i.e. it would not affect the kinetics of transmitter release (N) (Katz, 1968). If this were the case, the amplitude of the PSP would increase, while the shape of the waveform would remain constant.

In order to determine whether synapsin I and CaM kinase II altered the release kinetics, the maximum rate of rise (MRR) of the postsynaptic response and the peak amplitude (R_{peak}) were determined for each response. The normalized maximum rate

of rise (NMRR) was then calculated for each response as MRR/R_{peak}. Note that if two waveforms are scalar multiples of each other, then their NMRR values should be equal. In two typical uninjected synapses, postsynaptic currents were measured in response to stimulus pulses between 25 and 40 mV and the NMRR values calculated. The stimulus series were repeated twice in one and three times in

TABLE 2. Mean normalized maximal rate of rise (NMRR) values (±S.D.) for experimental subgroups in which voltage or current was recorded

	Voltage recording				Current recording			
	Synapsin I		CaM kinase II		Synapsin I		CaM kinase II	
Time (min)	0	22·56	0	14·5	0	19·4	0	29·667
NMRR	0·825 ± 0·387	0·722 ± 0·286	0·320 ± 0·037	0·400 ± 0·130	0·629 ± 0·075	0·630 ± 0·057	0·841 ± 0·258	0·700 ± 0·076
N	11		2		5		3	
t	1·663		−1·212		−0·050		1·253	
P	0·127		0·439		0·957		0·337	

Mean times of post-injection recordings are as noted. Paired t test values for within-group comparisons and P scores are shown. No within-group mean differences were significant.

the other synapse. The mean NMRR values at each stimulus amplitude for the five stimuli series was calculated and plotted against stimulus amplitude. A linear regression coefficient of $R^2 > 0{\cdot}95$ was found with a slope of $-5{\cdot}1 \times 10^{-4}$ mV ms^{-1} mV^{-1}. NMRR values for the same stimulus amplitude were quite close in successive stimulus runs, although the mean NMRR was significantly different for the two synapses (0·015 ms^{-1} and 0·030 ms^{-1} at 30 mV respectively).

A similar analysis of NMRR was carried out for synapsin I and CaM kinase II injection experiments. For each experiment, the NMRR was calculated for a time immediately pre-injection and again at a point 15–30 min later after significant inhibition or facilitation had occurred. Since the shapes of the postsynaptic response waveforms differed depending on whether postsynaptic voltage or current was being measured, they were analysed separately. The results of NMRR analysis for sixteen synapsin I and five CaM kinase II experiments are shown in Table 2, in which the means of the pre- and post-injection response amplitudes are given along with the mean post-injection measurement times. Note that for CaM kinase II, the mean facilitation is only 200–300% due to elimination of some of the largest responses in which saturation occurred. Within each of the four experimental subgroups (synapsin I or CaM kinase II) × (voltage or current)), the mean values were not significantly different ($P > 0{\cdot}1$, paired t test).

All experiments in which postsynaptic voltage was measured were then compared using an unpaired t test, and similarly, comparisons were made between all groups in which current was measured. In neither case were any significant differences found ($P > 0{\cdot}1$). Note that although the mean for the synapsin I voltage measurements is considerably larger than that for CaM kinase II, the latter is based on only two experiments. Finally, linear correlation analysis of NMRR was performed in several experiments in which multiple time points were measured (cf. Figs 3 and 10). In no

case was a significant correlation between NMRR and time post-injection found. These results indicate that the kinetics of vesicle release were unaffected by synapsin I or CaM kinase II. On the basis of these data, we conclude that during the time course of a given postsynaptic response, the probability of release was modified uniformly by synapsin I and by CaM kinase II.

DISCUSSION

The major findings of these experiments are as follows: (1) the degree of inhibition of transmitter release by dephosphorylated synapsin I is well correlated with the degree of invasion of the protein along the length of the presynaptic terminal. (2) Tail-phosphorylated synapsin I and heat-treated synapsin I have no effect on release. (3) Inhibition by dephosphorylated synapsin I is reversible. (4) CaM kinase II facilitates synaptic release. (5) The shape of the postsynaptic response waveform is not affected by either synapsin I or CaM kinase II over the duration of the response. We conclude from these data that the dynamics of synaptic transmission, specifically the number of vesicles available for release, are probably regulated by the ratio of tail-phosphorylated to dephosphorylated synapsin I which is determined enzymatically by CaM kinase II.

Synapsin I

The experiments involving injection of phosphorylated and dephosphorylated synapsin I showed that the rates of blockade of synaptic transmission were highly correlated with: (a) the state of phosphorylation of the protein, (b) the site of injection and (c) the rate of movement of the protein through the terminal. When the protein injections were large enough to fill rapidly most of the active release zone, the times to onset of blockade were short. Conversely, when synapsin I was injected far from the release site, the onset of the block was delayed. These data suggest that synapsin I acts specifically at the active zones to affect release.

The injection procedures *per se* did not appear to interfere with any aspect of synaptic transmitter release, including the availability of transmitter or the calcium current. Rather, three sets of experiments suggest that the effect of synapsin I on transmitter release is specific and dependent on the structure of this molecule. First, injections of synapsin I in which the tail only or both the head and tail were phosphorylated had no effect on release. Second, injection of heat-treated synapsin I also failed to affect release. Third, injection of avidin, a basic protein similar in size and pI to synapsin I did not alter synaptic transmission. In all these experiments, the injected proteins completely filled the presynaptic terminal. Therefore it is necessary for the tail site of synapsin I to be in the dephosphorylated state for it to block transmitter release.

As an additional test of the ability of synapsin I to bind to intracellular elements and inhibit vesicle movement, phosphorylated or dephosphorylated synapsin I was introduced into extruded squid axoplasm and the effect on the movement of subcellular organelles monitored by video-enhanced microscopy (McGuinness, Brady, Gruner, Sugimori, Llinás & Greengard, 1987; McGuinness *et al.* 1989). Following the injection of dephosphorylated synapsin I, both orthograde and

anterograde flow were significantly reduced. Injection of synapsin I phosphorylated only at the head partially inhibited organelle movement, and synapsin I phosphorylated only at the tail lacked any inhibitory effect. Injected CaM kinase II, in the presence of calcium and calmodulin, prevented the inhibitory effect of synapsin I. Dephosphorylated synapsin I does not appear to directly inhibit the transport mechanism subserving organelle movement, since the organelle movement along microtubules at the edges of the axoplasm (where the cytoskeletal structure was sparse) was unmodified by synapsin I (McGuinness *et al.* 1989). These data are consistent with the hypothesis that synapsin I immobilizes or restrains vesicles and/or other organelles by cross-linking them to cytoskeletal elements and that this cross-linking can be modulated by CaM kinase II.

CaM kinase II

CaM kinase II is capable of increasing transmitter release by up to sevenfold (Figs 9 and 10), which indicates that it plays a decisive role in the release process. At this time we cannot exclude the possibility that CaM kinase II has some minor effect on the calcium channel. However, the results obtained would require an approximately 50% increase in calcium entry even if a fourth-order relationship between I_{Ca} and transmitter release is assumed. This is totally inconsistent with the present data, which shows no detectable change in I_{Ca} within the limits of a measurement error of $< 5\%$.

In the present experiments, we observed an increase in the maximum rate of rise (MRR) of the postsynaptic response following CaM kinase II injections, confirming earlier findings (Llinás *et al.* 1985). Here we investigated the MRR in more detail to determine if the shape of the response (which is dependent on vesicle release kinetics) also changed following presynaptic protein injections. The rationale for this analysis is as follows. The variable N_{jR} (eqn (2)), which represents the number of vesicles released from a given compartment in response to a given depolarization, may be represented more explicitly as a function of time from the onset of the stimulus; i.e.

$$N_{jR} = \int_{t=0}^{\infty} P(t)\,dt,$$

where $P(t)$ represents the probability that a given vesicle will be released as a function of time after depolarization, and 'N' would be proportional to the number of vesicles available for release (Katz, 1968). Thus, doubling the number of available vesicles should, at least within certain limits, double the amplitude of the response. If $P(t)$ is unchanged, then the shape of the waveform should remain constant, depending only on N. In that case, then, the rate of change of response amplitude at any point on the curve should be proportional to the peak amplitude, and therefore the maximal rate of rise divided by the peak amplitude (NMRR) should be constant. This was in fact found when all successful injections of synapsin I or CaM kinase II were analysed either by comparing across experiments before and after injection, or within experiments as a function of time after injection. We conclude that these proteins do not alter dynamic aspects of vesicle release such as the duration of opening of ion channels or the rate of vesicle exocytosis. The most plausible mechanism, as initially suggested in a previous paper (Llinás *et al.* 1985) and

supported by *in vitro* studies (cf. Greengard *et al.* 1987), is that CaM kinase II acts to increase availability of synaptic vesicles by phosphorylating synapsin I. The ability of CaM kinase II to increase transmitter release from presynaptic terminals has recently been confirmed using rat brain synaptosomes (Nichols, Wu, Haycock & Greengard, 1989).

Model of preterminal protein diffusion, and of synaptic transmitter modulation by presynaptic protein injection

The simulations of postsynaptic inhibition and facilitation presented above were designed as a heuristic tool to test whether the observed rates of PSP inhibition and facilitation could be predicted by a unified model of vesicle release in which the amplitude of a PSP is dependent on phosphorylation of synapsin I by CaM kinase II. The data were, in fact, highly consistent with the model of release described by eqns (1) to (7) above. The compartmental model correctly describes the time courses of both inhibition by synapsin I and facilitation by CaM kinase II (eqns (7) and (8)). In both cases, limits on the number of vesicles available for release were included, and not found to affect the shape of the curves.

General hypothesis relating synapsin I to transmitter release: facilitation of transmitter release by calcium-dependent mobilization of synaptic vesicles

The ubiquitous nature of synapsin I in presynaptic terminals (DeCamilli *et al.* 1983), and the fact that its injection at the release site is capable of modulating transmitter release, raises the question of the mechanism by which synapsin I affects release. While we cannot exclude the possibility that synapsin I might be an integral part of the machinery for transmitter release itself, several facts argue against this view. First, if phosphorylated synapsin I were to directly promote vesicle release, one would expect that its injection would produce, following calcium entry, a continuous transmitter release leading to vesicle depletion and transmission failure. This was never observed. Furthermore, recent experiments failed to find any increase in miniature endplate potential frequency following such injections (Llinás, Sugimori, Lin, McGuinness & Greengard, 1988; Lin, Sugimori, Llinás, McGuinness & Greengard, 1990).

Another argument against synapsin I being a direct transmitter-release agent involves the time course of phosphorylation by CaM kinase II following calcium entry. The onset of transmitter release in the squid giant synapse begins as soon as 180 μs following calcium entry (Llinás *et al.* 1981*b*; Llinás *et al.* 1982) and peaks at about 1 ms. In contrast, the turnover rate for phosphorylation of synapsin I by CaM kinase II, calculated from data in McGuinness *et al.* (1985), is approximately 17 ms. It is thus difficult to see how this relatively slow phosphorylation reaction could produce the time course associated with a PSP, which is over within a few milliseconds.

Since synapsin I does not appear to be directly involved in vesicular release, we propose instead that it regulates the availability of vesicles for release. The biochemical and physiological studies noted above indicate that synapsin I restrains vesicles, probably close to the presynaptic release site, so that they cannot be released during depolarization. Calcium entry would thus trigger two events. First,

synaptic vesicles would be released, possibly by direct electrostatic shielding of negative charges by calcium or some other intermediate step. Second, a delayed effect independent of the release mechanism would occur after calcium had moved beyond the release site, by increasing the number of releasable vesicles following phosphorylation of synapsin I via activation of CaM kinase II. Physiological measurements indicate that the resting calcium conductance may have a powerful effect on the number of vesicles available at a given time (Simon, Sugimori & Llinás, 1984; Simon & Llinás, 1985). Indeed, resting calcium influx near the active zones may establish a steady-state level of phosphorylated synapsin I for regulation of vesicle availability close to the release site. The occurrence of an action potential would then increase the number of readily releasable vesicles by increasing the local calcium concentration and enhancing synapsin I phosphorylation. Such facilitation may underlie what has been considered to be calcium-dependent facilitation. This hypothesis is particularly attractive in the case of the squid giant synapse, as the large diameter of the preterminal would make it difficult to accumulate Ca^{2+} at the active zone.

This research was supported by Grant AFOSR850368 from the United States Air Force (R.L.) and MH 39327 (P.G.).

REFERENCES

AUGUSTINE, G. J. & CHARLTON, M. P. (1986). Calcium dependence of presynaptic calcium current and post-synaptic response at the squid giant synapse. *Journal of Physiology* **381**, 619–40.

AUGUSTINE, G. J., CHARLTON, M. P. & SMITH, S. J. (1985). Calcium entry into voltage-clamped presynaptic terminals of squid. *Journal of Physiology* **367**, 143–62.

AUGUSTINE, G. J., CHARLTON, M. P. & SMITH, S. (1987). Calcium action in synaptic transmitter release. *Annual Reviews* **10**, 633–693.

BAHLER, M. & GREENGARD, P. (1987). Synapsin I bundles F-actin in a phosphorylation-dependent manner. *Nature* **326**, 704–707.

BENFENATI, F., BAHLER, M., JAHN, R. & GREENGARD, P. (1989). Interactions of synapsin I with small synaptic vesicles: Distinct sites in synapsin I bind to vesicle phospholipids and vesicle proteins. *Journal of Cell Biology* **108**, 1863–1872.

BULLOCK, T. & HAGIWARA, S. (1957). Intracellular recording from the giant synapse of the squid. *Journal of General Physiology* **40**, 565–577.

CZERNICK, A. J., PANG, D. T. & GREENGARD, P. (1987). Amino acid sequences surrounding the cAMP-dependent and calcium/calmodulin-dependent phosphorylation sites in rat and bovine synapsin I. *Proceedings of the National Academy of Sciences of the USA* **84**, 7518–7522.

DECAMILLI, P., BENFENATI, F., VALTORTA, F. & GREENGARD, P. (1990). The synapsins. *Annual Review of Cell Biology* **6**, 433–460.

DECAMILLI, P., CAMERON, R. & GREENGARD, P. (1983). Synapsin I (protein I), a nerve terminal-specific phosphoprotein. I. Its general distribution in synapses of the central and peripheral nervous system demonstrated by immunofluorescence in frozen and plastic sections. *Journal of Cell Biology* **96**, 1337–1354.

DECAMILLI, P. & GREENGARD, P. (1986). Synapsin I: A synaptic vesicle-associated neuronal phosphoprotein. *Biochemical Pharmacology* **35**, 4348–4355.

GRAND, R. J. A., PERRY, S. V. & WEEKS, R. A. (1979). Troponin C-like proteins (calmodulins) from mammalian smooth muscle and other tissues. *Biochemical Journal* **177**, 521–529.

GREENGARD, P., BROWNING, M. D., MCGUINNESS, T. L. & LLINÁS, R. (1987). Synapsin I, a phosphoprotein associated with synaptic vesicles: possible role in regulation of neurotransmitter release. *Advances In Experimental Medicine and Biology* **221**, 135–153.

HACKETT, J. T., COCHRAN, S. L., GREENFIELD, L. J., BROSIUS, D. C. JR & UEDA, T. (1990). Synapsin I injected presynaptically into goldfish Mauthner axons reduces quantal synaptic transmission. *Journal of Neurophysiology* **63**, 701–706.

HAGIWARA, S. & TASAKI, I. (1958). A study on the mechanism of impulse transmission across the giant synapse of the squid. *Journal of Physiology* **143**. 114–137.

HUTTNER, W. B., DEGENNARO, L. J. & GREENGARD, P. (1981). Differential phosphorylation of multiple sites in purified protein I by cyclic AMP-dependent and calcium-dependent protein kinases. *Journal of Biological Chemistry* **256**. 1482–1488.

HUTTNER, W. B. & GREENGARD, P. (1979). Multiple phosphorylation sites in protein I and their differential regulation by cyclic AMP and calcium. *Proceedings of the National Academy of Sciences of the USA* **76**. 5402–5406.

HUTTNER, W. B., SCHEIBLER, W., GREENGARD, P. & DECAMILLI, P. (1983). Synapsin I (protein I), a nerve terminal-specific phosphoprotein: its association with synaptic vesicles studied in a highly purified synaptic vesicle preparation. *Journal of Cell Biology* **96**. 1374–1388.

KACZMAREK, L. K., JENNINGS, K. R., STRUMWASSER, I., NAIRN, A. C., WALTER, U., WILSON, F. D. & GREENGARD, P. (1980). Microinjection of catalytic subunit of cyclic AMP-dependent protein kinase enhances calcium action potentials of bag cell neurons in cell culture. *Proceedings of the National Academy of Sciences of the USA* **77**. 7487–7491.

KATZ, B. (1968). *The Release of Neuronal Transmitter Substances*. Charles C. Thomas. Liverpool.

KATZ, B. & MILEDI, R. (1967). A study of synaptic transmission in the absence of nerve impulses. *Journal of Physiology* **192**. 407–436.

KENNEDY, M. B. & GREENGARD, P. (1981). Two calcium/calmodulin-dependent protein kinases, which are highly concentrated in brain, phosphorylate protein I at distinct sites. *Proceedings of the National Academy of Sciences of the USA* **78**. 1293–1297.

KENNEDY, M. B., MCGUINNESS, T. & GREENGARD, P. J. (1983). A calcium/calmodulin-dependent protein kinase from mammalian brain that phosphorylates synapsin. I. Partial purification and characterization. *Journal of Neuroscience* **3**. 818–831.

LIN, J. W., SUGIMORI, M., LLINÁS, R., MCGUINNESS, T. & GREENGARD, P. (1990). Effects of synapsin I and calcium/calmodulin-dependent protein kinase II on spontaneous neurotransmitter release in the squid giant synapse. *Proceedings of the National Academy of Sciences of the USA* **87**. 8257–8261.

LLINÁS, R., MCGUINNESS, T., LEONARD, C. S., SUGIMORI, M. & GREENGARD, P. (1985). Intraterminal injection of synapsin I or calcium/calmodulin-dependent protein kinase II alters neurotransmitter release at the squid giant synapse. *Proceedings of the National Academy of Sciences of the USA* **82**. 3035–3039.

LLINÁS, R., STEINBERG, I. Z. & WALTON, K. (1976). Presynaptic calcium currents and their relation to synaptic transmission: voltage clamp study in squid giant synapse and theoretical model for the calcium gate. *Proceedings of the National Academy of Sciences of the USA* **73**. 2913–2922.

LLINÁS, R., STEINBERG, I. Z. & WALTON, K. (1981*a*). Presynaptic calcium currents in squid giant synapse. *Biophysical Journal* **33**. 289–321.

LLINÁS, R., STEINBERG, I. Z. & WALTON, K. (1981*b*). Relationship between presynaptic calcium current and postsynaptic potential in squid giant synapse. *Biophysical Journal* **33**, 323–352.

LLINÁS, R. & SUGIMORI, M. (1978). Double voltage clamp study in squid giant synapse. *Biological Bulletin* **155**. 454.

LLINÁS, R., SUGIMORI, M., LIN, J. W., MCGUINNESS, T. & GREENGARD, P. (1988). Effects of synapsin I and CAM kinase II on evoked and spontaneous transmitter release in the squid giant synapse. *Biological Bulletin* **175**. 307.

LLINÁS, R., SUGIMORI, M. & SIMON, S. M. (1982). Transmission by presynaptic spike-like depolarization in the squid *Loligo pealii* giant synapse. *Proceedings of the National Academy of Sciences of the USA* **79**. 2415–2419.

MCGUINNESS, T., BRADY, S. T., GRUNER, J. A., SUGIMORI, M., LLINÁS, R. & GREENGARD, P. (1987). Inhibition by synapsin I of membranous organelle movement in isolated squid axoplasm. *Society for Neuroscience Abstracts* **13**. 1239.

MCGUINNESS, T. L., BRADY, S. T., GRUNER, J. A., SUGIMORI, M., LLINÁS, R. & GREENGARD, P. (1989). Phosphorylation-dependent inhibition by synapsin I of organelle movement in squid axoplasm. *Journal of Neuroscience* **9**. 4138–4149.

MCGUINNESS, T., LAI, Y. & GREENGARD, P. (1985). Ca^{2+}/calmodulin-dependent protein kinase. II. Isozymic forms from rat forebrain and cerebellum. *Journal of Biological Chemistry* **260**, 1696–1704.

MARTIN, R. & MILEDI, R. (1986). The form and dimensions of the giant synapse of the squid. *Philosophical Transactions of the Royal Society* B **312**, 355–377.

MILEDI, R. & SLATER, C. R. (1966). The action of calcium on neuronal synapses in the squid. *Journal of Physiology* **184**, 473–498.

NAIRN, A. & GREENGARD, P. (1987). Purification and characterization of Ca^{2+}/calmodulin-dependent protein kinase I from bovine brain. *Journal of Biological Chemistry* **262**, 7273–7281.

NICHOLS, R. A., WU, W. C., HAYCOCK, J. W. & GREENGARD, P. (1989). Introduction of impermeant molecules into synaptosomes using freeze/thaw permeabilization. *Journal of Neurochemistry* **52**, 521–529.

PETERSON, G. L. (1977). A simplification of the protein assay method of Lowry *et al.* which is more generally applicable. *Analytical Biochemistry* **83**, 346–356.

PETRUCCI, T. C. & MORROW, J. S. (1987). Synapsin I: An actin-binding protein under phosphorylation control. *Journal of Cell Biology* **105**, 1355–1363.

SCHIEBLER, W., JAHN, R., DOUCET, J.-P., ROTHLEIN, J. & GREENGARD, P. (1986). Characterization of synapsin I binding to small synaptic vesicles. *Journal of Biological Chemistry* **261**, 8383–8390.

SIEGHART, W., FORN, J. & GREENGARD, P. (1979). Ca^{2+} and cyclic AMP regulate phosphorylation of same two membrane-associated proteins specific to nerve tissue. *Proceedings of the National Academy of Sciences of the USA* **76**, 2475–2479.

SIMON, S. M. & LLINÁS, R. R. (1985). Compartmentalization of the submembrane calcium activity during calcium influx and its significance in transmitter release. *Biophysical Journal* **48**, 485–498.

SIMON, S. M., SUGIMORI, M. & LLINÁS, R. (1984). Modeling of submembranous calcium concentration changes and their relation to rate of presynaptic transmitter release in the squid giant synapse. *Biophysics Journal* **45**, 264a.

TITUS, J. A., HAUGLAND, R., SHARROW, S. O. & SEGAL, D. M. (1982). Texas red, a hydrophilic, red-emitting flurophore for use with fluorescein in dual parameter flow microfluorometric and fluorescence microscopic studies. *Journal of Immunological Methods* **50**, 193–204.

UEDA, T. & GREENGARD, P. (1977). Adenosine 3′,5′-monophosphate-regulated phosphoprotein system of neuronal membranes. I. Solubilization, purification, and some properties of an endogenous phosphoprotein. *Journal of Biological Chemistry* **252**, 5155–5163.

The Journal of Neuroscience, December 1989, 9(12): 4138–4149

Phosphorylation-Dependent Inhibition by Synapsin I of Organelle Movement in Squid Axoplasm

Teresa L. McGuinness,[1,a] Scott T. Brady,[2] John A. Gruner,[3] Mutsuyuki Sugimori,[3] Rodolfo Llinas,[3] and Paul Greengard[1]

[1]Laboratory of Molecular and Cellular Neuroscience, The Rockefeller University, New York, New York 10021, [2]Department of Cell Biology, University of Texas Health Science Center, Dallas, Texas 75235, [3]Department of Physiology and Biophysics, New York University Medical Center, New York, New York 10016, and Marine Biological Laboratory, Woods Hole, Massachusetts 02543.

Synapsin I, a neuron-specific, synaptic vesicle-associated phosphoprotein, is thought to play an important role in synaptic vesicle function. Recent microinjection studies have shown that synapsin I inhibits neurotransmitter release at the squid giant synapse and that the inhibitory effect is abolished by phosphorylation of the synapsin I molecule (Llinas et al., 1985). We have considered the possibility that synapsin I might modulate release by regulating the ability of synaptic vesicles to move to, or fuse with, the plasma membrane. Since it is not yet possible to examine these mechanisms in the intact nerve terminal, we have used video-enhanced microscopy to study synaptic vesicle mobility in axoplasm extruded from the squid giant axon. We report here that the dephosphorylated form of synapsin I inhibits organelle movement along microtubules within the interior of extruded axoplasm and that phosphorylation of synapsin I on sites 2 and 3 by calcium/calmodulin-dependent protein kinase II removes this inhibitory effect. Phosphorylation of synapsin I on site 1 by the catalytic subunit of cAMP-dependent protein kinase only partially reduces the inhibitory effect. In contrast to the inhibition of movement along microtubules seen within the interior of the axoplasm, movement along isolated microtubules protruding from the edges of the axoplasm is unaffected by dephospho-synapsin I, despite the fact that the synapsin I concentration is higher there. Thus, synapsin I does not appear to inhibit the fast axonal transport mechanism itself. Rather, these results are consistent with the possibility that dephospho-synapsin I acts by a crosslinking mechanism involving some component(s) of the cytoskeleton, such as F-actin, to create a dense network that restricts organelle movement. The relevance of the present observations to regulation of neurotransmitter release is discussed.

Synapsin I is a neuron-specific phosphoprotein that is concentrated in presynaptic nerve terminals, where it appears to be associated primarily with the cytoplasmic surface of small synaptic vesicles (Ueda et al., 1973; Ueda and Greengard, 1977; De Camilli et al., 1979, 1983a, b; Huttner et al., 1983; Navone et al., 1984). It is a major substrate for cAMP-dependent protein kinase as well as calcium/calmodulin-dependent protein kinases I and II (CaM kinases I and II) (Huttner and Greengard, 1979; Sieghart et al., 1979; Huttner et al., 1981; Kennedy and Greengard, 1981; Czernik et al., 1987; Nairn and Greengard, 1987). cAMP-dependent protein kinase and CaM kinase I both phosphorylate a single serine residue (site 1) located in the collagenase-resistant head region of the synapsin I molecule, CaM kinase II phosphorylates a pair of serine residues (sites 2 and 3) located in the collagenase-sensitive tail region of the molecule. A variety of studies using intact nerve cell preparations have shown that physiological and pharmacological agents that affect synaptic function also produce alterations in the state of phosphorylation of synapsin I (for reviews, see Nestler and Greengard, 1984; Greengard et al., 1987). *In vitro* studies have shown that, under certain conditions, phosphorylation of the tail region of synapsin I by CaM kinase II reduces the affinity of synapsin I for the synaptic vesicle membrane (Huttner et al., 1983; Schiebler et al., 1986; Benfenati et al., 1989). Taken together, these studies led to the hypothesis that synapsin I might be involved in the regulation of some aspect of synaptic vesicle function.

The possibility that synapsin I might regulate neurotransmitter release was tested directly by injection of synapsin I into the preterminal digit of the squid giant synapse (Llinas et al., 1985). Injection of the dephosphorylated form of synapsin I decreased neurotransmitter release, whereas injection of synapsin I that had been phosphorylated at sites 2 and 3 in the tail region by CaM kinase II was without effect. Moreover, injection of CaM kinase II itself enhanced release. More recent studies (R. Llinas et al., unpublished observations) have expanded these initial findings and have shown that phosphorylation of site 1 in the head region of synapsin I by cAMP-dependent protein kinase is less effective than tail phospho-synapsin at reducing the ability of synapsin I to inhibit transmitter release at the squid giant synapse.

Received Feb. 13, 1989; revised Apr. 19, 1989; accepted Apr. 26, 1989.

We are grateful to Dr. Raymond Lasek for the use of his microscope. We also thank Philip Leopold and Bea Beverly for valuable technical assistance, Dr. Martin Bähler for performing the synapsin I-vesicle binding studies, Dr. Andrew Czernik for some of the synapsin I used in these experiments, and Dr. Angus C. Nairn for the cAMP-dependent protein kinase catalytic subunit. This work was supported by a Medical Scientist Training Program Fellowship GM-07205 (to T.L.M.), U.S.P.H.S. grants NS-23868 (to S.T.B.), NS-23320 (to S.T.B.), NS-14014 (to R.L.), A.A. 06944 (to P.G.), NS-21550 (to P.G.) and MH-39327 (to P.G.), NSF grant BNS-8511764 (to S.T.B.), and U.S. Air Force Office of Scientific Research grant 85-0368 (to R.L.)

Correspondence should be addressed to Dr. Paul Greengard, Laboratory of Molecular and Cellular Neuroscience, The Rockefeller University, 1230 York Ave., New York, NY 10021.

[a] Present address: Department of Psychiatry, University of Colorado Health Sciences Center, Denver, CO 80262.

We believe that synapsin I is more likely to be involved in modulating than in mediating release, since the fusion-release process per se can occur in less than 200 μsec (Llinas et al., 1981), and the turnover rates for the protein kinases are on the order of tens of milliseconds. Furthermore, it is unlikely that synapsin I, which is enriched only in neurons, regulates the exocytotic event itself, a process that is common to all secretory cells. Finally, within nerve terminals, synapsin I appears to be associated only with small (40–60 nm diameter) and not with large (>60 nm diameter) synaptic vesicles (De Camilli et al., 1983a, b; Huttner et al., 1983; Navone et al., 1984; De Camilli and Greengard, 1986). Thus, we think that synapsin I is most likely to be involved in modulating some prefusion property that is unique to small synaptic vesicles.

We have proposed that phosphorylation of synapsin I might regulate the availability of synaptic vesicles for release and that it might do so by regulating the ability of the vesicles to move to or fuse with the plasma membrane (Llinas et al., 1985). Since it is not yet possible to examine these mechanisms in the intact nerve terminal, a number of model systems are currently being used to study the mechanism of action of synapsin I. One of these systems, the extruded axoplasm of the squid giant axon, is the focus of the present report. The present studies were designed to test the possibility that synapsin I regulates the availability of synaptic vesicles for release by affecting the ability of the vesicles to move within the cytoplasm. This required a relatively intact system in which we could directly and clearly visualize vesicle movement. We therefore chose to use video-enhanced contrast-differential interference contrast (VEC-DIC) microscopy techniques to examine the effect of synapsin I on vesicle movement in the extruded squid axoplasm.

VEC-DIC microscopy techniques (Allen et al., 1981; Inoue, 1981) make it possible to detect structures as small as one-tenth the traditional limit of resolution of the light microscope. With these techniques, one can observe subcellular structures the size of individual small synaptic vesicles and microtubules (Allen et al., 1981; Allen and Allen, 1983). The extruded axoplasm preparation from the squid giant axon permits one to perform a variety of manipulations with macromolecules that do not ordinarily cross the plasma membrane and to use VEC-DIC microscopy to observe directly the effects of these manipulations on organelle movement (Brady et al., 1982, 1984, 1985). In addition, the extruded axoplasm preparation provides a useful means for determining if interactions between proteins and subcellular organelles that are suggested on the basis of reconstitution studies with purified components can occur within the axonal milieu. The present results indicate that synapsin I can restrict the ability of vesicles to move within the axoplasm and that this effect is dependent on the state of phosphorylation of the synapsin I molecule. A preliminary report of this work has been published (McGuinness et al., 1987).

Materials and Methods

Preparation of proteins. Synapsin I was purified in the dephosphorylated form from bovine brain by a modification (Bahler and Greengard, 1987) of the procedure of Schiebler et al. (1986). CaM kinase II was purified from rat forebrain as described by McGuinness et al. (1985), with the addition of hydroxylapatite chromatography inserted between the DEAE-cellulose chromatography and ammonium sulfate precipitation steps. Purified CaM kinase II (0.4–0.5 mg/ml) was dialyzed extensively against buffer A (10 mM HEPES, pH 7.2, 150 mM potassium aspartate, 5 mM $MgSO_4$) and stored at −70°C. The catalytic subunit of cAMP-dependent protein kinase was purified as described by Kaczmarek et al. (1980). Calmodulin was purified as described by Grand et al. (1979). Protein determinations were performed by the method of Peterson (1977), using BSA as standard.

Synapsin I (0.35 mg/ml) was phosphorylated by incubation for 30 min at 30°C in 50 mM Tris-HCl, pH 7.5, 150 mM NaCl, 0.4 mM EGTA, 1 mM dithioerythritol, 10 mM $MgCl_2$, 100 μM ATP, with trace amounts of γ-^{32}P-ATP, with either CaM kinase II (3.4 μg/ml), 0.7 mM $CaCl_2$, 30 μg/ml calmodulin or the catalytic subunit of cAMP-dependent protein kinase (60 nM), 0.1% Nonidet-P40. "Mock"-phospho-synapsin I was treated as above except that both kinases, $CaCl_2$, calmodulin, and Nonidet-P40 were added, and ATP was omitted from the reaction mixture. Phosphorylation reactions were terminated by the addition of EDTA to a final concentration of 20 mM. One- and 2-dimensional peptide mapping (Kennedy and Greengard, 1981; Huttner et al., 1981; Kennedy et al., 1983) revealed that synapsin I was phosphorylated to a stoichiometry of 1.0 mol/mol on site 2 and on site 3 by CaM kinase II and to a stoichiometry of 0.95 mol/mol on site 1 by the catalytic subunit of cAMP-dependent protein kinase.

Some of the phosphorylated and dephosphorylated synapsin I preparations were fluorescently labeled with Texas red (Molecular Probes, Inc., Eugene, OR) according to the method of Titus et al. (1982) as described by Llinas et al. (unpublished obervations). The various forms of synapsin I were re-purified from kinases and/or unbound Texas red by CM-cellulose chromatography at pH 8.0 as described by Llinas et al. (unpublished observations), using buffer A for elution. The re-purified synapsin I was concentrated, dialyzed against buffer A, centrifuged in a Beckman TL 100 centrifuge at 450,000 *g* for 15 min to remove large aggregates, stored at 0–4°C, and used within 7 d of preparation or stored at −70°C and thawed immediately before use. Labeled and unlabeled synapsin I preparations were assayed for the ability to be phosphorylated by CaM kinase II using the procedure of McGuinness et al. (1985), to bind to purified synaptic vesicles using the procedure of Schiebler et al. (1986), to inhibit neurotransmitter release using the procedure of Llinas et al. (1985), and to inhibit organelle movement using the methods described in the present report.

Manipulation of axoplasm. Squid (*Loligo pealei*) having a mantle length of 10–20 cm were obtained daily from the Department of Marine Resources, Marine Biological Laboratory (Woods Hole, MA). Postganglionic squid giant axons were dissected, and each axoplasm was extruded onto a glass coverslip. The axoplasm was then covered with a second glass coverslip for viewing by VEC-DIC microscopy as previously described (Brady et al., 1985; Schroer et al., 1985). After recording baseline organelle movement, axoplasm was incubated with 20–40 μl of either buffer B (buffer A plus 1 mM ATP) alone or buffer B containing 1.3–10 μM synapsin I.

For the kinase injection experiments, axoplasm was extruded onto a glass coverslip, and CaM kinase II (0.4 mg/ml in buffer A) was injected from a microelectrode by means of short pressure pulses (20–65 psi, ~100 msec in duration) into a small region of the axoplasm. The axoplasm was then covered with a second coverslip for viewing by VEC-DIC microscopy. After recording baseline organelle movement, 20–40 μl of buffer B containing 1.3–10 μM dephosphosynapsin I, 40 μM $CaCl_2$, and 0.15 mg/ml calmodulin was applied to the chamber.

The rapid directed movement of membranous organelles within extruded axoplasm occurs in both the anterograde (from the cell body to the terminals) and the retrograde (from the terminals to the cell body) directions and, in neurons, is referred to as fast axonal transport (for review, see Grafstein and Forman, 1980). Fast transport has been shown, using VEC-DIC techniques, to occur along individual microtubules (Hayden et al., 1983; Allen et al., 1985; Schnapp et al., 1985). Recent evidence suggests that the translocating enzyme that may be responsible for anterograde transport is different from that responsible for retrograde transport (Vale et al., 1985 a, c; Paschal and Vallee, 1987; Paschal et al., 1987). In all the figures, the axoplasm was oriented horizontally such that the proximal or cell body end of the axoplasm is to the left and the distal or terminal end is to the right. Thus, movement from left to right is in the anterograde direction, and movement from right to left is in the retrograde direction.

Video-enhanced microscopy. Organelle movement was visualized using DIC optics on a Zeiss Axiomat microscope (with 100× objective, zoom set at 2.5×) using a Chalnicon videocamera (Hamamatsu Systems, Inc., Waltham, MA). A silicon-intensified target camera (Hamamatsu) and rhodamine filter set (Carl Zeiss, Inc., Thornwood, NY) were used for fluorescence imaging. Video images were processed with a Hamamatsu C-1440 or C-1966 Image Processor (Photonics Micros-

copy, Inc., Oak Brook, IL) to enhance contrast and to eliminate background optical noise. Video signals were recorded in real-time (30 frames/sec) on a Sony VO-5850 videotape recorder.

Depending on the particular biological preparation used, one can examine various parameters of fast axonal transport, including the number and types of organelles moving, their velocity, and the direction of movement. However, the intact extruded axoplasm preparation is not amenable to quantitation of the number of organelles moving per unit time. The number of moving particles in a single plane of focus within a healthy axoplasm is so numerous and the smallest organelles, which are the ones of interest in the present studies, have such low contrast that they are detected primarily as a continuous streaming across the screen. Because such organelles are well below the limit of resolution of the light microscope, it is physically impossible to distinguish these small moving particles as individual elements. Any estimate of the number of particles moving across even a short line drawn on the screen could be in error by orders of magnitude. In previous studies using intact axons (e.g., Allen et al., 1982; Adams and Bray, 1983; Forman et al., 1983; Koenig, 1986) or neurites in culture (e.g., Hollenbeck and Bray, 1987), only a fraction of the total number of moving particles was detected. In fact, the inability to detect the small synaptic vesicle-sized particles in these preparations reduced the total number of visible moving particles so that the small number of larger moving organelles could be counted. In previous studies using dissociated axoplasm (e.g., Allen et al., 1985; Schnapp et al., 1985; Vale et al., 1985b; Weiss, 1986), individual translocation events could be easily examined. For some of the intact and dissociated preparations, estimates were presented of the number of moving particles. However, no attempt was made in any of these studies to evaluate the sampling procedure to determine the population of organelles being counted or how these relate to the complete set of organelles in transport. Fortunately, in the present study, the effect of the dephosphorylated form of synapsin I on organelle movement was so dramatic that precise quantitation of the number of organelles affected was not critical.

Velocity measurements were performed with a Hamamatsu C-2117 video manipulator, which generates white pixels that move across the monitor. The direction and rate of these pixels were adjusted by eye to correspond alternately to the average velocity of particles moving in the anterograde or retrograde directions. Velocities are expressed as mean ± SEM.

The "trace" images were obtained using the Hamamatsu C-1966 Image Processor to extract a trace of moving objects by sequentially subtracting frames at specified intervals and accumulating the successive subtracted images. We had hoped to calculate the total intensities of the trace images and to use the intensity values as a quantitative measure of total movement. This could be done by using a root-mean-square average of the subtracted images as described by Forscher et al. (1987). However, several limitations inherent in the trace technique precluded its routine use in the present studies. Situations that limit the usefulness of this technique include too many moving particles for their trajectories to be resolved from one another, variation in intensity of illumination due to fluctuations of the light source or differences in the depth of focus, and particles moving in and out of the plane of focus. The first limitation is the reason why only the trajectories of the high-contrast, medium-sized and large organelles could be clearly seen in Figure 2A. Unfortunately, we were most interested in the movements of the low-contrast, small (synaptic vesicle-sized) organelles, which were lost in the background video noise. In addition, fluctuations in the illuminator and slight changes in the depth of focus during the course of a 1 hr experiment often made it impossible to compare directly the trace image or total intensity of the image before and after the experimental manipulation. As a result, this procedure provided a qualitative means of comparison but was not well suited for quantitative comparison of movement in axoplasm.

Results

Effect of dephospho-synapsin I on organelle movement within the interior of the axoplasm

In agreement with previous reports (Brady et al., 1982, 1984, 1985), in preparations that were not exposed to synapsin I, transport of organelles along microtubules was maintained for several hours after extrusion of the axoplasm. The situation in the presence of the dephosphorylated form of synapsin I is illustrated in Figure 1 and Table 1, where it can be seen that incubation of isolated axoplasm with dephospho-synapsin I resulted in an almost complete inhibition of directed organelle movement. Immediately before addition of dephospho-synapsin I, organelles of all sizes were seen moving in both anterograde and retrograde directions (Fig. 1, *A, B*). In contrast, by 1 hr after addition of dephospho-synapsin I to the axoplasm, virtually all directed organelle movement within the interior of the axoplasm came to a complete halt (Fig. 1, *C, D*). The smallest organelles appeared to be the most quickly and completely affected, but by 30 min to 1 hr after addition of dephospho-synapsin I, organelles of all sizes were clearly affected. In the absence of dephospho-synapsin I, the average velocity of particles moving in the anterograde and retrograde directions was 1.72 ± 0.098 μm/sec (n = 33) and 1.29 ± 0.042 μm/sec (n = 33), respectively (S. T. Brady and G. S. Bloom, unpublished observations; and the present report). After equilibration of the axoplasm with dephospho-synapsin I, the average velocity in both directions for most particles was essentially zero.

No detectable change in the structural organization of the axoplasm was noted on the addition of dephospho-synapsin I. For example, in contrast to results obtained with purified microtubules (Baines and Bennett, 1986), no dephospho-synapsin I-induced bundling of microtubules was detected in the intact axoplasm. Furthermore, there was no loss of order or increase in Brownian motion, which can be seen in disrupted axoplasm or axoplasm depleted of ATP (Brady et al., 1985). Instead, the axoplasm appeared to virtually freeze in the presence of dephospho-synapsin I, with many organelles undergoing repeated short "tugging" movements. This tugging behavior could represent constrained Brownian movement of particles trapped

→

Figure 1. Effect of dephospho-synapsin I on organelle movement within the interior of the axoplasm. Stills from video records show organelle movement within the interior of extruded axoplasm immediately before (*A, B*) and 1 hr after (*C, D*) addition of 10 μM dephospho-synapsin I. *Arrows* and *arrowhead* in *A* point to a few of the numerous organelles that had moved during the 5.5 sec interval between frames *A* and *B*. The corresponding symbols in *B* point to the positions originally occupied by the respective organelles. *Solid, curved arrow* in *A* points to a mitochondrion that moved to the left, as seen in *B*. *Open, curved arrow* in *A* points to a large organelle that moved upward and to the right, as seen in *B*. *Solid, thin arrow* and *solid arrowhead* in *A* point to 2 smaller organelles that moved out of the field in *B*. *Open, straight arrow* in *A* points to 2 organelles that moved in opposite directions in *B*. These 2 organelles are marked with an * in both *A* and *B*; the top organelle moved in the retrograde direction, whereas the bottom organelle moved in the anterograde direction. In contrast to the movement observed between frames *A* and *B*, almost no organelles moved during the 5.5 sec interval between frames *C* and *D*. *Arrows* and *arrowheads* in *C* and *D* indicate just a few of the various-sized organelles that remained stationary in the presence of dephospho-synapsin I. Stills were made by playing the original videotape into the C-1966 Image Processor, performing a rolling average of 4 frames, and recording the averaged image onto an optical disc using a Panasonic TQ-2028F Optical Memory Disc Recorder. Single frames from the optical disc were photographed from a high-resolution monochrome monitor with a 35 mm camera onto Kodak Tech-pan film. Scale bar, 2 μm.

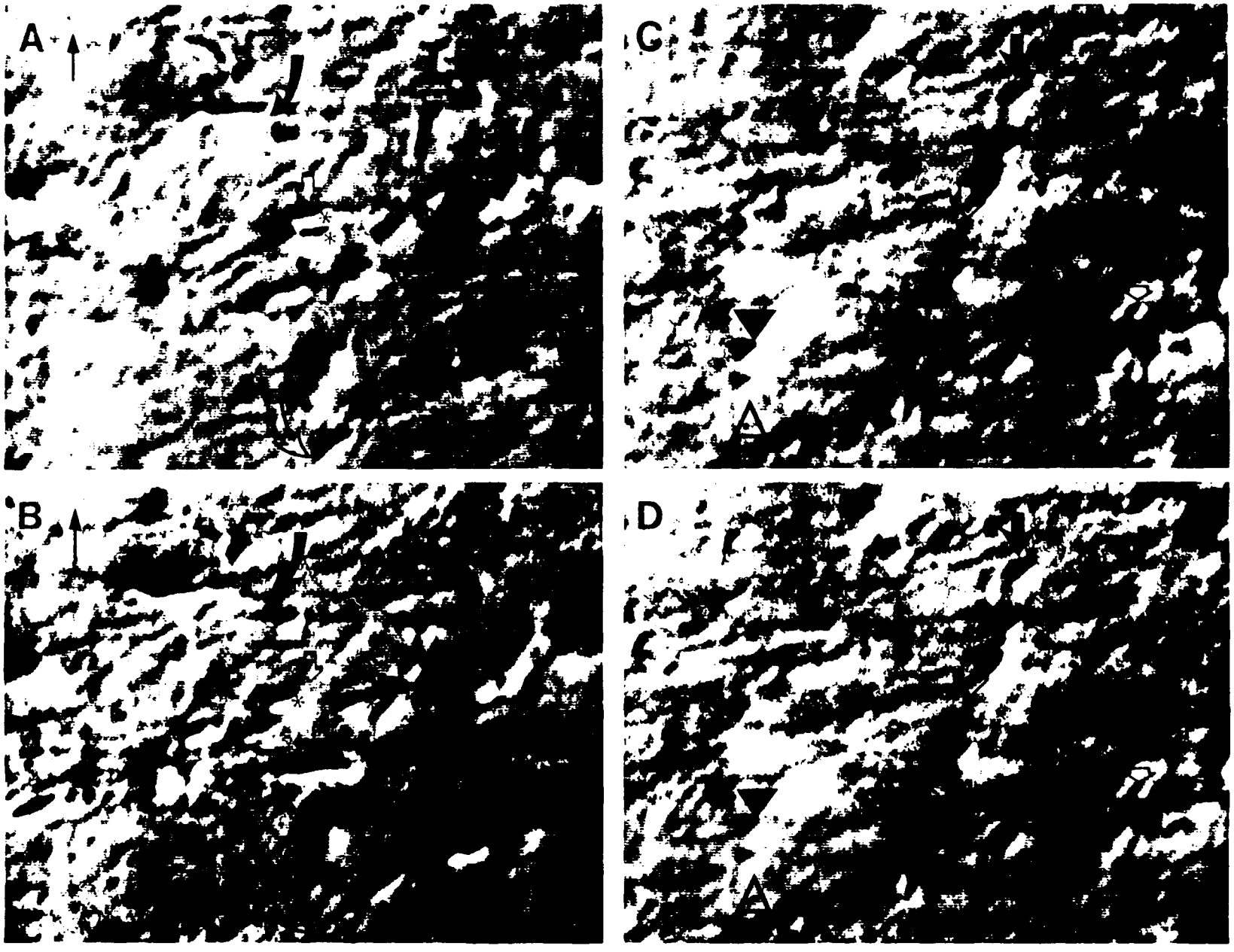
A
C
B
D

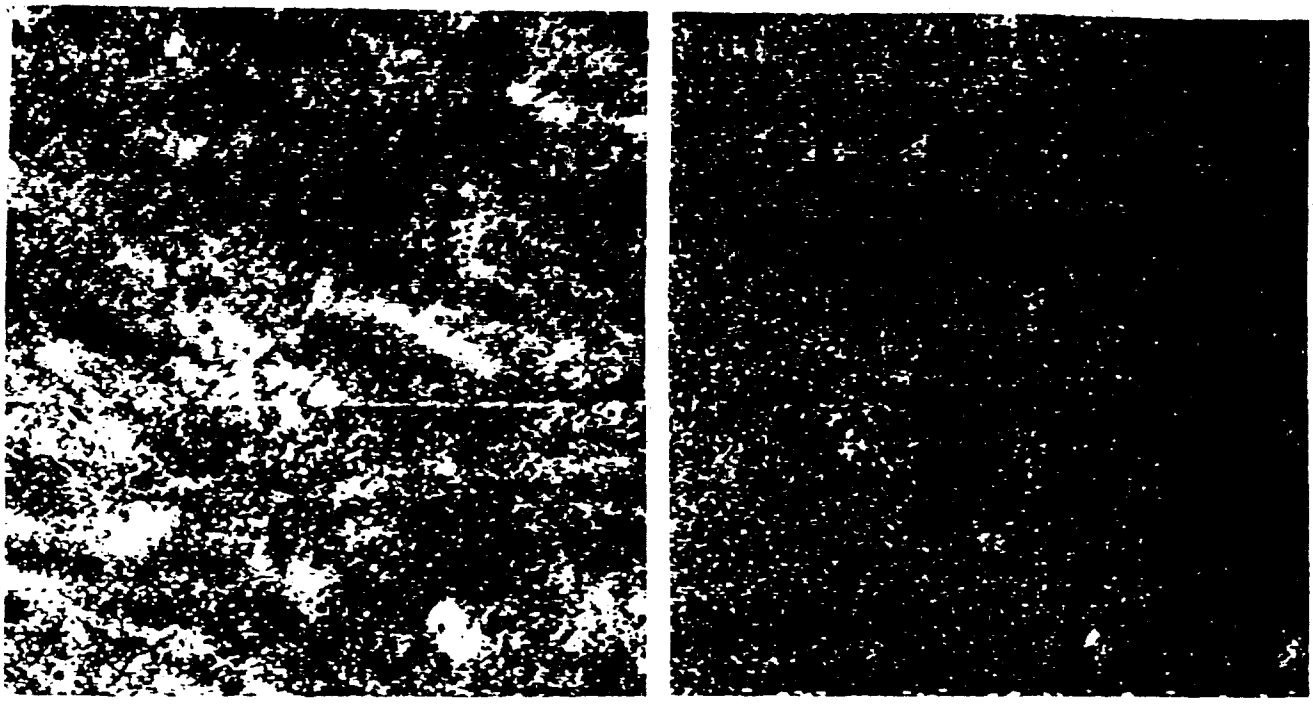

Figure 2. Trace images illustrating the effect of dephospho-synapsin I on organelle movement within the interior of the axoplasm. Traces were obtained by subtracting every third frame (0.1 sec intervals) and accumulating the subtracted images of 60 frames, as described in Materials and Methods. *A*, Linear paths produced by moving organelles within the axoplasm immediately before addition of dephospho-synapsin I. *B*, No such paths can be detected in the same axoplasm 1 hr after addition of 10 μM dephospho-synapsin I. Stills were made by copying the original videotape onto an optical disc and photographing single frames as described in the legend to Figure 1. Scale bar, 2 μm.

within the matrix of the axoplasm (Brady et al., 1985) or could represent attempted movement of organelles that are actually tethered to some component of the axoplasmic matrix. Replenishing the ATP did not reverse the inhibitory effect of dephospho-synapsin I on axonal transport.

Regions in which directed movement had ceased within the axoplasm were first detected within 5 min after dephospho-synapsin I addition and were detected throughout the axoplasm by 30 min. To monitor the diffusion of synapsin I into the axoplasm, the protein used for most of these experiments was fluorescently labeled with the rhodamine derivative Texas red. Labeled synapsin I was comparable to unlabeled synapsin I in terms of its ability to be phosphorylated by CaM kinase II, to bind to purified synaptic vesicles, to inhibit organelle movement (present report), and to inhibit neurotransmitter release (Llinas et al., unpublished observations). Fluorescent dephospho-synapsin I was found to penetrate the axoplasm with a time course similar to that found for the appearance of the inhibitory effect. This time course is consistent with that expected for diffusion of molecules the size of synapsin I in squid axoplasm (Brady et al., 1984, 1985; Morris and Lasek, 1984).

Table 1. Effect of dephospho-synapsin I and phospho-synapsin I on organelle movement within extruded axoplasm

Condition	Synapsin concentration (mg/ml)	Organelle movements (after 30 min)
Control	0	+ + + +
Dephospho-synapsin I	0.1	+
	1.0	0
Mock phospho-synapsin I	0.1	+
	1.0	0
Tail phospho-synapsin I (calmodulin kinase II treated)	0.1	+ + + +
	1.0	+ + +
Head phospho-synapsin I (cAMP-dependent protein kinase treated)	0.1	+ + +

Dynamic movement observed in real-time using video-enhanced microscopy cannot be adequately represented in still photographs. The isolated axoplasm preparation contains so many moving organelles that frames selected at 2 different times may look very similar because almost all organelles have moved in the interframe interval and other organelles have taken their place. Often, only the positions of medium-sized and large organelles can unequivocally be identified in successive still photographs. Furthermore, the ability to even detect the small synaptic vesicle-sized particles within the complex interior of the axoplasm is almost completely lost in the still picture. The changes in contrast generated by the movement of these particles contribute significantly to one's ability to study them.

Figure 2 represents an attempt to circumvent these limitations. The trace images in Figure 2 were obtained by sequentially subtracting DIC images captured at 0.1 sec intervals and accumulating 60 of the subtracted images. Trajectories of moving particles were visualized by changes in pixel brightness caused by movement during the interframe interval. The trajectories created by organelles moving within the axoplasm were clearly seen before addition of dephospho-synapsin I (Fig. 2*A*). In con-

trast, no trajectories were evident 1 hr after dephospho-synapsin I was applied to the axoplasm (Fig. 2B). This trace imaging technique provided a qualitative measure of the extent to which dephospho-synapsin I reduced movement of organelles.

Effect of dephospho-synapsin I on organelle movement at the periphery of the axoplasm

The most peripheral region of the extruded axoplasm preparation, i.e., the region nearest the buffer–axoplasm interface, has a less dense and less ordered organization than does the interior of the axoplasm proper (cf. Fig. 3, *A, B* to *C, D*, and see Brady et al., 1982; Miller and Lasek, 1985). In the periphery, organelle movement is not inhibited by dephospho-synapsin I. In contrast to the immobilization of particles produced by dephospho-synapsin I within the interior of the axoplasm (Fig. 3, *A, B*), organelle movement along microtubules near the boundary between the buffer and axoplasm (Fig. 3, *C, D*) was unaffected by dephospho-synapsin I. Typically, regions of the axoplasm more than 5–6 μm away from the boundary between buffer and axoplasm were clearly reduced in the amount of organelle movement within 10 min of dephospho-synapsin I addition. As the incubation continued, almost all organelle movement ceased within the interior of the axoplasm (Fig. 3, *A, B*). Throughout the course of the experiment, however, organelles of all sizes in the most superficial regions of axoplasm continued to move along easily resolved microtubules (Fig. 3, *C, D*). Similarly, organelle movement along isolated microtubules protruding from the edge of the axoplasm continued in the presence of dephospho-synapsin I (Fig. 4). Thus, axonal transport along individual microtubules in the periphery of the axoplasm and in the surrounding buffer continued unabated, despite the fact that the dephospho-synapsin I concentration was higher in these peripheral regions than in the interior of the axoplasm, as determined by fluorescent monitoring of Texas red-labeled synapsin I.

Effect of phospho-synapsin I on organelle movement

Phosphorylation of sites 2 and 3 in the tail region of the synapsin I molecule by CaM kinase II abolishes the ability of synapsin I to inhibit transmitter release at the squid giant synapse (Llinas et al., 1985; unpublished observations). Therefore, we examined whether phosphorylation of synapsin I by CaM kinase II would also reduce the ability of synapsin I to inhibit organelle movement in the squid giant axoplasm. As shown in the previous section, organelle movement was almost completely inhibited when axoplasm was incubated with 1.3–10 μM dephospho-synapsin I. In contrast, incubation of axoplasm with 1.3 μM tail phospho-synapsin I (synapsin I that had been phosphorylated on sites 2 and 3 in the tail region of the molecule by CaM kinase II) had no effect on organelle movement (see Table 1), and incubation with 10 μM tail phosphosynapsin I had only a slight inhibitory effect (Fig. 5). This minor effect at the higher concentration might have resulted from sites 2 and 3 being incompletely phosphorylated or partially dephosphorylated by endogenous squid protein phosphatase(s). The fact that 10 μM tail phospho-synapsin I had little effect on transport indicates that this concentration of dephospho-synapsin I, which abolished organelle movement, did not per se cause a nonspecific perturbation of axonal transport.

Phosphorylation of site 1 in the head region of the synapsin I molecule by cAMP-dependent protein kinase only partially reduced the ability of synapsin I to inhibit organelles from being transported along microtubules. Phosphorylation by cAMP-dependent protein kinase was not as effective as phosphorylation by CaM kinase II in preventing the inhibitory effect of synapsin I, but far more movement was seen in axoplasm treated with head phospho-synapsin I than if treated with dephospho-synapsin I (see Table 1).

The relative lack of effect of the phospho-synapsin I preparations was not due to nonspecific inactivation of the molecule by the phosphorylation conditions, since mock phospho-synapsin I (synapsin I that had been treated identically to phospho-synapsin I except that ATP was omitted from the phosphorylation reaction mixture) was indistinguishable from dephospho-synapsin I in its inhibitory effect. The relative lack of effect of the phospho-synapsin I preparations was also not due to poor penetration into the axoplasm, since fluorescence monitoring of Texas red-labeled synapsin I showed similar diffusion for the dephospho- and phospho-forms. The differences in transport blocking ability between dephospho- and phospho-synapsin I were also observed when the proteins were pressure-injected from a microelectrode directly into a small region of the axoplasm. In these experiments, dephospho-synapsin I inhibited movement in the region surrounding the injection site, whereas axonal transport proceeded normally at distances farther away. In contrast, phospho-synapsin I had no effect.

The microinjection technique was also used to test whether phosphorylation of synapsin I within the axoplasm itself by CaM kinase II would prevent the inhibitory action of synapsin I on organelle movement. CaM kinase II was pressure-injected into a small area at the distal end of the axoplasm. Organelle movement and the integrity of the axoplasm in the vicinity of the injection site were not noticeably different from that seen in other regions. The axoplasm was then incubated with buffer containing 1.3–10 μM dephospho-synapsin I in the presence of 40 μM calcium and 0.15 mg/ml calmodulin to promote phosphorylation. Incubation with these concentrations of calcium and calmodulin without dephospho-synapsin I had no detectable effect on organelle movement (Brady et al., 1984, 1985; and this study). Dephospho-synapsin I inhibited movement throughout the axoplasm except in the immediate vicinity of the kinase injection site. Near the injection site, normal organelle movement was observed. Decreases in organelle movement were seen with increasing distance from the site of injection. The distribution and intensity of the fluorescent synapsin I was the same at the injection site as in other regions. Thus, inhibition by dephospho-synapsin I can be prevented by CaM kinase II within the axoplasm itself.

Discussion

The present studies utilized the isolated axoplasm from the squid giant axon as one model for studying the mechanism by which synapsin I might regulate neurotransmitter release. These studies were undertaken to test the following hypothesis. If synapsin I regulates availability of synaptic vesicles for release by restricting the ability of vesicles to move within the cytoplasm of the presynaptic terminal, then adding concentrations of synapsin I that would be expected to exist within the terminal to the isolated axoplasm might inhibit vesicle movement in the axoplasm. This is, in fact, what was found (see Table 1). The dephosphorylated form of synapsin I virtually abolished all vesicle movement within the interior of the isolated axoplasm. Phosphorylation of synapsin I by CaM kinase II removed the inhibitory effect and phosphorylation by cAMP-dependent pro-

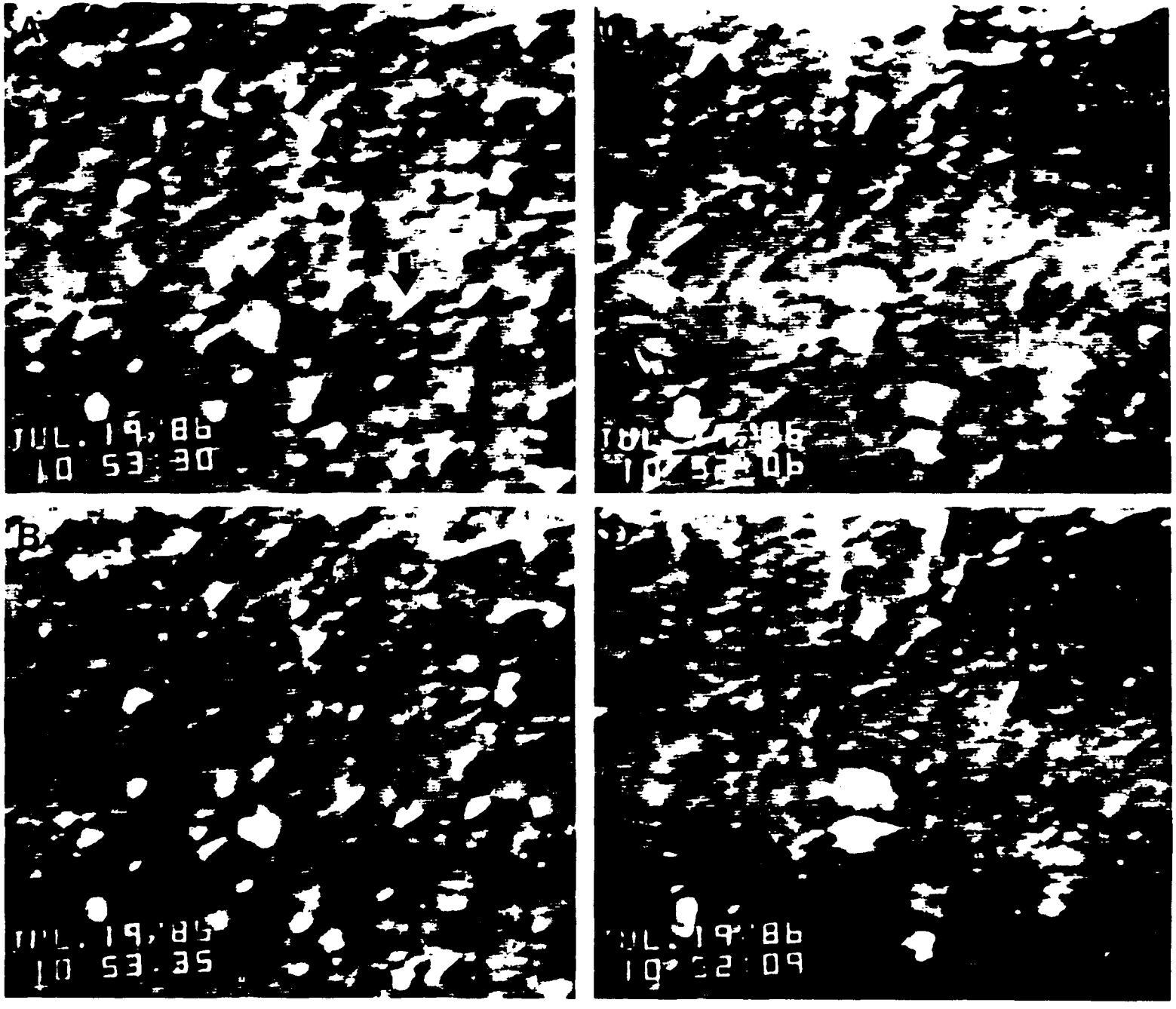
A
JUL. 19, 86
10 53 30
B
JUL. 19, 86
10 53 35

tein kinase partially reduced the inhibitory effect on vesicle movement. These results are analogous to the inhibition of neurotransmitter release by dephospho-synapsin I and the reduction of that inhibition by phosphorylation of synapsin I. Thus, the results are consistent with the possibility that the mechanism by which synapsin I affects organelle movement in the isolated axoplasm is similar or identical to the mechanism by which it regulates synaptic vesicle availability in the presynaptic terminal.

The small vesicles in the axoplasm were clearly not the only organelles affected by synapsin I. Movement of all organelles was dramatically inhibited. This nonselective effect raises the possibility that synapsin I directly inhibits the microtubule-based motor mechanism for fast axonal transport. Several factors, however, suggest that synapsin I does not directly affect the transport mechanism itself. First, synapsin I had no apparent effect on the movement of organelles along microtubules in the periphery of the axoplasm or along isolated microtubules protruding into the buffer, where the concentration of synapsin I was the highest. Furthermore, the ability of synapsin I to inhibit organelle movement was critically dependent on a closely packed cytoskeletal matrix. For example, when the axoplasm was improperly extruded so that the original linear organization of the cytoskeletal network was disturbed, synapsin I was much less effective in inhibiting movement. Also, if a single axoplasm had highly organized regions adjacent to regions where the microtubules were disorganized and extending haphazardly in all directions, then significant inhibition was seen only in the organized regions. This ability of synapsin I to inhibit movement only within the interior of axoplasm in which the original cytoskeletal architecture has been maintained is not consistent with a direct effect on the fast axonal transport mechanism. It is also not consistent with the inhibitory effect depending solely on the concentration of a particular component that may have been diluted below a critical concentration in the buffer surrounding the axoplasm. Rather, it suggests that synapsin I may indirectly inhibit fast axonal transport by crosslinking neighboring axoplasmic structures, thus restricting the ability of organelles to move within the resulting network. However, the absence of an effect of dephospho-synapsin I on organelles moving along individual microtubules or in the periphery of the axoplasm suggests that the organelles are not crosslinked to the microtubules. Instead, some other axoplasmic structure must be required.

One possible mechanism for the inhibition of movement of membranous organelles reported here is the following. Dephospho-synapsin I inhibits synaptic vesicle mobility by crosslinking the vesicles to some component(s) of the cytoskeleton, thereby creating a dense meshwork or cage, which then indirectly restricts the movement of other organelles as well. Indeed, it has previously been proposed that synapsin I crosslinks synaptic vesicles to cytoskeletal structures and that this interaction is regulated by phosphorylation of the synapsin I molecule (De Camilli et al., 1983b; Huttner et al., 1983; Navone et al., 1984). In support of this proposal, synapsin I has been shown to bind with high affinity to isolated synaptic vesicles (Huttner et al., 1983; Schiebler et al., 1986; Steiner et al., 1987; Benfenati et al., 1989) and to interact *in vitro* with various cytoskeletal structures, including spectrin (Baines and Bennett, 1985; Kanda et al., 1986; Krebs et al., 1987), microtubules (Baines and Bennett, 1986; Goldenring et al., 1986), neurofilaments (Goldenring et al., 1986; Steiner et al., 1987), and F-actin (Bahler and Greengard, 1987; Petrucci and Morrow, 1987; Petrucci et al., 1988; Bahler et al., 1989).

Only in the synaptic vesicle (Huttner et al., 1983; Schiebler et al., 1986; Benfenati et al., 1989) and actin (Bahler and Greengard, 1987; Petrucci and Morrow, 1987; Bahler et al., 1989) studies was the effect of phosphorylation of synapsin I by cAMP-dependent protein kinase examined. Phosphorylation by cAMP-dependent protein kinase had only a slight effect on the interaction of synapsin I with purified vesicles (Schiebler et al., 1986) and with actin (Bahler and Greengard, 1987). It is not known whether these relatively minor effects are of physiological significance. Phosphorylation of synapsin I by CaM kinase II has been shown to decrease its interaction with purified synaptic vesicles (Huttner et al., 1983; Schiebler et al., 1986; Benfenati et al., 1989) and neurofilaments (Steiner et al., 1987) and to nearly abolish its ability to bundle F-actin (Bahler and Greengard, 1987; Petrucci and Morrow, 1987). Thus, phosphorylation-dependent interactions of synapsin I with any of these components could be responsible for the present findings on organelle movement.

Interaction with neurofilaments is unlikely to explain the effects of synapsin I in both the axoplasm and the presynaptic terminal, since neurofilaments are thought not to extend into the synaptic vesicle-containing region of the terminal (Roots, 1983; Walker et al., 1985). Interaction with microtubules is also unlikely to be the sole explanation for the effects of synapsin I, since no microtubule bundling was observed in the present experiments and phosphorylation of synapsin I, if anything, may enhance the interaction of synapsin I with microtubule proteins (Petrucci and Morrow, 1987). In addition, microtubules are thought not to extend into the synaptic vesicle region of the presynaptic nerve terminal (Roots, 1983; Walker et al., 1985), although evidence for some microtubules extending into the presynaptic terminal does exist (Hirokawa et al., 1989). Regardless, the absence of inhibition by dephospho-synapsin I when organelles are moving along individual microtubules in the absence of other structures (Fig. 4) makes it unlikely that interaction with microtubules is involved.

Interaction with F-actin, on the other hand, could explain both effects. The ability of synapsin I to bundle F-actin in *in vitro* systems (Bahler and Greengard, 1987; Petrucci and Morrow, 1987; Petrucci et al., 1988) is consistent with synapsin I

—

Figure 3. Comparison of the effect of dephospho-synapsin I on organelle movement within the interior and near the periphery of the axoplasm. Stills from video records showing organelle movement within the interior (*A*, *B*) and near the periphery (*C*, *D*) of extruded axoplasm 20–22 min after addition of 1.3 μM dephospho-synapsin I. *Arrows* in *A* and *B* indicate 2 of the numerous organelles in the field that did not move during the 5 sec interval between frames *A* and *B*. *Open arrows* in *C* and *D* indicate a single microtubule. *Solid arrows* in *C* and *D* indicate the positions of a single organelle that moved along another microtubule during the 3 sec interval between frames *C* and *D*. In such peripheral regions, movement was generally active to the extent that few organelles remained in the field for more than 2 or 3 sec. *Arrowhead* in *C* indicates an organelle that is not seen in *D* because it had moved out of the field. Stills were made by accumulating 4 frames (0.13 sec) from the original videotape using the C-1966 Image Processor and photographing the accumulated image from the monitor onto Kodak TMAX 100 film. Scale bar, 2 μm.

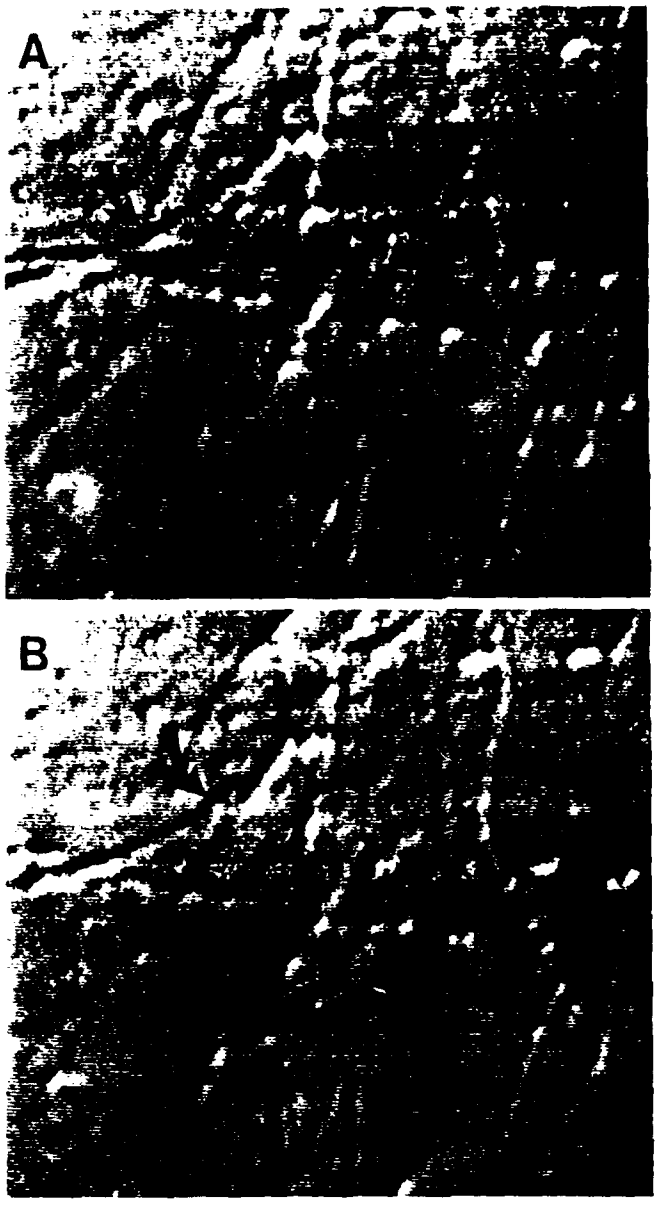

Figure 4. Effect of dephospho-synapsin I on organelle movement along isolated microtubules protruding from the axoplasm into the buffer. Stills from video records show that organelles continue to move along these isolated microtubules 1 hr after addition of 10 μM dephospho-synapsin I. *Arrows* in *A* point to organelles that moved during the 5.5 sec interval between frames *A* and *B*. *Solid, curved arrows* in *A* and *B* point to an organelle that moved upward to the left. *Dashed, curved arrows* in *A* point to two smaller organelles that are not seen in *B* because they had moved out of the field. *Dashed, straight arrows* in *B* point to the positions originally occupied by these organelles. *Short, solid* and *short, open arrows* in the lower right corners of *A* and *B* point to two organelles that moved upward along the indicated microtubule. Stills were made as described in the legend to Figure 1. The axoplasm used for this figure is the same axoplasm used for Figure 1. Scale bar, 2 μm.

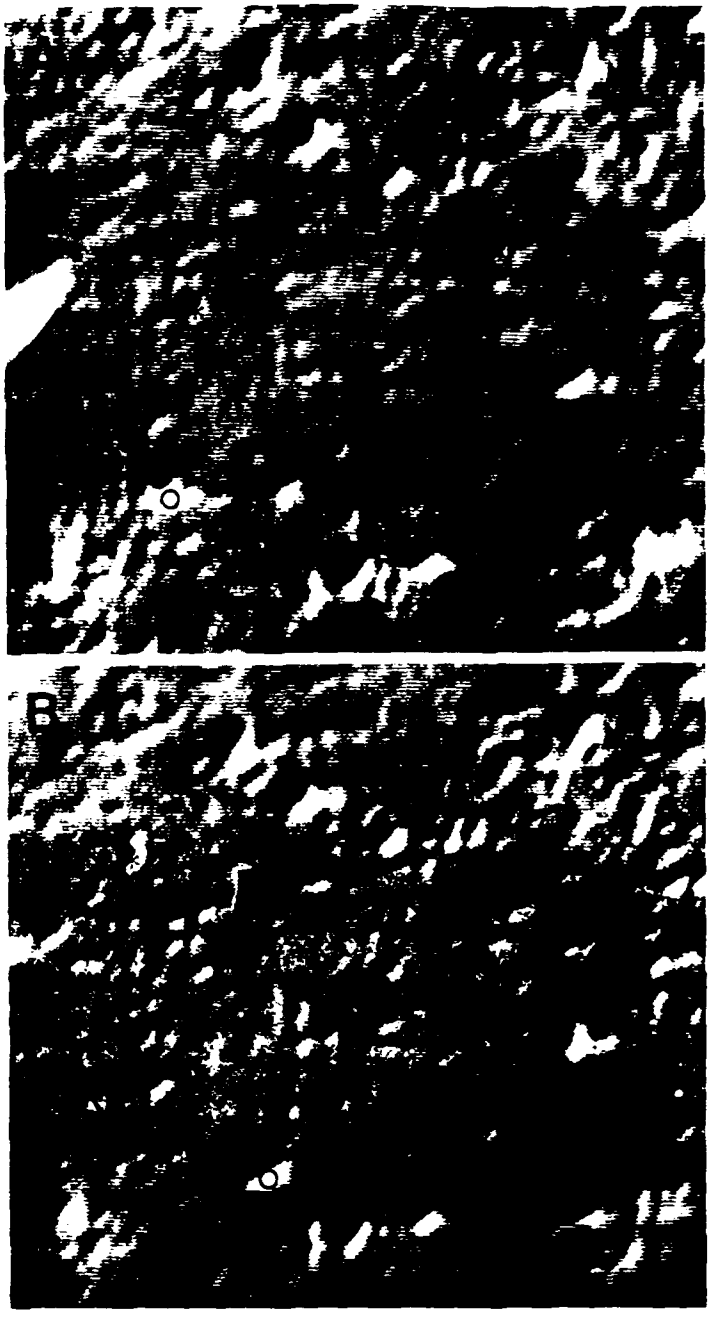

Figure 5. Effect of phosphorylation of synapsin I by CaM kinase II on organelle movement within the interior of the axoplasm. Stills from video records show organelle movement within the interior of isolated axoplasm 1 hr after addition of 10 μM tail phospho-synapsin I. *Straight arrows* and *large, curved arrows* in *A* point to a few of the many organelles that moved during the 5.5 sec interval between frames *A* and *B*. The corresponding symbols in *B* point to the positions originally occupied by the respective organelles. *Solid, curved arrow* in *A* points to an organelle (•) that moved upward to the left, as seen in *B*. *Open, curved arrow* in *A* points to an organelle (o) that moved to the right in *B*. *Solid, straight* and *open, straight arrows* in *A* point to organelles that had moved out of the field in *B*. The *short, curved arrow* in the upper right corner of *B* points to an organelle that was not present in *A*. Stills were made as described in the legend to Figure 1. Scale bar, 2 μm.

affecting organelle motility via a crosslinking mechanism involving actin microfilaments. The question as to whether actin-containing filaments are distributed predominantly under the axolemma (Kuang and Goodman, 1978; Isenberg and Small, 1978; Mercadal and Lasek, 1978; Herokawa, 1982; Schnapp and Reese, 1982; Lee and Kuo, 1983) or are also present in significant amounts in the central microtubule-containing domain of the axon or neurite (Yamada et al., 1971; LeBeux and Wallace, 1978; Jockusch et al., 1979; Kuczmarski and Rosenbaum, 1979; Spooner and Holladay, 1981; Papasozomenos and Payne, 1986; Fath and Lasek, 1988) has been the subject of

some dispute. However, actin is clearly present in high concentration in the extruded squid axoplasm (Morris and Lasek, 1984; Fath and Lasek, 1988) and is also found in the presynaptic nerve terminal (LeBeux and Willemot, 1975; Toh et al., 1976; Walker et al., 1985). Moreover, although actin is not necessary for fast axonal transport (Allen et al., 1985; Brady et al., 1985; Schnapp et al., 1985), several actin-binding and microfilament depolymerizing agents have been shown to disrupt fast axonal transport (Goldberg et al., 1980; Goldberg, 1982; Brady et al., 1984). Significantly, these microfilament depolymerizing agents are not effective at inhibiting organelle movement along individual microtubules (Brady, 1987), and the individual microtubules on the periphery do not contain detectable microfilaments (Schnapp et al., 1985; Brady, 1987). Further studies will be required to determine if synapsin I inhibits organelle movement within the squid axoplasm by crosslinking synaptic vesicles with F-actin, by crosslinking F-actin with F-actin, or by some mechanism involving other cytoplasmic component(s) and to determine if such interactions have physiological relevance to synaptic transmission.

Associations between synapsin I and various subcellular components that were produced under the *in vitro* conditions used in the present study may not occur in vivo. However, it should be noted that the axoplasm studies more nearly resemble physiologically relevant conditions than do studies that examine interactions between synapsin I and purified subcellular components. A variety of other proteins, including myosin fragments, calcium-free gelsolin, antitubulin antibodies, antimyosin antibodies, and calmodulin (Brady et al., 1985; Johnston et al., 1987; S. T. Brady, unpublished observations; and this report), had little or no effect on transport, indicating that the perturbation of axonal transport by synapsin I was highly specific. In support of the specificity of the action of synapsin I on transport, addition of only 2 phosphate groups to the tail region of the synapsin I molecule virtually abolish its inhibitory effect. Furthermore, it is unlikely that the inhibitory effect of dephosphosynapsin I is an artifact due to the overall surfactant (M. Ho et al., unpublished observations) or basic properties of the molecule, since phosphorylation of synapsin I has no detectable effect on its surface activity (M. Ho et al., unpublished observations) and has only a minimal effect on its isoelectric point. In addition, perfusion of axoplasm with the basic protein avidin had no detectable effect on movement of organelles (unpublished observations).

Synapsin I constitutes ~0.4% of mammalian cerebral cortex protein (corresponding to approximately 1.0% of total neuronal protein) (Goelz et al., 1981) and most of the synapsin I appears to be localized to presynaptic terminals (De Camilli et al., 1983a, b; Huttner et al., 1983). Indeed, synapsin I represents 6% of the total protein present in synaptic vesicle fractions isolated from nerve terminal endings (Huttner et al., 1983). Squid axoplasm contains approximately 25 mg/ml protein (Morris and Lasek, 1984); thus, the effective concentrations of synapsin I used in the present experiments, namely 1.3–10 μM, correspond to about 0.4–3.0% of total protein in the extruded axoplasm. These concentrations are probably higher than that which exists in axons, since synapsin I constitutes only 0.02% of total protein in the corpus callosum (Goelz et al., 1981). In addition, it appears that only a portion of the synapsin I present in the axon is associated with vesicles during their transport down the axon, with the remainder undergoing slow axonal transport independent of membranous organelles (Baitinger and Willard, 1987). Thus, the concentrations of synapsin I used in the present experiments are most likely reached only in synaptic terminals where synapsin I is specifically localized. Therefore, we do not propose that synapsin I regulates release by blocking fast axonal transport. In fact (Llinas et al., unpublished observations), disruption of microtubules or axonal transport could not account for the inhibition of neurotransmitter release by synapsin I. Instead, we suggest that the ability of synapsin I to block axonal transport might reflect its ability to modulate organelle movement in the nerve terminal. Such modulation might involve regulating release of the vesicles from the microtubules, targeting the released vesicles to a cytoskeletal (actin?) matrix, or regulating detachment of the vesicles from such a cytoskeletal matrix.

References

Adams, R. J., and D. Bray (1983) Rapid transport of foreign particles microinjected into crab axons. Nature (London) *303:* 718–720.

Allen, R. D., and N. S. Allen (1983) Video-enhanced microscopy with a computer frame memory. J. Microsc. *129:* 3–17.

Allen, R. D., N. S. Allen, and J. L. Travis (1981) Video-enhanced contrast, differential interference contrast (AVEC-DIC) microscopy: A new method capable of analyzing microtubule-related motility in the reticulopodial network of *Allogromia laticollaris.* Cell Motil. *1:* 291–302.

Allen, R. D., J. Metuzals, I. Tasaki, S. T. Brady, and S. P. Gilbert (1982) Fast axonal transport in squid giant axon. Science *218:* 1127–1129.

Allen, R. D., D. G. Weiss, J. H. Hayden, D. T. Brown, H. Fujiwake, and M. Simpson (1985) Gliding movement of and bidirectional transport along single native microtubules from squid axoplasm: Evidence for an active role of microtubules in cytoplasmic transport. J. Cell Biol. *100:* 1736–1752.

Bahler, M., and P. Greengard (1987) Synapsin I bundles F-actin in a phosphorylation-dependent manner. Nature (London) *326:* 704–707.

Bahler, M., Benfenati, F., Valtorta, F., Czernik, A. J. and P. Greengard (1989) Characterization of synapsin I fragments produced by cysteine-specific cleavage: A study of their interactions with F-actin. J. Cell Biol. *108:* 1841–1849.

Baines, A. J., and V. Bennett (1985) Synapsin I is a spectrin-binding protein immunologically related to erythrocyte protein 4.1. Nature (London) *315:* 410–413.

Baines, A. J., and V. Bennett (1986) Synapsin I is a microtubule-bundling protein. Nature (London) *319:* 145–147.

Baitinger, C., and M. Willard (1987) Axonal transport of synapsin I-like proteins in rabbit retinal ganglion cells. J. Neurosci. *7:* 3723–3735.

Benfenati, F., M. Bähler, R. Jahn, and P. Greengard (1989) Interactions of synapsin I with small synaptic vesicles: Distinct sites in synapsin I bind to vesicle phospholipids and vesicle proteins. J. Cell Biol. *108:* 1863–1872.

Brady, S. T. (1987) Fast axonal transport in isolated axoplasm from squid giant axon. In *Axonal Transport,* R. S. Smith and M. Bisby, eds., pp. 113–138, Liss, New York.

Brady, S. T., R. J. Lasek, and R. D. Allen (1982) Fast axonal transport in extruded axoplasm from squid giant axon. Science *218:* 1129–1131.

Brady, S. T., R. J. Lasek, R. D. Allen, H. L. Yin, and T. P. Stossel (1984) Gelsolin inhibition of fast axonal transport indicates a requirement for actin microfilaments. Nature (London) *310:* 56–58.

Brady, S. T., R. J. Lasek, and R. D. Allen (1985) Video microscopy of fast axonal transport in extruded axoplasm: A new model for study of molecular mechanisms. Cell Motil. *5:* 81–101.

Chang, C.-M., and R. D. Goldman (1973) The localization of actin-like fibers in cultured neuroblastoma cells as revealed by heavy meromyosin binding. J. Cell Biol. *57:* 867–874.

Czernik, A. J., D. T. Pang, and P. Greengard (1987) Amino acid sequences surrounding the cAMP-dependent and calcium/calmodulin-dependent phosphorylation sites in rat and bovine synapsin I. Proc. Natl. Acad. Sci. USA *84:* 7518–7522.

De Camilli, P., and P. Greengard (1986) Synapsin I: A synaptic vesicle-associated neuronal phosphoprotein. Biochem. Pharmacol. *35:* 4349–4357.

spread distribution of protein I in the central and peripheral nervous systems. Proc. Natl. Acad. Sci. USA *76:* 5977–5981.

De Camilli, P., R. Cameron, and P. Greengard (1983a) Synapsin I (protein I), a nerve terminal-specific phosphoprotein. I. Its general distribution in synapses of the central and peripheral nervous system demonstrated by immunofluorescence in frozen and plastic sections. J. Cell Biol. *96:* 1337–1354.

De Camilli, P., S. M. Harris, Jr., W. B. Huttner, and P. Greengard (1983b) Synapsin I (protein I), a nerve terminal-specific phosphoprotein. II. Its specific association with synaptic vesicles demonstrated by immunocytochemistry in agarose-embedded synaptosomes. J. Cell Biol. *96:* 1355–1373.

Fath, K., and R. J. Lasek (1988) Two classes of actin microfilaments are associated with the inner cytoskeleton of axons. J. Cell Biol. *107:* 613–621.

Forman, D. S., K. J. Brown, and D. R. Livengood (1983) Fast axonal transport in permeabilized lobster giant axons is inhibited by vanadate. J. Neurosci. *3:* 1279–1288.

Forscher, P., L. K. Kaczmarek, J. Buchanan, and S. J. Smith (1987) Cyclic AMP induces changes in distribution and transport of organelles within growth cones of *Aplysia* bag cell neurons. J. Neurosci. *7:* 3600–3611.

Goelz, S. E., E. J. Nestler, B. Chehrazi, and P. Greengard (1981) Distribution of protein I in mammalian brain as determined by a detergent-based radioimmunoassay. Proc. Natl. Acad. Sci. USA *78:* 2130–2134.

Goldberg, D. J. (1982) Microinjection into an identified axon to study the mechanism of fast axonal transport. Proc. Natl. Acad. Sci. USA *74:* 4818–4822.

Goldberg, D. J., D. A. Harris, B. W. Lubit, and J. H. Schwartz (1980) Analysis of the mechanism of fast axonal transport by intracellular injection of potentially inhibitory macromolecules: Evidence for a possible role of actin filaments. Proc. Natl. Acad. Sci. USA *77:* 7448–7452.

Goldenring, J. R., R. S. Lasher, M. L. Vallano, T. Ueda, S. Naito, N. H. Sternberger, L. A. Sternberger, and R. J. DeLorenzo (1986) Association of synapsin I with neuronal cytoskeleton. J. Biol. Chem. *261:* 8495–8504.

Grafstein, B., and D. S. Forman (1980) Intracellular transport in neurons. Physiol. Rev. *60:* 1167–1283.

Grand, R. J. A., S. V. Perry, and R. A. Weeks (1979) Troponin C-like proteins (calmodulins) from mammalian smooth muscle and other tissues. Biochem. J. *177:* 521–529.

Greengard, P., M. D. Browning, T. L. McGuinness, and R. Llinas (1987) Synapsin I, a phosphoprotein associated with synaptic vesicles: Possible role in regulation of neurotransmitter release. In *Molecular Mechanisms of Neuronal Responsiveness*, Y. H. Ehrlich, R. H. Lenox, E. Kornecki, and W. O. Berry, eds., pp. 135–153, Plenum, New York.

Hayden, J. H., R. D. Allen, and R. D. Goldman (1983) Cytoplasmic transport in keratocytes: Direct visualization of particle translocation along microtubules. Cell Motil. *3:* 1–19.

Hirokawa, N. (1982) Cross-linker system between neurofilaments, microtubules and membranous organelles in frog axons revealed by the quick-freeze, deep-etching method. J. Cell Biol. *94:* 129–142.

Hirokawa, N., K. Sobue, K. Kanda, A. Harada, and H. Yorifuji (1989) The cytoskeletal architecture of the presynaptic terminal and molecular structure of synapsin I. J. Cell Biol. *108:* 111–126.

Hollenbeck, P. J., and D. Bray (1987) Rapidly transported organelles containing membrane and cytoskeletal components: Their relation to axonal growth. J. Cell Biol. *105:* 2827–2835.

Huttner, W. B., and P. Greengard (1979) Multiple phosphorylation sites in protein I and their differential regulation by cyclic AMP and calcium. Proc. Natl. Acad. Sci. USA *76:* 5402–5406.

Huttner, W. B., L. J. DeGennaro, and P. Greengard (1981) Differential phosphorylation of multiple sites in purified protein I by cyclic AMP-dependent and calcium-dependent protein kinases. J. Biol. Chem. *256:* 1482–1488.

Huttner, W. B., W. Schiebler, P. Greengard, and P. De Camilli (1983) Synapsin I (protein I), a nerve terminal-specific phosphoprotein. III. Its association with synaptic vesicles studied in a highly purified synaptic vesicle preparation. J. Cell Biol. *96:* 1374–1388.

Inoue, S. (1981) Video image processing greatly enhances contrast, quality, and speed in polarization-based microscopy. J. Cell Biol. *89:* 346–356.

and microtubules in neuroblastoma cells. Their distribution in relation to sites of movement and neuronal transport. Eur. J. Cell Biol. *16:* 326–344.

Jockusch, H., B. M. Jockusch, and M. M. Burger (1979) Nerve fibers in culture and their interaction with non-neural cells visualized by immunofluorescence. J. Cell Biol. *80:* 629–641.

Johnston, K. M., S. T. Brady, D. van der Kooy, and J. A. Connolly (1987) A unique tubulin antibody which disrupts particle movement in squid axoplasm. Cell Motil. Cytoskel. *7:* 110–115.

Kaczmarek, L. K., K. R. Jennings, F. Strumwasser, A. C. Nairn, U. Walter, F. D. Wilson, and P. Greengard. (1980) Microinjection of catalytic subunit of cyclic AMP-dependent protein kinase enhances calcium action potentials of bag cell neurons in cell culture. Proc. Natl. Acad. Sci. USA *77:* 7487–7491.

Kanda, K., T. Tanaka, and K. Sobue (1986) Calspectin (fodrin or nonerythroid spectrin)–actin interaction: A possible involvement of 4.1-related protein. Biochim. Biophys. Res. Commun. *140:* 1051–1058.

Kennedy, M. B., and P. Greengard (1981) Two calcium/calmodulin-dependent protein kinases, which are highly concentrated in brain, phosphorylate protein I at distinct sites. Proc. Natl. Acad. Sci. USA *78:* 1293–1297.

Kennedy, M. B., T. McGuinness, and P. Greengard (1983) A calcium/calmodulin-dependent protein kinase from mammalian brain that phosphorylates synapsin I: Partial purification and characterization. J. Neurosci. *3:* 818–831.

Koenig, E. (1986) Isolation of native Mauthner cell axoplasm and an analysis of organelle movement in non-aqueous and aqueous media. Brain Res. *398:* 288–297.

Krebs, K. E., I. S. Zagon, and S. R. Goodman (1987) Amelin: A 4.1-related spectrin-binding protein found in neuronal cell bodies and dendrites. J. Neurosci. *7:* 3907–3914.

Kuczmarski, E. R., and J. L. Rosenbaum (1979) Studies on the organization and localization of actin and myosin in neurons. J. Cell Biol. *80:* 356–371.

LeBeux, Y. J., and J. Willemot (1975) An ultrastructural study of the microfilaments in rat brain by means of E-PTA staining and heavy meromyosin labeling. II. The synapses. Cell Tissue Res. *160:* 37–68.

Letourneau, P. C. (1983) Differences in the organization of actin in the growth cones compared with the neurites of culture neurons from chick embryos. J. Cell Biol. *97:* 963–973.

Llinas, R., I. Z. Steinberg, and K. Walton (1981) Relationship between presynaptic calcium current and postsynaptic potential in squid giant synapse. Biophys. J. *33:* 323–352.

Llinas, R., T. L. McGuinness, C. S. Leonard, M. Sugimori, and P. Greengard (1985) Intraterminal injection of synapsin I or calcium/calmodulin-dependent protein kinase II alters neurotransmitter release at the squid giant synapse. Proc. Natl. Acad. Sci. USA *82:* 3035–3039.

McGuinness, T. L., Y. Lai, and P. Greengard (1985) Ca^{2+}/calmodulin-dependent protein kinase II: Isozymic forms from rat forebrain and cerebellum. J. Biol. Chem. *260:* 1696–1704.

McGuinness, T. L., S. T. Brady, J. A. Gruner, M. Sugimori, R. Llinas, and P. Greengard (1987) Inhibition by synapsin I of membranous organelle movement in isolated squid axoplasm. Soc. Neurosci. Abstr. *13:* 1239.

Metuzals, J., and I. Tasaki (1978) Subaxolemmal filamentous network in the giant nerve fiber of the squid (*Loligo pealei* L.) and its possible role in excitability. J. Cell Biol. *78:* 597–621.

Miller, R. H., and R. J. Lasek (1985) Cross-bridges mediate anterograde and retrograde vesicle transport along microtubules in squid axoplasm. J. Cell Biol. *101:* 2181–2193.

Morris, J. R., and R. J. Lasek (1984) Monomer–polymer equilibria in the axon: Direct measurement of tubulin and actin as polymer and monomer in axoplasm. J. Cell Biol. *98:* 2064–2076.

Nairn, A. C., and P. Greengard (1987) Purification and characterization of Ca^{2+}/calmodulin-dependent protein kinase I from bovine brain. J. Biol. Chem. *262:* 7273–7281.

Navone, F., P. Greengard, and P. De Camilli (1984) Synapsin I in nerve terminals: Selective association with small synaptic vesicles. Science *226:* 1209–1211.

Nestler, E. J., and P. Greengard (1984) *Protein Phosphorylation in the Nervous System*, pp. 144–153, Wiley, New York.

Papasozomenos, S. C., and M. R. Payne (1986) Actin immunoreactivity localizes with segregated microtubules and membranous organelles and in the subaxolemmal region in the β,β'-iminodipropionitrile axon. J. Neurosci. *6:* 3483–3491.

Paschal, B. M., and R. B. Vallee (1987) Retrograde transport by the microtubule-associated protein MAP 1C. Nature (London) *330:* 181–183.

Paschal, B. M., H. S. Shpetner, and R. B. Vallee (1987) MAP-1C is a microtubule-activated ATPase which translocates microtubules *in vitro* and has dynein-like properties. J. Cell Biol. *105:* 1273–1282.

Peterson, G. L. (1977) A simplification of the protein assay method of Lowry et al. which is more generally applicable. Anal. Biochem. *83:* 346–356.

Petrucci, T. C., and J. S. Morrow (1987) Synapsin I: An actin-bundling protein under phosphorylation control. J. Cell Biol. *105:* 1355–1363.

Petrucci, T. C., M. S. Mooseker, and J. S. Morrow (1988) A domain of synapsin I involved with actin bundling shares immunologic cross-reactivity with villin. J. Cell Biochem. *36:* 25–35.

Roots, B. I. (1983) Neurofilament accumulation induced in synapses by leupeptin. Science *221:* 971–972.

Schiebler, W., R. Jahn, J.-P. Doucet, J. Rothlein, and P. Greengard (1986) Characterization of synapsin I binding to small synaptic vesicles. J. Biol. Chem. *261:* 8383–8390.

Schnapp, B. J., and T. S. Reese (1982) Cytoplasmic structure in rapid-frozen axons. J. Cell Biol. *94:* 667–679.

Schnapp, B. J., R. D. Vale, M. P. Sheetz, and T. S. Reese (1985) Single microtubules from squid axoplasm support bidirectional movement of organelles. Cell *40:* 455–462.

Schroer, T. A., S. T. Brady, and R. B. Kelly (1985) Fast axonal transport of foreign synaptic vesicles in squid axoplasm. J. Cell Biol. *101:* 568–572.

Sieghart, W., J. Forn, and P. Greengard (1979) Ca^{2+} and cyclic AMP regulate phosphorylation of the same two membrane-associated proteins specific to nerve tissue. Proc. Natl. Acad. Sci. USA *76:* 2475–2479.

Spooner, B. S., and C. R. Holladay (1981) Distribution of tubulin and actin in neurites and growth cones of differentiating nerve cells. Cell Motil. *1:* 167–178.

Steiner, J. P., E. Ling, and V. Bennett (1987) Nearest neighbor analysis for brain synapsin I. J. Biol. Chem. *262:* 905–914.

Titus, J. A., R. Haugland, S. O. Sharrow, and D. M. Segal (1982) Texas red, a hydrophilic, red-emitting fluorophore for use with fluorescein in dual paramater flow microfluorometric and fluorescence microscopic studies. J. Immunol. Methods *50:* 193–204.

Toh, B. H., H. A. Gallichio, P. L. Jeffrey, B. G. Livett, H. K. Muller, M. N. Cauchi, and F. M. Clarke (1976) Anti-actin stains synapses. Nature (London) *264:* 648–650.

Ueda, T., and P. Greengard (1977) Adenosine 3',5'-monophosphate-regulated phosphoprotein system of neuronal membranes. I. Solubilization, purification, and some properties of an endogenous phosphoprotein. J. Biol. Chem. *252:* 5155–5163.

Ueda, T., H. Maeno, and P. Greengard (1973) Regulation of endogenous phosphorylation of specific proteins in synaptic membrane fractions from rat brain by adenosine 3',5'-monophosphate. J. Biol. Chem. *248:* 8295–8305.

Vale, R. D., B. J. Schnapp, T. Mitchison, E. Steuer, T. S. Reese, and M. P. Scheetz (1985a) Different axoplasmic proteins generate movement in opposite directions *in vitro.* Cell *43:* 623–632.

Vale, R. D., B. J. Schnapp, T. S. Reese, and M. P. Scheetz (1985b) Movement of organelles along filaments dissociated from the axoplasm of the squid giant axon. Cell *40:* 449–454.

Vale, R. D., B. J. Schnapp, T. S. Reese, and M. P. Scheetz (1985c) Identification of a novel force-generating protein, kinesin, involved in microtubule-based motility. Cell *42:* 39–50.

Walker, J. H., C. M. Boustead, V. Witzemann, G. Shaw, K. Weber, and M. Osborn (1985) Cytoskeletal proteins at the cholinergic synapse: Distribution of desmin, actin, fodrin, neurofilaments, and tubulin in *Torpedo* electric organ. Eur. J. Cell Biol. *38:* 123–133.

Weiss, D. G. (1986) Visualization of the living cytoskeleton by video-enhanced microscopy and digital image processing. J. Cell Sci. [Suppl.] *5:* 1–15.

Yamada, K. M., B. S. Spooner, and N. K. Wessells (1971) Ultrastructure and function of growth cones and axons of cultured nerve cells. J. Cell Biol. *49:* 614–635.

Proc. Natl. Acad. Sci. USA
Vol. 86, pp. 5656–5660, July 1989
Neurobiology

ATP-dependent directional movement of rat synaptic vesicles injected into the presynaptic terminal of squid giant synapse

R. LLINÁS*, M. SUGIMORI*, J.-W. LIN*, P. L. LEOPOLD†, AND S. T. BRADY†

*Department of Physiology and Biophysics, New York University Medical School, New York, NY 10016; and †Department of Cell Biology and Anatomy, University of Texas, Southwestern Medical Center, Dallas, TX 75235

Contributed by R. Llinás, March 22, 1989

ABSTRACT **The question as to whether synaptic vesicles prepared from vertebrate brain can be transported to the active zones of the squid giant synapse was studied by using a combined optical and electrophysiological approach. In order to visualize the behavior of the vertebrate synaptic vesicles *in situ*, synaptic vesicles isolated from rat brain were labeled with a fluorescent dye (Texas red) and injected into the presynaptic terminal of the squid giant synapse. The pattern of fluorescence that would result from passive diffusion was determined by coinjection of an unconjugated fluorescent dye (fluorescein). The patterns obtained with fluorescent synaptic vesicles were strikingly different from that obtained by simple diffusion of fluorescein. Although the fluorescein diffused freely in both directions, the vesicles moved preferentially into the terminal—i.e., toward the release sites—at a rate of 0.5 μm/sec. The final distribution of the injected fluorescent synaptic vesicles displayed a discrete localization that suggested a distribution coincident with the active zones of the presynaptic terminal. Like fast axonal transport, but unlike fluorescein movements in the terminal, the vesicle movement was energy dependent, since the addition of 2,4-dinitrophenol blocked the redistribution of vesicles completely. In addition, reduction of extracellular calcium concentration reversibly blocked vesicular movement as well. In conclusion, mammalian synaptic vesicles retain the cytoplasmic surface components necessary for translocation, sorting, and targeting to the proper locations by the native machinery of the squid giant synapse.**

The movement and disposition of synaptic vesicles (SVs) in presynaptic terminals have been areas of intensive research in recent years. Several different lines of investigation have led to the conclusion that SVs or their precursors are delivered to the presynaptic terminal by fast axonal transport (for review, see refs. 1 and 2). Many questions remain, however, about the fate of these vesicles during and after transport to the presynaptic terminal. For example, how are these vesicles targeted to the terminal rather than to the axonal plasmalemma? What occurs once the SV enters the presynaptic terminal: Do they proceed directly to the junctional areas or are they distributed stochastically? Moreover, what effect does activity have on these processes? Are the same molecular motors involved in moving vesicles in the terminal and in the axoplasm? Answers to most of these questions have been difficult or impossible to obtain because of limitations in the preparations and tools available to researchers. A combination of microinjection and intracellular recording with video microscopy techniques has now provided us with the means of addressing these fundamental questions in the presynaptic terminal of the squid giant synapse.

Several methods are now available for preparation of highly purified SVs from vertebrate neural tissue (3–6). These homogeneous fractions can be stripped of peripheral proteins and labeled with fluorescent probes without losing biological activity (neurotransmitter content and enzymatic activities). Previous studies with labeled SVs from vertebrate neural tissue have demonstrated that once they are introduced into isolated axoplasm from squid, the labeled SVs can interact with the motile machinery of fast axonal transport present in the axoplasm and can then be transported along the endogenous organelles (7). When the surface properties of the SVs were modified prior to injection into the axoplasm, the ability of the SVs to move and the directionality of movement were affected (refs. 1 and 7; S.T.B. and L. Yamasaki, unpublished observations). The principle of using a heterologous system that combined SVs from vertebrate sources with molluscan giant neurons and manipulating these constituent elements independently was thereby established as feasible. However, this type of preparation was primarily suited for studying the molecular mechanisms of fast axonal transport, particularly with regard to questions about putative molecular motors (i.e., kinesin or cytoplasmic dynein), and could not readily address questions about targeting or function in the terminal.

Extensive electrophysiological studies of the giant synapse have been conducted to characterize the physiological properties of synaptic transmission in the squid (8). In most respects, the squid giant synapse is a prototypical chemical synapse with the characteristic features of many vertebrate synapses such as the vertebrate neuromuscular junction. However, the large size and relative accessibility of the giant synapse of the squid permit intracellular recording within the terminal itself as well as microinjection of materials directly into the presynaptic terminal and adjacent axonal regions (9). As a result, the presynaptic terminal of the giant synapse is uniquely amenable to experimental manipulations for exploration of the molecular mechanisms underlying synaptic transmission. The ability to microinject materials into this presynaptic terminal has been particularly useful for examining possible functions for specific proteins associated with the terminal. For example, the injection of synapsin I has allowed the study of phosphorylation in the modulation of transmitter availability (9), and the injection of calcium indicators (10–12) enabled the visualization of the distribution of inward calcium current during synaptic release. A logical extension of these two approaches is to inject intact organelles into the terminal instead of proteins.

Microinjection of fluorescently labeled vertebrate SVs into the presynaptic terminal represents a powerful paradigm for understanding synaptic function. The ability to modify independently the SV components permits analysis of those vesicle components involved in the movement of organelles in the terminal, in the targeting of organelles to the junctional regions, and in the release of neurotransmitter. The electrophysiological properties of the giant synapse can be readily evaluated and continuously monitored, so the effects of an

The publication costs of this article were defrayed in part by page charge payment. This article must therefore be hereby marked "*advertisement*" in accordance with 18 U.S.C. §1734 solely to indicate this fact.

Abbreviations: SV, synaptic vesicle; TRSV, Texas red SV; DNP, 2,4-dinitrophenol.

experimental manipulation can be quantitatively analyzed, while simultaneously evaluating movements of the previously injected fluorescent SVs. We describe here the ATP-dependent, directional movement of vertebrate SVs in the presynaptic terminal of the squid giant synapse. The present set of experiments demonstrates that vesicles injected into a functional synapse are treated as intrinsic vesicles and are carried to the site of synaptic release in the presynaptic terminal.

MATERIAL AND METHODS

The following work was performed at the Marine Biology Laboratory in Woods Hole, MA. Reagents were obtained from Sigma unless otherwise stated. The squid giant synapse in the stellate ganglion of *Loligo pealeii* was removed from squid mantle under running seawater following standard protocol (13). Typically, squid with mantle lengths between 7 and 10 cm were utilized. Following removal of the stellate ganglion, it was placed in the recording chamber, and connective tissue was removed to allow presynaptic and postsynaptic recording and to facilitate visualization of the presynaptic terminal. The design of the experiment requires a clear visualization of the complete synaptic terminals, so only those stellate ganglia having superficial presynaptic terminals and simple structures were chosen. A synapse with simple structure was defined as having presynaptic terminals that ran longitudinally over the postsynaptic axons as opposed to those that either dive into the ganglion and contact the lower surface or those that wrap around the postsynaptic axon. In these cases, visualization of vesicular movement is very much impaired, although electrophysiological recordings could still be feasible. Preparations were perfused with oxygenated, running artificial seawater to maintain viability. In some experiments, Ca^{2+}-free artificial seawater, prepared by replacement of $CaCl_2$ with $MgCl_2$, was employed to eliminate activity.

Electrophysiological Techniques. Methods for electrophysiological studies were essentially as described previously (13). The presynaptic terminal was stimulated with extracellular electrodes located in the presynaptic bundle, and intracellular recordings were obtained at the presynaptic terminal near the point of entry of the presynaptic axon into the ganglion, prior to its ramification into the presynaptic digits. Intracellular recordings were required to characterize the presynaptic terminal, to assess its viability, and to check its ability to maintain a proper resting potential during the injection procedure. The identification of the presynaptic terminal could also be obtained optically as the injection of presynaptic dye immediately outlined the shape of the preterminal.

Preparation and Injection of Fluorescent Vertebrate SVs. Synaptosomal fractions were prepared from rat cortex, and SVs were purified from these synaptosomes by using a minor modification of the method of Huttner *et al.* (5). Following purification, 33-μg samples of SVs were resuspended in 200 μl of precleared Texas red (Molecular Probes) in labeling buffer (0.67 mg of Texas red per ml/0.4 M NaCl/10 mM Hepes, pH 7.4/10 mM EGTA) and incubated for 4 hr at 4°C. This step removes peripheral proteins and labels integral membrane proteins of the vesicle fraction. Following labeling, the Texas red SVs (TRSVs) were pelleted by a 15-min spin at 260,000 × g in a Beckman TL-100 ultracentrifuge and washed several times by resuspension into labeling buffer without Texas red. TRSVs could then be stored as aliquots either at −80°C for 4–8 wk or on ice for up to 10 days. Prior to use, TRSVs were pelleted, washed, and resuspended in injection buffer (0.1 M potassium aspartate/10 mM Hepes, pH 7.2). Previous studies had shown that this treatment does not interfere with the ability of TRSVs to move in fast axonal transport (7).

Unconjugated fluorescein was added to the injection fluid along with the TRSVs so that two fluorescent dyes were simultaneously injected. The fluorescein served several important functions. It was utilized as a control for the diffusion of any nonvesicular components and defined the morphology of the terminals and adjacent axon. In addition, the fluorescein provided a measure of the relative thickness in different regions of the presynaptic terminal and axon. The choice of unconjugated fluorescein as the second dye was made on the basis of two criteria. (*i*) Fluorescein and Texas red have sufficiently different excitation and emission wavelengths so that the two dye distributions could be compared at all times by switching filters and that observation at one wavelength would not contribute to bleaching for the other fluorochrome. (*ii*) Fluorescein did not significantly interact with other structures of the presynaptic terminal (SVs, plasmalemma, cytoskeletal structures, etc.).

Injection of TRSVs and fluorescein solutions into the presynaptic terminal were accomplished by using carefully beveled micropipettes. The beveling step was crucial as vesicular material was difficult to inject if the micropipette opening was not large enough. Conversely, a very large micropipette opening invariably leads to presynaptic terminal death, due to the influx of seawater, with a consequent disruption of synaptic organization and paralysis of vesicular mobility. Two important parameters were taken into consideration: (*i*) to bevel the electrode with an angle sufficiently steep in order to combine a low resistance (<1 MΩ) with a diameter sufficiently small so as to prevent injury to the presynaptic terminal and (*ii*) to ensure good suspension of SVs, as they tend to aggregate and form large masses that could prevent injection by blockage of the electrode. If injected, these aggregated vesicular masses exhibited a general lack of mobility. The actual injection was performed by use of pressure pulses. These pulses had a duration of 100–150 msec and the pressure varied from 20–35 psi (1 psi = 6.89 kDa).

Microscopic Techniques. The fluorescence was imaged by using a ×10 objective with an optical aperture of 0.22, which provided images to a double microchannel plate image intensifier coupled to a videcon camera (C1966-20 VIM System; Hammamatsu Photonics). This system allowed the visualization of fluorescence at extremely low light levels. Though fine structures could not be resolved by using this optic, this system gave excellent images of the bulk of the injected material in the interior of the presynaptic terminal. The image was then fed to an image processor (C1966; Hammamatsu Photonics), which allowed a variety of image enhancements, including a running average of fluorescence, the subtraction of background, and greyscale or pseudocolor manipulations. Fluorescent images were also recorded directly on video tape using a conventional VHS-type videocassette recorder, and the taped image was used for further analysis after the experiment. The fluorescent images were then displayed either as grey level images or using pseudocolor to emphasize fluorescent profile of injected materials.

RESULTS

Movement of TRSVs in the Presynaptic Terminal of the Squid Giant Synapse. After the pressure injection of presynaptic vesicles, SVs—i.e., Texas red fluorescence—were eventually distributed throughout the terminal area and outlined the complete structure of the synapse (Fig. 1). Similar results were obtained in four additional experiments. The image in Fig. 1 was taken 50 min after the initial injection. The injection site was located at the base of the upward pointing digit (arrow). It is clear from the illustration that the vesicles

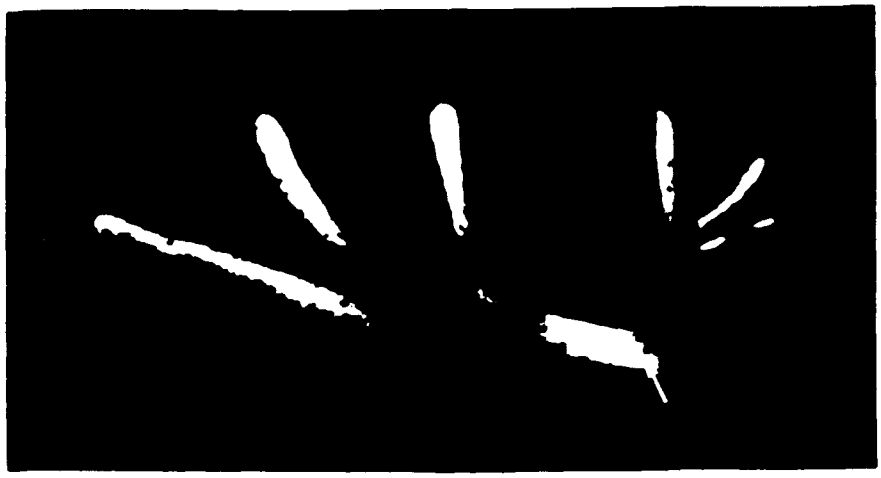

FIG. 1. Distribution of SVs in the squid giant synapse. This image highlights the distribution of Texas red fluorescence—i.e., the SVs—50 min after the initial TRSV and fluorescein coinjection. The density of the fluorescence is not uniform over the entire synapse. Instead, the distal portions of the digits have higher density and indicate a higher concentration of the TRSVs. The injection site was located at the base of the upward pointing digit (arrow), which contained three branchlettes. By contrast, coinjected fluorescein never concentrated in any portions of the presynaptic terminal.

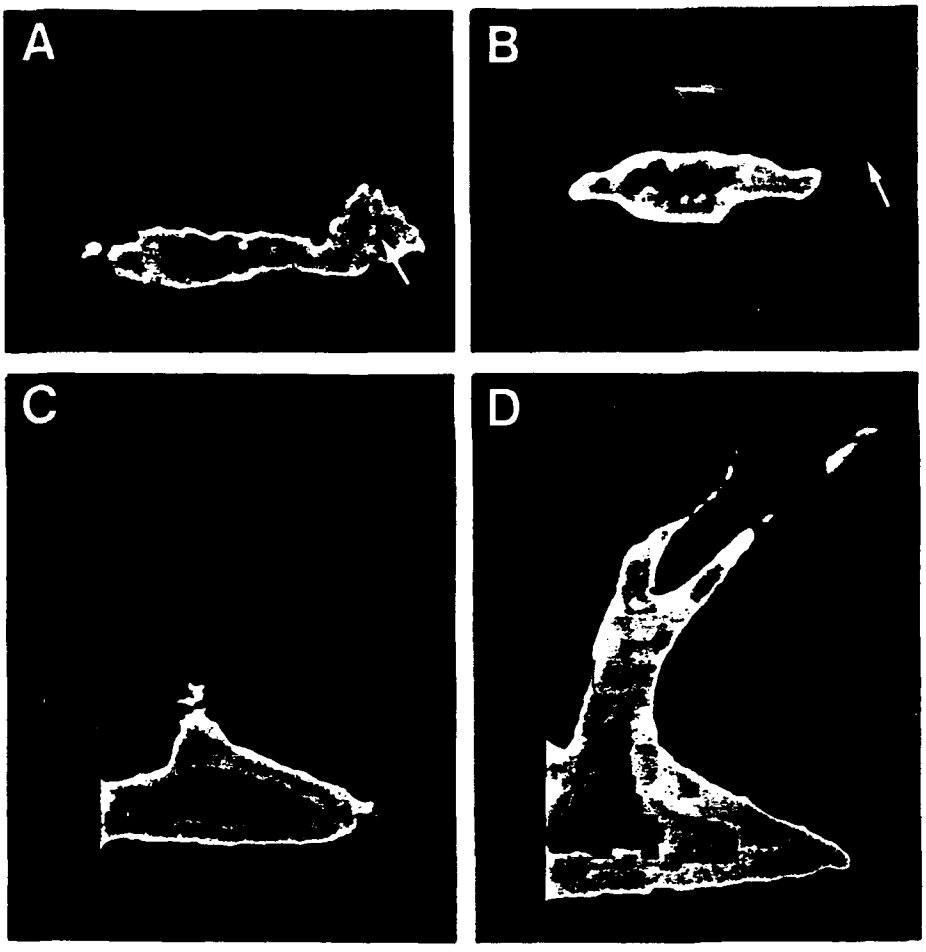

FIG. 2. Distribution of fluorescein and TRSV at different times after the initial injection. These images were obtained from the same synapse as that in Fig. 1 and have the same orientations. The fluorescein distribution 10 min after the injection (*A*) was mostly in the main trunk of the synapse and the axon. The latter corresponds to the area toward the right of the upward pointing digit. The TRSV distribution (*B*) has a similar distribution except that it is more restricted. The injection sites are indicated by arrows. A clear difference in the distribution of TRSV and fluorescein was observed 27 min after the initial injection (*C* and *D*). These images were taken under a higher magnification than that shown in *A* and *B*, and the terminal region to the left is not included. Due to prolonged diffusion, the fluorescein density is relatively low (*C*) such that its profile is smaller than the actual size of the synapse, which is better delineated by the distribution of TRSVs (*D*). In contrast to the distribution of fluorescein, TRSVs move along the terminal digit "purposefully" and penetrate deep into the branches (*D*). The distance that TRSVs travel along the digit is far longer than that on the retrograde direction—i.e., to the right.

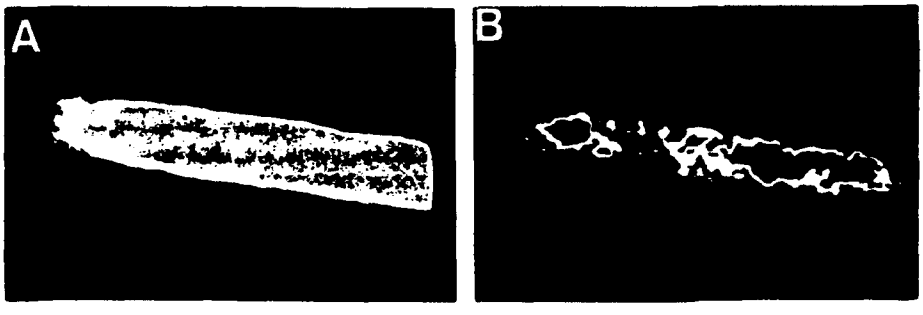

FIG. 4. Vesicular movement is energy dependent. In the presence of 0.66 mM DNP, the distribution of TRSV remained unchanged 35 min after injection (*B*), whereas fluorescein faded away rapidly after the initial injection. Terminal digits pointing toward the left in this preparation were not invaded by TRSVs. The picture in *A* was taken shortly after a second injection to highlight the initial distribution of fluorescein.

only moved anterogradely as there was virtually no fluorescence in the axon to the right. Furthermore, the SVs were preferentially concentrated in the areas corresponding to synaptic junctions—i.e., the last few hundred microns of the digits. In the case of the terminal digit, the horizontal one on the left, the vesicular material was seen to cover a large portion of the digit but was less concentrated near its base. The density of fluorescence in this digit is not entirely uniform, not unlike that observed from direct measurement of calcium entry using Fura II (12), and suggests a correlation with the localized distribution of the active zones in the terminal.

In order to provide a chronological description of the vesicular movement in the presynaptic arbor illustrated in Fig. 1, the distribution of fluorescence observed at earlier times after the injection is illustrated in Fig. 2. The initial distributions of the fluorescein (Fig. 2*A*) and the Texas red (Fig. 2*B*) fluorescence provide a direct measure of the location of the injected presynaptic vesicles within the terminal. This image was taken 10 min after the injection of a 10-pl volume of fluid containing TRSVs (0.44 mg/ml), fluorescein (0.14 mg/ml), and ATP (14 mM) in injection buffer. Following the initial injection, the presynaptic electrode was removed and the movement of vesicles was monitored by using the epifluorescence microscopy system.

As illustrated in Fig. 2*B*, the TRSVs were still largely confined to the general area of injection at 10 min, while the fluorescein had clearly diffused beyond the original injection site, moving both proximally and distally. After a period of 27 min, much of the fluorescence associated with the injected fluorescein had diffused away and consequently outlined an image smaller than the actual size of the synapse (Fig. 2*C*). In contrast, movement of TRSVs during the last 17 min covered a distance of ≈500 μm, measured from injection site to the tip of right branch (Fig. 2*D*). This measurement provides a transport rate of 0.5 μm/sec. By comparison, fast axonal transport in the isolated axoplasm has an average rate of 1.9 μm/sec in the anterograde direction and 1.3 μm/sec in the retrograde direction. Instead of measuring the rate of fluorescent vesicular movement by direct observation of individual vesicles (7), our imaging system only allowed us to estimate the transport rate by the movement of fluorescence boundary. This approach provided a lower limit of the transport rate because the criterion for defining the boundary was to find a line where there was an abrupt change in the fluorescence density. By this criterion, there was clearly weak fluorescence beyond the line but change in fluorescence density was too gradual to provide a consistent boundary definition. A quantitative description of TRSV movement, measured from the same synapse as that of Figs. 1 and 2, is illustrated in Fig. 3, where the movements to the terminal digit (square) and to the upward-pointing digit (circle) were plotted separately. The linear fits provide a transport rate of 0.5 and 0.4 μm/sec, respectively.

Movement of TRSVs was preferential in the anterograde direction. In fact, TRSVs were always observed to advance into the digits and to concentrate in the distal portions of the presynaptic terminals, there being essentially no detectable fluorescence in the retrograde direction. A clear demonstration of this point can be seen in Fig. 2*D*, where the distance of Texas red distribution into the digit is far longer than that into the larger proximal part of the axon (toward the right).

In contrast, injected fluorescein diffused quickly both forward into the presynaptic terminal and back into the proximal portion of the presynaptic axon. As a result, the fluorescein signal soon became widely distributed and thus attenuated. In fact, qualitatively the largest movement of fluorescein occurred in the retrograde direction, reflecting the larger sink for diffusion.

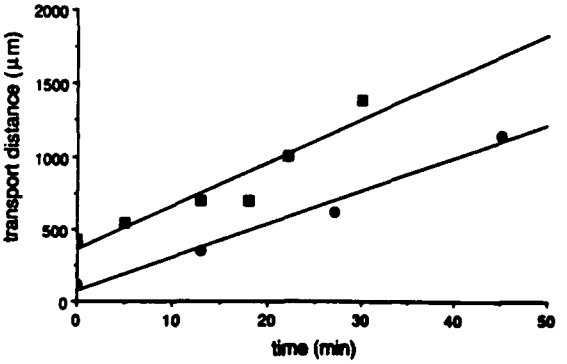

FIG. 3. Rate of vesicular movement. The measurements were obtained from the same synapse as that in Fig. 1. TRSV fluorescence movement in the horizontal direction (■)—i.e., toward the terminal digit to the left—and in vertical direction (●)—i.e., into the pointing digit—are plotted in the same graph. The distances were measured upward from the injection site to the boundary of fluorescence (see text). The straight lines are the linear regression fits for each direction. The data points do not start at zero distance because the fluorescence distribution covered a significant area instantaneously; presumably it was forced by the pressure applied through the injection electrode.

Distribution of Labeled SVs Following Inhibition of ATP Synthesis. In order to determine whether the movement required ATP, 2,4-dinitrophenol (DNP) (0.66 mM) was added to the extracellular fluid in place of the ATP. This has been shown to produce a total blockage of axonal transport (14, 15). If the movement of presynaptic vesicles in the terminals were to be an active process, dependent on ATP, then inhibition of ATP synthesis should block the redistribution of TRSVs as it blocks fast axonal transport. Coinjection of TRSVs and fluorescein with DNP demonstrated that although distribution of material due to passive diffusion (fluorescein) was not modified by the treatment, the redistribution of SVs did not occur following inhibition of axonal transport (see Fig. 4). Specifically, the fluorescein fluorescence typically faded away rapidly and required multiple injections to outline the profile of the synapse (Fig. 4*A*), whereas TRSV distribution remained stationary even after multiple injections (Fig. 4*B*). These experiments, which were repeated three times, demonstrated no movement of vesicles for periods up to 40 min after injection.

Distribution of Labeled SVs Following the Removal of Extracellular Calcium. Extracellular calcium was removed from the bathing medium to evaluate its role on the movement of TRSVs in a series of experiments similar to those described in previous sections. In this case, the extracellular calcium was removed from the bathing medium from the time of fine dissection in the recording chambers for a period of at least 30 min prior to injections of TRSVs and fluorescein. After this treatment, the extracellular calcium concentration was sufficiently low to prevent transmitter release, although presynaptic action potentials still exhibited a normal amplitude. As a result of this treatment, repeated in four synapses, no movement of TRSVs away from the initial site of injection could be detected. The movement of TRSVs under these conditions of low extracellular calcium resembled those following blockage of axonal transport by DNP. Furthermore, in three of these four experiments, partial or complete movement of the TRSVs could be recovered when the extracellular calcium concentration was raised to 10 mM. By contrast, removal of intracellular calcium in the axoplasm by perfusion with buffers containing as much as 10–20 mM EGTA had no detectable effect on the transport of organelles in fast axonal transport (14–16).

DISCUSSION

The results described above indicate that mammalian SVs moved when injected into the axoplasm of the squid giant synapse. Furthermore, the vesicles were specifically transported to the site of synaptic release. The rate and directionality of this movement are consistent with the view that movement occurs via the normal transport systems of the presynaptic terminal. In some respects, this movement bears a certain resemblance to vesicle movement due to fast axonal transport obtained in isolated axoplasm (1, 14, 15).

As in the isolated axoplasm, TRSVs in the presynaptic terminal move preferentially in the anterograde direction and in an ATP-dependent fashion. When the injection electrode was located near the base of the distal-most digit, SVs were seen to move toward that digit alone, again suggesting that vesicular movement is preferentially in an anterograde direction. There are, however, some differences. For example, the average velocity of movement for fluorescent vesicles in the terminal is only 0.5 μm/sec as compared to 1.9 μm/sec for fast axonal transport in the anterograde direction. Several mechanisms might be invoked to explain all or part of this apparent reduction in velocity. These include differences in the methods used for rate measurement in the two preparations (i.e., movement of large groups of organelles as opposed to movement of individual organelles), differences between the cytoskeleton of the terminal regions and the axoplasm, and multiple mechanisms for movement in the terminal. Another difference is that the reduction of extracellular calcium seems to completely block the movement of TRSVs in the presynaptic terminal, but fast axonal transport appears unaffected by low calcium levels (14–16). Some investigators have reported inhibition of fast axonal transport following application of a calcium channel blocker (17) or inhibitors of calmodulin (18). Such differences may reflect either an effect of the extracellular calcium on a regulatory process in the terminal (and possibly the axon) or the fact that cytoskeletal organization is primarily actin microfilaments in the presynaptic terminal as opposed to microtubules and neurofilaments in the axon. The extent to which vesicle movements in the terminal regions are homologous to fast axonal transport remains to be determined, but study of the movements of vertebrate SVs in the squid giant presynaptic terminal should permit elucidation of the underlying molecular mechanisms of vesicle movements in the terminal.

A striking feature of the redistribution of TRSVs in these studies is the specificity of targeting. No gross unevenness of vesicular distribution among the terminal digits was observed, suggesting that the base of the terminal arborization is a strategic site for injection that allows vesicular distribution to all presynaptic digits. The mechanisms for sorting and targeting of endogenous vesicles in the presynaptic terminal appear to function equally well on the injected vertebrate TRSVs. Apparently the information required for sorting and targeting must be present on the vesicles themselves and is sufficiently well conserved to be operational even when mammalian SVs are directed by the molluscan presynaptic terminal. Systematic modification of the vesicle surface prior to injection should permit identification of the vesicle surface features that determine the targeting and sorting of SVs in the presynaptic terminal. Similar studies have already determined that certain protein components of the vesicles affect the directionality of transport in axonal transport (7).

The fact that agents known to block axonal transport or to interfere with synaptic release were also capable of modifying vesicular movement indicates that the movement of TRSVs is well correlated with vesicular movement in the presynaptic terminal *per se*. SVs appear to move only when the preterminal is fully functional and capable of releasing transmitter. This is to be expected if the vesicle movements do relate to the mechanisms of transport, sorting, and release. Moreover, it is probable that the final distribution of vesicular material in these experiments concerns not only the actual accumulation of vesicles but also the apposition of vesicles onto the presynaptic axolemma. These experiments not only demonstrate that presynaptic vesicles move in the proper direction and accumulate in appropriate locations but also suggest that the system may in fact allow the vesicles to fuse with the membrane of the presynaptic terminal.

The small size and inaccessibility of most presynaptic terminals have hindered studies on the molecular mechanism of synaptic release and associated phenomena. A similar impasse had been reached in the study of molecular mechanisms of fast axonal transport prior to the application of video microscopy imaging methods to the study of fast axonal transport in the isolated axoplasm (14, 15). The result was the discovery of a new class of mechanochemical enzymes, the kinesins (19, 20). Analyses of the movements of vertebrate SVs in the presynaptic terminal of the squid giant axon using a combination of electrophysiological and video microscopic methods promise to provide comparable insights into the molecular mechanisms of synaptic release and transport of vesicles in the presynaptic terminal.

This research was supported by Grant AFOSR850368 from the United States Air Force.

1. Brady, S. T. (1987) *Neurol. Neurobiol.* **25**, 113–137.
2. Grafstein, B. & Forman, D. (1980) *Physiol. Rev.* **60**, 1167–1283.
3. Carlson, S. C., Wagner, J. A. & Kelly, R. B. (1978) *Biochemistry* **17**, 1188–1198.
4. Wagner, J. A., Carlson, S. C. & Kelly, R. B. (1978) *Biochemistry* **17**, 1199–1206.
5. Huttner, W. B., Schiebler, W., Greengard, P. & DeCamilli, P. (1983) *J. Cell Biol.* **96**, 1374–1388.
6. Hell, J. W., Maycox, P. R., Stadler, H. & Jahn, R. (1988) *EMBO J.* **7**, 3023–3029.
7. Schroer, T. A., Brady, S. T. & Kelly, R. B. (1985) *J. Cell Biol.* **101**, 568–572.
8. Llinás, R., Steinberg, I. Z. & Walton, K. (1981) *Biophys. J.* **33**, 323–352.
9. Llinás, R., McGuinness, T. L., Leonard, C., Sugimori, M. & Greengard, P. (1985) *Proc. Natl. Acad. Sci. USA* **82**, 3035–3039.
10. Llinás, R. & Nicholson, C. (1975) *Proc. Natl. Acad. Sci. USA* **72**, 187–190.
11. Miledi, R. & Parker, I. (1981) *Proc. Roy. Soc. London Ser. B* **212**, 197–211.
12. Smith, S. J., Augustine, G. J., Buchanan, J., Charlton, M. P. & Osses, L. (1988) *Biol. Bull.* **175**, 317–318.
13. Llinás, R., Steinberg, I. Z. & Walton, K. (1981) *Biophys. J.* **33**, 289–322.
14. Brady, S. T., Lasek, R. J. & Allen, R. D. (1982) *Science* **218**, 1129–1131.
15. Brady, S. T., Lasek, R. J. & Allen, R. D. (1985) *Cell Motil. Cytoskel.* **5**, 81–101.
16. Adams, R. (1982) *Nature (London)* **297**, 327–329.
17. Kanje, M., Edstrom, A. & Ekstrom, P. (1982) *Brain Res.* **241**, 67–74.
18. LaVoie, P. & Tiberi, M. (1986) *J. Neurobiol.* **17**, 681–695.
19. Brady, S. T. (1985) *Nature (London)* **317**, 73–75.
20. Vale, R. D., Reese, T. S. & Sheetz, M. P. (1985) *Cell* **42**, 39–50.

Proc. Natl. Acad. Sci. USA
Vol. 86, pp. 1689–1693, March 1989
Neurobiology

Blocking and isolation of a calcium channel from neurons in mammals and cephalopods utilizing a toxin fraction (FTX) from funnel-web spider poison

(ion-channel blocker/Purkinje cell/squid synapse)

R. LLINÁS, M. SUGIMORI, J.-W. LIN, AND B. CHERKSEY

Department of Physiology and Biophysics, New York University Medical School, New York, NY 10016

Contributed by R. Llinás, November 22, 1988

ABSTRACT **A Ca^{2+}-channel blocker derived from funnel-web spider toxin (FTX) has made it possible to define and study the ionic channels responsible for the Ca^{2+} conductance in mammalian Purkinje cell neurons and the preterminal in squid giant synapse. In cerebellar slices, FTX blocked Ca^{2+}-dependent spikes in Purkinje cells, reduced the spike afterpotential hyperpolarization, and increased the Na^{+}-dependent plateau potential. In the squid giant synapse, FTX blocked synaptic transmission without affecting the presynaptic action potential. Presynaptic voltage-clamp results show blockage of the inward Ca^{2+} current and of transmitter release. FTX was used to isolate channels from cerebellum and squid optic lobe. The isolated product was incorporated into black lipid membranes and was analyzed by using patch-clamp techniques. The channel from cerebellum exhibited a 10- to 12-pS conductance in 80 mM Ba^{2+} and 5–8 pS in 100 mM Ca^{2+} with voltage-dependent open probabilities and kinetics. High Ba^{2+} concentrations at the cytoplasmic side of the channel increased the average open time from 1 to 3 msec to more than 1 sec. A similar channel was also isolated from squid optic lobe. However, its conductance was higher in Ba^{2+}, and the maximum opening probability was about half of that derived from cerebellar tissue and also was sensitive to high cytoplasmic Ba^{2+}. Both channels were blocked by FTX, Cd^{2+}, and Co^{2+} but were not blocked by ω-conotoxin or dihydropyridines. These results suggest that one of the main Ca^{2+} conductances in mammalian neurons and in the squid preterminal represents the activation of a previously undefined class of Ca^{2+} channel. We propose that it be termed the "P" channel, as it was first described in Purkinje cells.**

While different Ca^{2+}-channel blockers have been described in past years (1), a true blocker for the main Ca^{2+}-dependent action potential in mammalian and in some molluscan neurons had not been encountered. This lack of a suitable blocker suggested that at least one of the main Ca^{2+} conductances present in the central nervous system (CNS) does not belong to the categories proposed by Tsien and co-workers (2, 3), as those channels respond quite specifically to dihydropyridines and ω-conotoxins. The use of funnel-web spider toxin (FTX) as a CNS Ca^{2+}-channel blocker was first described in Purkinje cells, where it blocked dendritic spiking (4). At that time the fragment utilized was known as AG1 and was obtained from Bioactives (Salt Lake City, UT). Because of the variability in the blocking observed, we attempted to isolate the main factor involved in this blockage from crude venom. We report here on the specific neuronal Ca^{2+}-channel blocking properties of FTX and its use in the isolation of functional channels, which we have studied in the black lipid membranes. That the Ca^{2+}-channel blocking fraction, which we call FTX, is different from that initially described as AG1 relates to its molecular mass as determined chromatographically, which is one-fifth that of AG1, and its high affinity for Ca^{2+} conductance both in the mammalian CNS and the squid giant synapse. Some of these results have been presented as short communications (4–7).

MATERIALS AND METHODS

Electrophysiological Techniques. The methods utilized for the brain slice work on the cerebellum and for the giant synapse are the same as those described in previous papers from our laboratory (8, 9). Purkinje cell recordings were obtained from *in vivo* adult guinea pig cerebellar slices. These cells were impaled at either the soma or the dendrites. Electrical excitability of the cell was determined by direct stimulation of the neurons. Sodium conductances were blocked by using tetrodotoxin (TTX).

The experiments on the squid (*Loligo Pealeii*) giant synapse were performed at the Marine Biological Laboratory (Woods Hole, MA). Pre- and postsynaptic recordings from the giant synapse were utilized to test the action of FTX on synaptic transmission, and presynaptic voltage-clamp was used to determine the effect of the toxin fraction on the inward presynaptic Ca^{2+} current and on synaptic transmitter release in the absence of action potentials.

Toxin. Crude venom from American funnel-web spiders, including *Agelenopsis aperta*, *Hololina curta*, and *Calilena*, was obtained commercially (Spider Pharm, Black Canyon, AZ). FTX, a factor with a molecular mass in the 200- to 400-Da range, was purified chromatographically from the venom. We estimate the concentration of toxin used to block Ca^{2+} conductance to be submicromolar, based on the elution profile (OD_{280}) of the FTX fraction on column chromatography and the dilution factors of the chamber.

Affinity Gel Construction. Purified toxin, the activity of which had been previously verified, was coupled to Sepharose 4B via 1,4-butanediol diglycidyl ether. The purified toxin obtained from 100 μl of the *A. aperta* venom was treated with 50 ml of the spacer-attached gel to form the final affinity gel.

Biochemical Methods. *Animals.* Adult Hartley guinea pigs (400–600 g) were decapitated with a small-animal guillotine under sodium pentobarbital (Nembutal, 40 mg/kg, i.p.) anesthesia. A rapid craniotomy was performed to remove the squamous portion of the occipital bone. The cerebellum was then separated from the brainstem and placed in ice-cold 400 mM sucrose/5 mM Tris·HCl, pH 7.4/0.1% phenylmethylsulfonyl fluoride/0.1% bacitracin/5 mM EDTA containing approximately 2 units of aprotinin per ml.

Adult squid (*Loligo Pealeii*) with a 10- to 13-cm mantle size were decapitated, and the optic lobe was excised and rapidly frozen in liquid nitrogen.

The publication costs of this article were defrayed in part by page charge payment. This article must therefore be hereby marked "*advertisement*" in accordance with 18 U.S.C. §1734 solely to indicate this fact.

Abbreviations: FTX, funnel-web spider toxin; TTX, tetrodotoxin.

Purification Procedure. Published protocols for the affinity purification of membrane proteins (10) were followed for the isolation of the toxin-binding components of the cerebellar and optic lobe membranes. The membrane pellet was resuspended to a concentration of 20 mg of protein per ml into 100 mM sodium citrate, pH 7.4/ 3% sodium choleate to solubilize the membrane protein in a Dounce homogenizer. The solution was stirred overnight at 4°C and centrifuged at 47,000 × *g* for 30 min; the supernatant was filtered under vacuum. The resulting filtrate was then subjected to affinity chromatography. The solution containing the solubilized membrane protein was allowed to react batchwise with 20 ml of the toxin-Sepharose gel by gently stirring overnight at 4°C. The gel was separated from the detergent solution by vacuum filtration. The resulting gel cake was resuspended into 20 ml of 1 M $CaCl_2$/1% sodium choleate/10 mM Hepes, pH 7.4, and was stirred for 2 hr at 4°C. The suspension was then filtered, and the filtrate was retained. The elution procedure was repeated a second time, and the resulting filtrates were combined. The volume of the solution was reduced by dialysis against polyethylene glycol 35,000 (Merck). The protein-containing concentrate was desalted on a 1.0 × 25 cm column of Sephadex G-25 equilibrated with 100 mM Hepes (pH 7.4) and was dialyzed extensively against 400 mM sucrose/10 mM Hepes, pH 7.4. Samples were taken at each step of the procedure for determination of protein by the Bradford assay (11). The product obtained with this procedure typically had a final yield of 0.0005% or less, consistent with the purification of a membrane protein such as an ionic channel.

Ca^{2+}-Channel Reconstitution and Recording. The purified protein was reconstituted into lipid vesicles by using a 4:1 mixture of phosphatidylethanolamine/phosphatidylcholine (Sigma) in 400 mM sucrose formed by the sonication–dialysis procedure of Racker (12, 13). After vesicle formation, the dialysate was applied to a 1.0 × 35 cm column of Sephadex G-25, and the void volume was collected. The resulting vesicle suspension was used for the bilayer studies.

The functional activity of the reconstituted protein was studied by using the lipid bilayer technique. Vesicles containing affinity-gel-processed protein were fused to a planar lipid bilayer, and the electrical activity was determined. Bilayers were formed on two-pull micropipettes with opening diameters near 1 μm by using a lipid solution composed of a 3:1 mixture of phosphatidylcholine/phosphatidylethanolamine (Avanti Polar Lipids). Voltage was applied via the micropipette by using a Dagan 8900 patch/whole-cell clamp with a 10-GΩ head stage (Dagan Instruments, Minneapolis). The bathing solution was held at ground. Data obtained in the channel studies were amplified to a level of 500 mV/pA, and the membrane current was recorded on an HP 3960 FM instrumentation recorder for subsequent analysis. Data were filtered at 1 kHz and were digitized at 2500 or 5000 samples per sec. The digitized records could then be viewed on a computer-generated display, and amplitude and open-time and closed-time distributions were obtained.

RESULTS

The Effect of FTX on the Intact Mouse. The activity of the toxin fraction was tested on mice. The results indicate that for a 30-g mouse, a 5-μl i.p. injection of a solution diluted 1:9 from the spider venom fraction produced death in 15–20 min, apparently by respiratory failure. No effect was observed on neuromuscular transmission. With half of the lethal dose, the animal became sleepy and rarely responded to auditory, visual, or tactile stimuli; when present, the response was phasic and short-lasting, emulating abrupt awakening from deep sleep. The results suggest that FTX crosses the brain–blood barrier, directly affecting the CNS. This is in contrast with results reported for the dihydropyridines (14, 15) and conotoxins (16, 17), which have little effect on mammalian CNS.

The Effect of FTX on Purkinje Cells. Intracellular recordings from Purkinje cells were obtained from cerebellar slices (4, 8). The two types of spike responses typically recorded from these neurons under control conditions are shown in Fig. 1. Depolarization of the neuron by square current pulses produced rapid sodium-dependent firing, which culminated in a set of long, low-amplitude, repetitive Ca^{2+}-dependent spikes (Fig. 1*A*). After bath application of FTX, the Ca^{2+}-dependent spikes disappeared, and the duration of the after-potential hyperpolarization was reduced (Fig. 1*B*). This blocking occurred 5–10 min after bath application of the toxin at a calculated 0.5 μM final concentration and was partly reversible after washing for about 30 min. In addition to blocking the Ca^{2+}-dependent action potentials, FTX increased the likelihood of plateau potentials (Fig. 1*B*), which are produced by the activation of the persistent Na^+ conductance (8, 9). Both of these plateau potentials and the initial fast spikes were blocked by the addition of TTX (10^{-6} g/ml) to the bath (Fig. 1*C*). Nearly identical results were obtained with FTX from the three different types of funnel-web spiders tested.

In a second set of experiments, recordings were made from the Purkinje cell soma after TTX administration. Under these

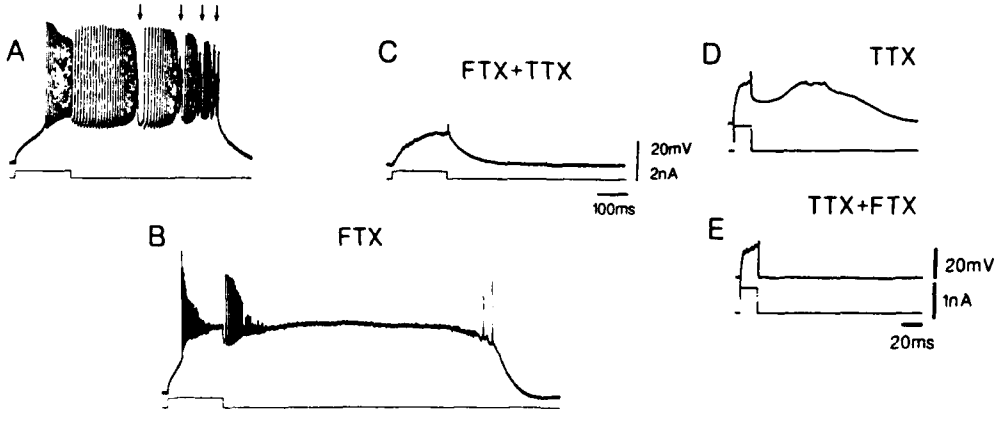

FIG. 1. (*A*) Intracellular recording from a Purkinje cell shows fast Na^+-dependent spikes and Ca^{2+}-dependent action potentials (arrows). (*B*) Five minutes after application of FTX, Ca^{2+} spiking disappeared, and a prolonged Na^+-dependent plateau potential is observed that far outlasts the duration of the stimulation (lower trace). (*C*) Addition of TTX to the bath blocks the fast action potentials and the plateau potentials shown in *B*. (*D*) Ca^{2+}-dependent slow action potential is generated by direct stimulation of the Purkinje cell in the presence of TTX. (*E*) Addition of FTX to the bath produces a blockage of the voltage-dependent Ca^{2+} electroresponsiveness.

conditions, Purkinje cell stimulation is known to elicit a slow Ca^{2+}-dependent plateau potential (8, 9). One such response is illustrated in Fig. 1*D*. In this case, a short, direct depolarization of the soma initiated a prolonged dendritic potential that outlasted the pulse by about 20 msec. However, after application of FTX ($\approx$0.5 μM), this Ca^{2+}-dependent conductance was blocked (Fig. 1*E*).

Single-Channel Properties. The functional activity of the isolated protein was assessed by the lipid-bilayer technique. Electrical activity was measured in asymmetric solutions containing 80 mM $BaCl_2$ and 10 mM Hepes (pH 7.4) on the cis side and 120 mM CsCl, 1 mM $MgCl_2$, and 10 mM Hepes (pH 7.4) on the trans side or in the patch pipette. Recordings were also obtained with the solutions reversed. When vesicles containing the purified protein were added to the bilayer chamber, an increase in the conductance of the bilayer was usually detected within 10 min. In general, it was difficult to obtain recordings of only a single channel when vesicles were added to the Ba^{2+}-containing solutions because of the fusion-promoting effect of divalent cations.

Two types of single-channel activity were found. The first was seen when Ba^{2+} was present on the extracellular face of the channel protein and was characterized by short-duration openings. Fig. 2 *A–C* illustrates this activity from the cerebellar preparation at holding potentials of −45, −30, and −15 mV. The voltage dependence of the open probability is shown in Fig. 2*F*. The channel was closed at −60 mV and began to exhibit openings as depolarizing potentials were applied. The maximum open probability, 0.6–0.65, occurred at holding potentials greater than 0 mV. The mean open time was also found to be voltage-dependent and ranged from less than 0.6 msec to 5 msec. The *I–V* relationship constructed from six experiments is nonlinear as shown in Fig. 2*E*, where each point represents the mean of the current at each voltage step. Voltage steps above 0 mV generated unitary currents too low to be measured reliably (Figs. 2*E* and 4 *F* and *G*). A conductance of 10–12 pS in Ba^{2+} and 6–8 pS in 100 mM Ca^{2+} was obtained from these data. The extrapolated reversal potential was between −90 and −120 mV, which, to the limit of the accuracy of the measurements, is the theoretical value for a Ba^{2+} permeable channel.

A second type of channel-like activity was found when the solutions were reversed so that the high-Ba^{2+} solution was on the cytoplasmic face of the channel. Typical recordings are shown in Fig. 2*D*, which were made at holding potentials of −45, −30, and −15 mV. In this particular experiment, three channels with identical conductances had fused with the bilayer. An unexpected characteristic was the predominance of openings longer than 1 sec. Also present are rapid openings with durations of less than 100 msec. From these data we estimated a unitary channel conductance of 20 pS.

The measured Ca^{2+} currents represent contributions from both the individual currents and the opening probabilities of the channels. Thus, it should be possible to approximate the macroscopic current by multiplying the single-channel currents by the opening probabilities at each potential as has been done for the "fast" Ca^{2+} channel (18). The voltage and time dependence of the current obtained in this way is comparable to the results from current clamp experiments in the dendrites of Purkinje cells (8). However, in the absence of Ca^{2+}-current measurements for Purkinje cell dendrites, only a qualitative statement can be offered. The effect of known blockers of the neuronal Ca^{2+} channels was determined for the reconstituted channels. Single channels were blocked by both Cd^{2+} and Co^{2+} at concentrations of less than 100 μM in a manner consistent with a fast-block mechanism (18). The single channels were also blocked by the microliter addition of a 1:10 dilution of FTX.

Cephalopod Ca^{2+} Channels. A set of experiments similar to those described for the Purkinje cell were carried out at the squid giant synapse. Two experimental paradigms were followed. Pre- and postsynaptic intracellular recordings were obtained, and synaptic transmission was tested by electrical activation of the presynaptic fiber. Presynaptic stimulation generated a presynaptic action potential that served as a trigger for transmitter release and the generation of a postsyn-

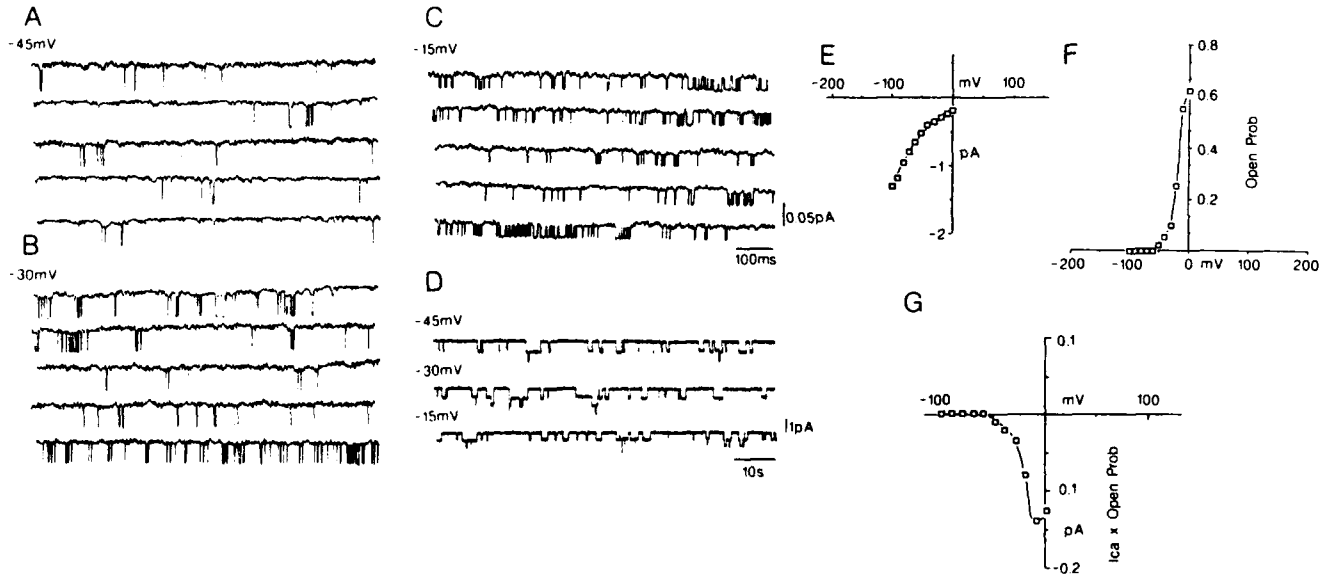

FIG. 2. Functional properties of channels isolated from guinea pig cerebellum by an FTX affinity gel. (*A–C*) Single-channel recording with 80 mM external Ba^{2+} obtained for protein reconstituted in lipid vesicles and fused with lipid bilayer. Holding potentials: −45 mV (*A*), −30 mV (*B*), and −15 mV (*C*). (*D*) Single-channel recordings obtained with 80 mM Ba^{2+} on the cytoplasmic face of the channel. Holding potentials of −45, −30, and −15 mV are shown. In this particular experiment, three identical channels had fused with the bilayer. The long duration of the open time seems to be an effect of the high amount of internal Ba^{2+}, as it can be converted into the short-duration channel (*A–C*) when Ba^{2+} is removed from the cytoplasmic side. (*E*) *I–V* curve in 80 mM Ba^{2+} for the "fast" channel of *A–C* constructed from the single-channel events obtained from six different experiments. Each point represents the mean current from 200 or more events at each voltage. (*F*) Plot of open probability vs. applied voltage showing the voltage dependence of the channel, which reaches a maximum value of 0.6–0.65 above 0 mV. (*G*) Values from *E–F* multiplied to give an approximation of the macroscopic current.

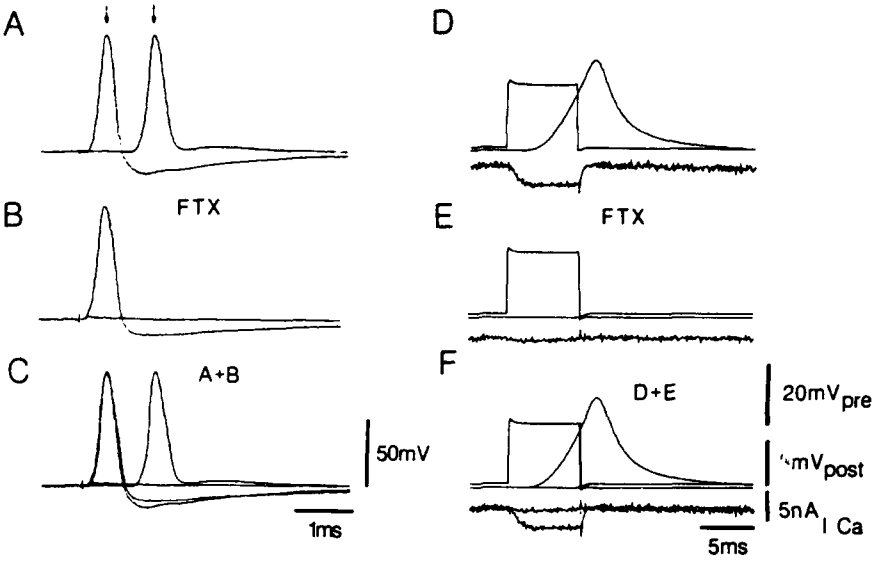

FIG. 3. Action of FTX on synaptic transmission at the squid giant synapse. (*A–C*) Effect of FTX on synaptic transmission evoked by presynaptic action potentials. Pre- (first arrow) and postsynaptic (second arrow) action potentials were evoked after direct stimulation of the preterminal fiber (*A*). Five minutes after the application of FTX, a total block of synaptic transmission was observed without affecting significantly the presynaptic action potential (*B*). Superimposition of the records in *A* and *B* (*C*) shows the small reduction in the amplitude of the afterpotential hyperpolarization after application of FTX. (*D–F*) Presynaptic voltage-clamp records and postsynaptic recording. Traces: upper, voltage step; middle, postsynaptic response; lower, inward calcium current. Results are shown before (*D*) and 10 min after (*E*) the application of FTX. Note the block of the calcium current and the postsynaptic response. Superimposition of records in *D* and *E* is shown in *F*.

aptic response (Fig. 3*A*). After administration of FTX in submicromolar concentrations, synaptic transmission was blocked within 5–8 min, and the presynaptic afterpotential hyperpolarization was slightly reduced (Fig. 3*B*). In a second set of experiments, the presynaptic terminal was voltage-clamped, and the relation between the presynaptic Ca^{2+} current and transmitter release was studied as shown in Fig. 3*D*. Addition of FTX at similar concentrations to that used in the experiment illustrated in Fig. 3*E* blocked the Ca^{2+} current within a few minutes. This was accompanied by a block of transmitter release, as judged by the absence of a postsynaptic response. The toxin fraction did not have a direct effect on postsynaptic channels, since no reduction of the postsynaptic response to pressure-injected glutamic acid was observed after the synaptic transmission was blocked by the toxin (not shown).

Isolation of Ca^{2+} Channels from the Squid Optic Lobe. Channel protein derived from the optic lobe was extracted and studied in the black lipid membranes. In Fig. 4 examples of the single-channel currents are illustrated. In the same asymmetric solutions used for the cerebellum, two types of channel-like activity were found. The first, shown at three holding potentials in Fig. 4 *A–C* was characterized by voltage-dependent openings with a mean duration of 1–3

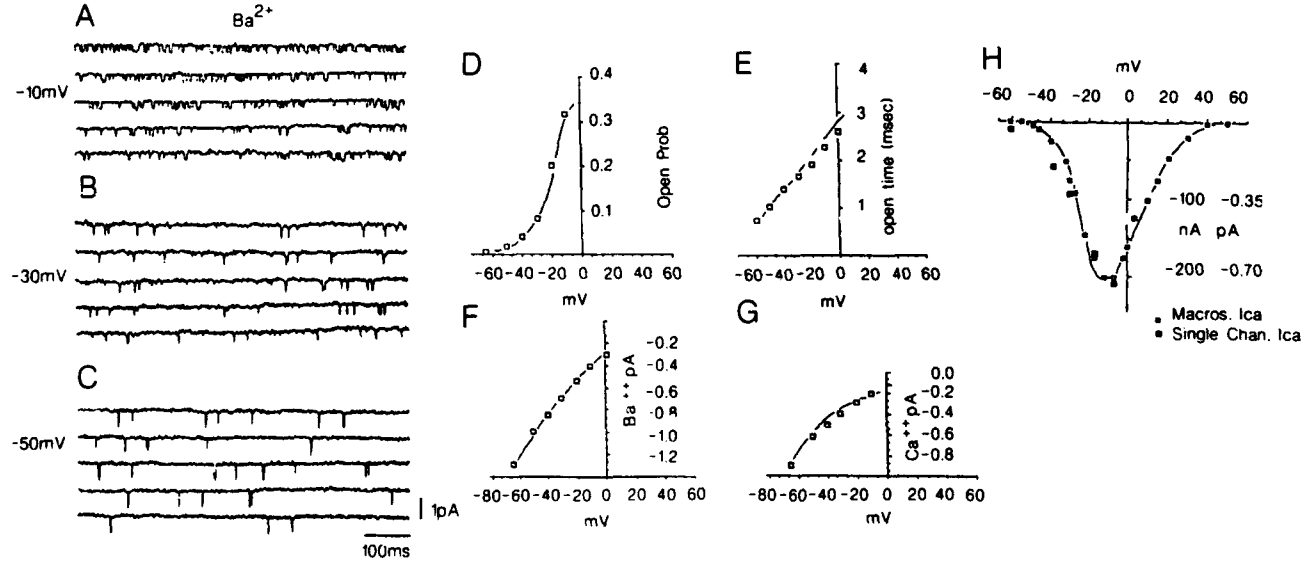

FIG. 4. Single-channel properties of protein from squid optic lobe. (*A–C*) Single-channel recordings at potentials of −10, −30, and −50 mV were obtained with 80 mM Ba^{2+} on the external face of the protein. (*D*) Opening probability of the channel reaches a maximum of 0.32–0.35 at 0 mV and above, exhibiting a clear voltage dependence ($n = 6$). (*E*) Mean open time vs. potential shows the voltage dependence of the length of time the channel remains open as the holding potential is varied ($n = 6$). (*F* and *G*) *I–V* curves obtained in 80 mM Ba^{2+} (*F*) and 100 mM Ca^{2+} (*G*). The conductance of the channel is 20 pS in Ba^{2+} and 8 pS in Ca^{2+} (200+ events at each potential). (*H*) □, Current obtained by multiplying values in *D* and *G* to approximate macroscopic behavior; ■, actual values for I_{Ca} in squid as previously published (9).

msec (Fig. 4*E*). The unitary conductance of the channel was 18–20 pS in 80 mM Ba^{2+} (Fig. 4*F*) and 5–8 pS in 100 mM Ca^{2+} (Fig. 4*G*). The opening probability, which was also voltage-dependent, reached a maximum of 0.35 at a membrane potential of 0 mV. When the cytoplasmic face of the protein was exposed to high-concentration Ba^{2+} solutions, long open times of the channel were induced, and replacement of the Ba^{2+} ions on the cytoplasmic side with Cs^{+} resulted in conversion of the long openings to short openings. High concentrations of internal Ca^{2+} (100 mM) did not induce the long open times. As both the probability of opening and the single-channel current are dependent on voltage, multiplication of these two parameters would give the current–voltage relationship for the macroscopic current. Such a plot for the fast channel, as shown in Fig. 4*H*, is quite similar to the macroscopic I_{Ca} recorded from the squid preterminal (19, 20).

Results similar to those determined for the cerebellar channel were found in the channels from squid optic lobe. Both long-duration and short-duration opening time were recorded. The squid fast channel differed from the cerebellar channel in two respects. First, the conductance of the squid channel was higher. The *I–V* curve constructed from a series of experiments on the short-duration channel is shown in Fig. 4 *F* and *G*. The unitary conductance was estimated to be 20 pS. A second difference between the two channels is that the cerebellar channel has a 2-fold higher maximum probability of opening. However, the voltage-dependence of the channels and their pharmacological characteristics are quite similar.

DISCUSSION

The present paper indicates that FTX, a fraction of funnel-web spider poison having a molecular mass of 200–400 Da, blocks Ca^{2+} channels both in mammalian Purkinje cells and at the presynaptic terminal of the squid giant synapse. Because this channel has unique pharmacological properties and kinetics that are somewhat different from those described for the L, N, and T channels (2, 3), we propose that it should be referred to as the "P" channel, since it was first described in Purkinje cells. Whether the P channel observed in Purkinje cells and in the squid giant synapse are indeed the same is difficult to say at this time. From an electrophysiological point of view, the macroscopic Ca^{2+} currents obtained from presynaptic voltage clamp studies (18, 19) and those obtained from black lipid membrane recordings of channels isolated from cerebellum show a similar *I–V* relation. Because reliable voltage-clamping of Purkinje cells so far has not been technically feasible, we cannot compare the computed *I–V* relation obtained from single Ca^{2+}-channel recordings with macroscopic I_{Ca}. However, the similarity between the kinetics of those observed in squid and Purkinje cells suggests that these two channels are similar.

A comparison of the P channel with previously described Ca^{2+} channels (2, 3) indicates clear differences. Indeed, the electrophysiological properties of both the squid giant synapse presynaptic spike as well as the action potential recorded from Purkinje cell dendrites are quite different from the low-threshold calcium spike observed in central neurons (20), which corresponds to the activation of the T channels (2, 3). Neither can the P channel be considered to be similar to the L channel, since the voltage-dependence of this channel is far more negative (−60 mV) (19, 20) than that reported for the L channel (2, 3). In addition, at least in the squid presynaptic terminal, a degree of inactivation may be observed. If anything, our channel may resemble the N channel. However, the P channel is not blocked by ω-conotoxin. In short, we must conclude on pharmacological and electrophysiological criteria that there exists yet another Ca^{2+} channel. This P channel is, in our estimation, one of a large variety of Ca^{2+} channels that will probably be encountered in the years to come.

In addition to the differences in pharmacology, single-channel conductances, and voltage-dependence kinetics, it is possible that the different channels have fundamentally different properties from a biochemical point of view as well. One of the interesting aspects of the present results relates to the action of calmodulin kinase II (CAMkinase II) on Ca^{2+} channels. This enzyme is known to phosphorylate the L-type Ca^{2+} channels, increasing their average open times, resulting in an increased Ca^{2+} current when these channels are phosphorylated (21). In the squid giant synapse, presynaptic injection of CAMkinase II has been shown to increase transmitter release as much as 7-fold without an observabie effect on the Ca^{2+} current (22), indicating that CAMkinase II may modulate transmitter release by phosphorylation of synapsin I at site 2 (23, 24), which would increase vesicular availability at the presynaptic release site (22). Thus, specific biochemical modulation of the different Ca^{2+} channels may be a fundamental variable in their role in nervous system function.

This work was supported by National Institute of Neurological and Communicative Disorders and Stroke Grants NS13742 and AFOSR85-0368.

1. Tsien, R. W., Lipscombe, D., Madison, D. V., Bley, K. R. & Fox, A. P. (1988) *Trends NeuroSci.* **11**, 431.
2. Fox, A. P., Nowycky, M. C. & Tsein, R. W. (1987) *J. Physiol. (London)* **394**, 149–172.
3. Fox, A. P., Nowycky, M. C. & Tsien, R. W. (1987) *J. Physiol. (London)* **394**, 173–200.
4. Sugimori, M. & Llinás, R. (1987) *Soc. Neurosci. Abst.* **13**.
5. Tank, D. W., Sugimori, M., O'Connor, J. A. & Llinás, R. (1988) *Science* **242**, 773–777.
6. Sugimori, M., Lin, J. W., Cherksey, B. & Llinás, R. (1988) *Biol. Bull.* **175**, 308.
7. Cherksey, B., Sugimori, M., Lin, J. W. & Llinás, R. (1988) *Biol. Bull.* **175**, 304.
8. Llinás, R. & Sugimori, M. (1980) *J. Physiol. (London)* **305**, 171–195.
9. Llinás, R., Steinberg, I. Z. & Walton, K. (1981) *Biophys. J.* **33**, 289–322.
10. Cherksey, B. D. (1988) *J. Comp. Physiol. Biochem.* **90A**, 771–773.
11. Bradford, M. (1976) *Anal. Biochem.* **12**, 248–254.
12. Racker, E., Knowles, A. F. & Eytan, E. (1975) *Ann. N.Y. Acad. Sci.* **264**, 17–33.
13. Cherksey, B. D. & Zeuthen, T. (1987) *Acta Physiol. Scand.* **129**, 137–138.
14. Fleckenstein, A. (1977) *Annu. Rev. Pharmacol. Toxicol.* **17**, 149–166.
15. Weiss, G. B., ed. (1981) *New Perspectives on Calcium Antagonists* (Am. Physiol. Soc., Bethesda, MD).
16. Gray, W. R., Luque, A., Olivera, B. M., Barret, J. & Cruz, L. J. (1981) *J. Biol. Chem.* **256**, 4734–4740.
17. Olivera, B. M., McIntosh, J. M., Cruz, L. J., Luque, F. A. & Gray, W. R. (1984) *Biochemistry* **23**, 5087–5090.
18. Hille, B. (1984) *Ionic Channels of Excitable Membranes* (Sinauer, Sunderland, MA).
19. Llinás, R., Steinberg, I. Z. & Walton, K. (1981) *Biophys. J.* **33**, 323–352.
20. Llinás, R. (1988) *Science* **242**, 1654–1664.
21. Armstrong, D. (1988) *J. Gen. Physiol.* **92**, 10a (abstr.).
22. Llinás, R., McGuinness, T. L., Leonard, C. S., Sugimori, M. & Greengard, P. (1985) *Proc. Natl. Acad. Sci. USA* **82**, 3035–3039.
23. DeCamilli, P., Cameron, R. & Greengard, P. (1983) *J. Cell Biol.* **96**, 1337–1354.
24. Huttner, W. B., Schiebler, W., Greengard, P. & DeCamilli, P. (1983) *J. Cell Biol.* **96**, 1374–1388.